VSP-ASSISTED SEISMIC INTERPRETATION: GLACIAL TERRACES, RED LODGE, MONTANA AND AVO EFFECTS, GARDEN BANKS, GULF OF MEXICO

A Thesis Presented to

the Faculty of the Department of Earth and Atmospheric Sciences

University of Houston

In Partial Fulfillment

of the Requirements for the Degree

Master of Science in Geophysics

By

Jingqiu Huang

August 2011

VSP-ASSISTED SEISMIC INTERPRETATION: GLACIAL TERRACES, RED LODGE, MONTANA AND AVO EFFECTS, GARDEN BANKS, GULF OF MEXICO

Jingqiu Huang

APPROVED:

Dr. Robert Stewart, Advisor
Professor

Dr. Fred Hilterman
Professor

Dr. Don Kouri
Professor

Dean, College of Natural Sciences & Mathematics

ACKNOWLEDGEMENTS

My special thanks go to Dr. Robert Stewart for his guidance and support throughout this endeavor. I would also like to thank Dr. Fred Hilterman, Dr. Don Kouri, Rick Kuzmiski, Joe Wong, and Carlos Montana. Last, but certainly not least; my deepest gratitude goes to my family for their constant encouragement and support in my attainment of this goal.

VSP-ASSISTED SEISMIC INTERPRETATION: GLACIAL TERRACES, RED LODGE, MONTANA AND AVO EFFECTS, GARDEN BANK, GULF OF MEXICO

An Abstract of a Thesis Presented to

the Faculty of the Department of Earth and Atmospheric Sciences

University of Houston

In Partial Fulfillment

of the Requirements for the Degree

Master of Science in Geophysics

By

Jingqiu Huang

August 2011

ABSTRACT

This study covers the analysis of two Vertical Seismic Profile (VSP) cases. In the first case, we conducted a series of geophysical surveys to characterize a glacial bench deposit and underlying strata near Red Lodge, Montana. The well logs and VSP data were acquired in a PVC-cased, 115m deep borehole. The well logs included measurements of conductivity, radioactivity (gamma ray), temperature, and sonic velocity. High-resolution 2D and 3D seismic surveys, using a sledgehammer source, were designed and acquired near the well GB-1. On the L-plot composite displaying well log data, and the VSPs corridor stack data. Three reliable reflections were identified, and the 50m depth one also shows on driller's report as a water zone. The VSPs velocities and sonic log show a velocity increase at 25m depth, which is interpreted as the base of the glacial deposits in this study.

A VSP was also acquired in the Garden Banks block at the Gulf of Mexico to provide a basic time-to-depth relationship. The resulting in situ velocities were used to calibrate surface seismic anomalies. During the modeling part of this study, the incident angle of a 3D numerical model was tested. The analysis result shows that the field VSP geometry does not have enough information to perform adequate AVO analysis. Vertical incidence VSP (VIVSP), Offset VSP (OVSP), and the sonic log show a velocity increase at 17,000ft (5200m) depth, which causes converted wavefields. The downgoing P-wave, downgoing PS-wave, upgoing PP-wave, and upgoing PS-wave energy partitions have been analyzed and compared with the theoretical calculations from the Zoeppritz

equation. The OVSP P-P reflection has been processed into a 150ft (45m) bin size CDP section, which resolves the horizon at 18,000ft (5500m) (5.0s), and shows the reflection amplitude decrease with the offset increase. At 20,000ft (6100m) (5.35s) is a horizon with uncertain thickness. Logging data show it may extend to 20,500ft (6250m) (5.45s), which is also has low velocity. The VIVSP-CDP with 40ft bin size mapping resolves the boundary between the two horizons.

CONTENTS

Section	*Page Number*
Acknowledgements	iii
Abstract	v
Chapter 1: Introduction	1
Chapter 2: Montana case study	3
2.1 Geology and motivation	3
2.2 Acquisition equipment	8
2.3 Data available	10
2.4 Forward modeling and synthetic VSP	23
2.5 Hydrophone walk-away VSP tube wave removal	25
2.6 Hydrophone VSP signal processing	33
2.7 Hydrophone walk-away VSP-AVO analysis	38
2.8 Hydrophone VSP tube wavefield processing	40
2.9 Near-offset geophone VSP processing	47
2.10 Wireline logs, 2D seismic, and VSP comparison	52
2.11 Discussion and conclusion	54
Chapter 3: Garden Banks case study	56
3.1 Geology and motivation	56
3.2 Target description	58
3.3 Data available	59
3.4 VIVSP synthetic and processing	62
3.5 OVSP synthetic and processing	73
3.6 VIVSP & OVSP AVO evaluation	95
3.7 Walk-away VSP design for AVO analysis	97
3.8 Discussion and conclusions	99

Chapter 4: Thesis summary **101**

4.1 Summary of glacial terraces, Red Lodge, Montana 101

4.2 Summary of Garden banks, Gulf of Mexico 102

References 105

Appendices 109

Appendix 2-1: The GB-1 well drilling report 109

Appendix 2-2: Critical offset calculation using Snell's law 110

Appendix 2-3: 2D forward model parameters 111

Appendix 2-4: 36m depth CRG AVO information table 112

Appendix 3-1: Schlumberger processed VIVSP and OVSP depth migration 113

Appendix 3-2: Forward model parameters 114

Chapter 1 Introduction

The main method involved in this study is the vertical seismic profile (VSP) with its acquisition, processing, and interpretation. The VSP is a measurement procedure in which a seismic signal generated at the surface of the earth is recorded by geophones secured, at various depths, to the wall of a drilled well (Hardage, 1983). The VSP often is recorded in a lower noise environment compared to surface seismic, because the geophones are down in the borehole. A principal use of the VSP is to determine the variation of seismic velocity with depth (Stewart, 1984). The VSP techniques (walk-away VSP, 3D VSP, and massive VSP) provide higher resolution than surface seismic, which can be inverted into rock properties of a target horizon including velocity, attenuation and anisotropy. Multi-offset VSP survey, specific for Amplitude-Versus-Offset (AVO) analysis, can transform the amplitude information into an estimate of lithology and pore-fluid saturation using the AVO technique.

For VSP data processing, a standard processing workflow has been used, illustrated in Figure 1-1. The first break pick for the downgoing wavefield is used to get the time, which is inverted to get the interval velocity. Wave field separation is achieved by applying a median filter to subtract the enhanced downgoing wavefield from the total traces. The VSP deconvolution operator is designed from the downgoing wavefield to apply to the upgoing wavefield, which is a good way to design the deconvolution operator to get absolute reflection coefficients (Hinds et al., 1999). To suppress noise and multiples, the corridor stack is windowed along the edge of the data to get the final VSP reflection coefficient series. The VSP data processing in this study is done using the VISTA software package and forward modeling is done using the OMNI package, both from GEDCO (Calgary).

There are two VSP cases in this study, Chapter 2 contains the Montana field camp case study,

and Chapter 3 contains the Garden Banks, Gulf of Mexico (GOM) case study. At the Montana field camp, different types of geophysical data have been acquired to study the thicknesses of glacial benches and water aquifer depth. In the Garden Banks field, vertical incidence VSP (VIVSP) and offset VSP (OVSP) were acquired for better velocity model analysis and time-depth conversion.

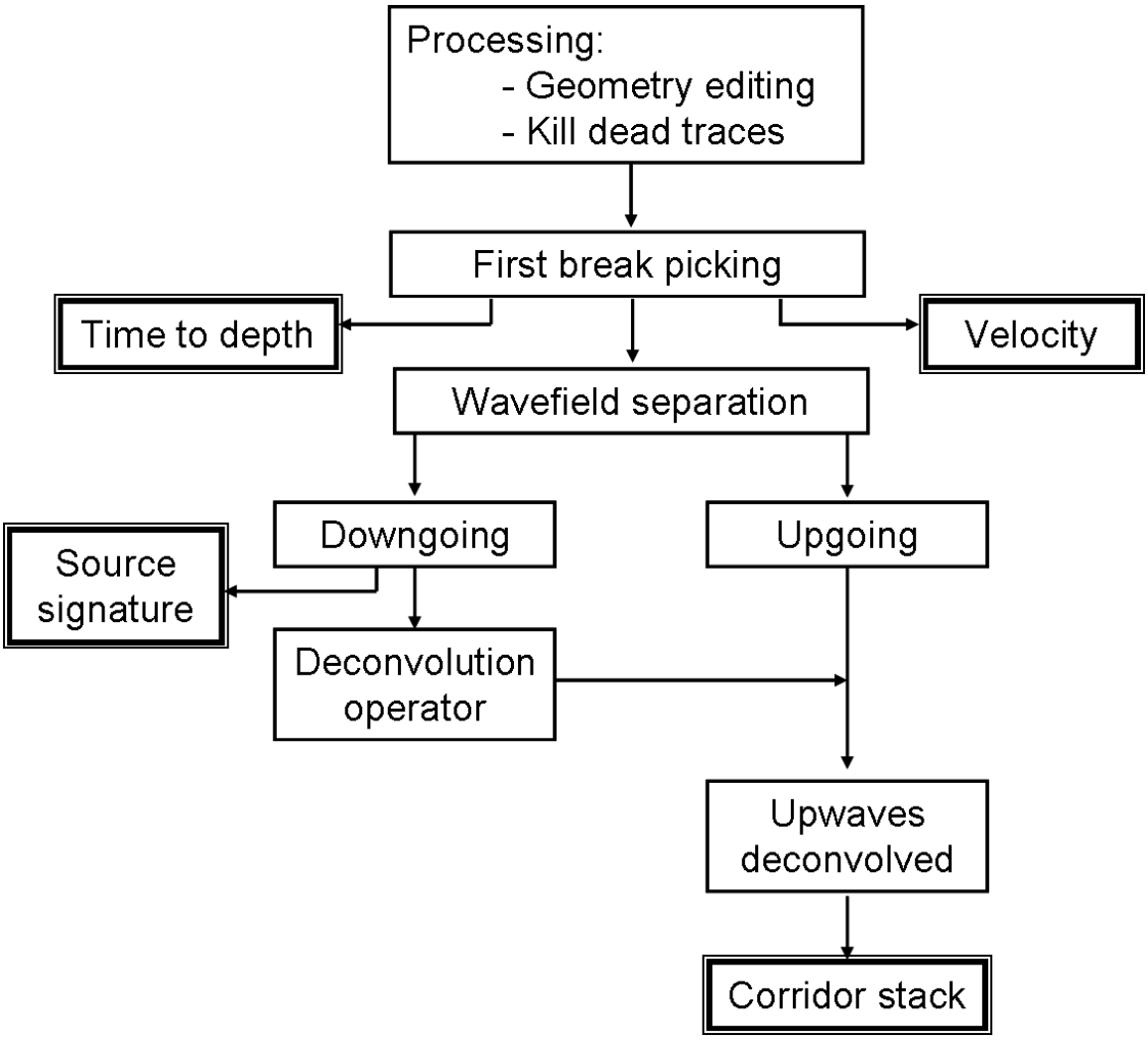

Figure 1-1: VSP data processing workflow used in this study, boxes with double outline are results (deliverables).

Chapter 2 Montana case study

2.1 Geology and motivation

The study area, near Red Lodge Montana, is close to the border of Montana and Wyoming (Fig. 2-1). The field survey lies in front of the Beartooth Mountains which locally comprise an overturned sequence with a thrust fold (Foose et al., 1961; Wise, 2000- Fig.2-2). During the last glacial maximum (approximately 12,000 to 20,000 years ago, locally called the Pinedale), mountain glaciers formed in the Montana area, picking up and transporting rock fragments. These rock fragments can be deposited as glacial till when the glacier recedes. In our case, the glacial deposits were formed by rivers and streams running from the glacier onto the plains. Nearby outcrops show three layers of glacial till deposits and boulders of granite ranging from 0.3m to 3m in diameter (Fig.2-3). The glacial benches in the area were formed during earlier glacial melts depositing sediment and the erosion scarps were formed by later glacier outwashes. The total thickness of glacial bench is around 23m (Ritter, 1964) (Fig. 2-4). The well is lined with cement casing. It encounters about 13m of unconsolidated overburden and then goes through a red rock and a fracture zone. Rock properties from the drillers log shows that the top 13m is soil and gravel (Fig. 2-5). This gravel may be the youngest pulse of glacial deposits. From 15m to 25m, there is a red-colored rock, interpreted as another pulse of glacial deposits. To assess the thickness of the overlying glacial till and provide information on the underlying stratigraphy, we have undertaken geophysical measurements. To understand it, a forward model to generate synthetic VSP was built.

Figure 2-1: General location map of Red Lodge, Montana, the location of study site is annotated with a red arrow.

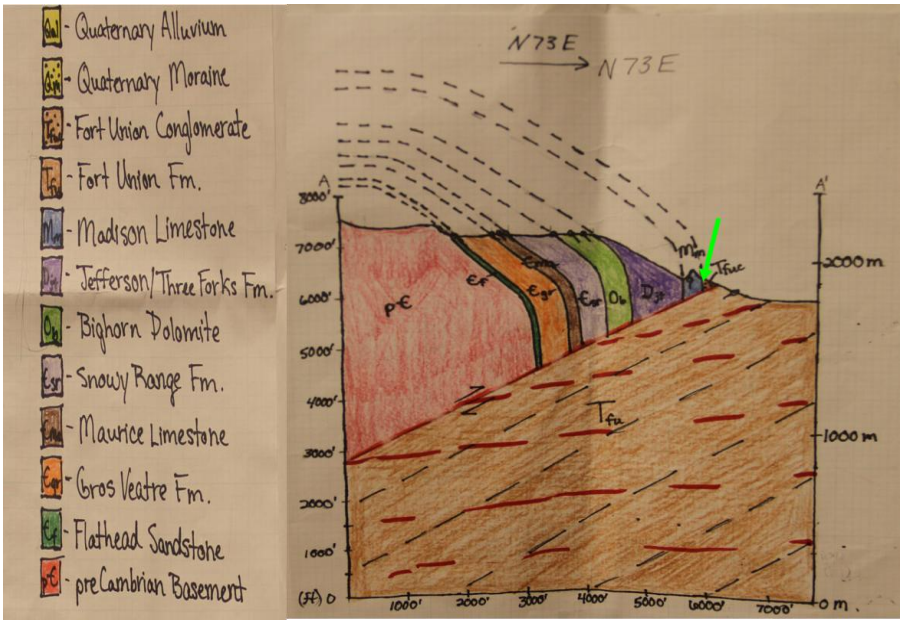

Figure 2-2: A geologic cross section (WE) of the glacial bench deposits near the site, the vertical structure at the study area is shown in green arrow (Adapted from Tiffany Henderson, 2010).

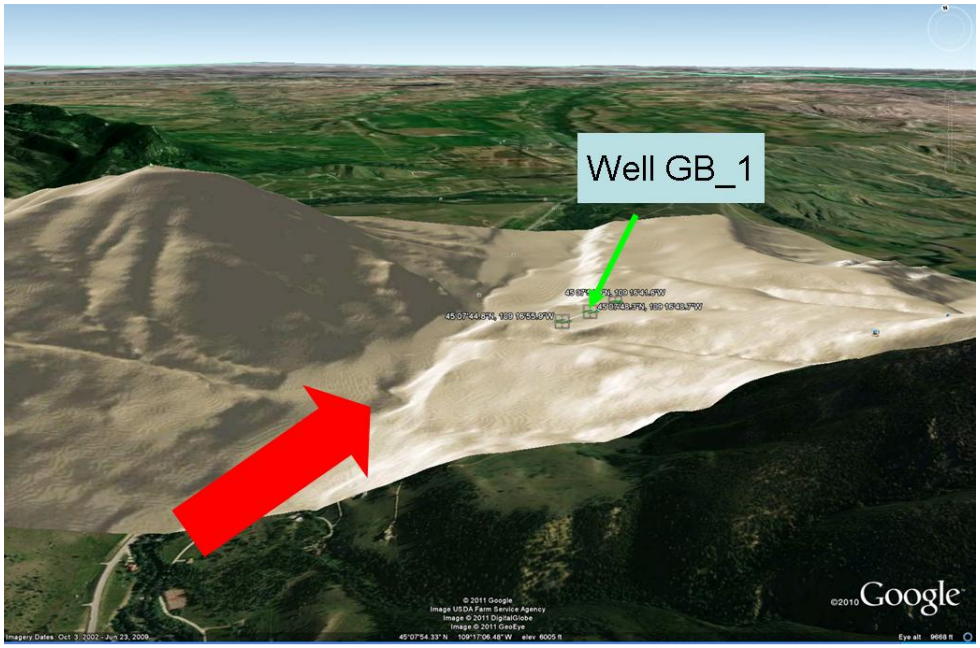

Figure 2-3: a) Plane view of the field site, the glacial movement direction shows in red arrow.

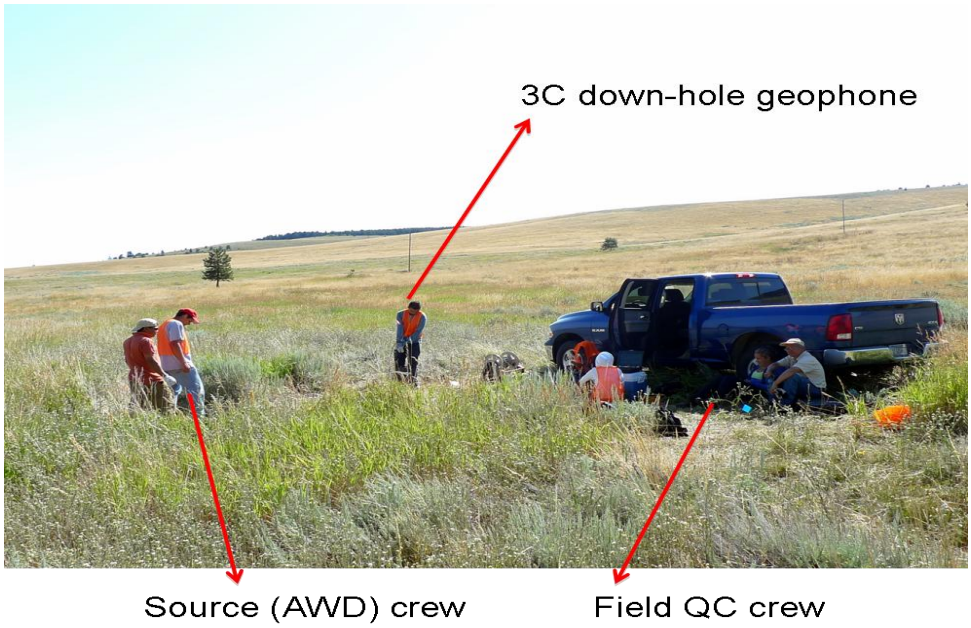

Figure 2-3: b) The field VSP acquisition in the GB-1 well.

Figure 2-3: c) The field site of the glacial bench out crops near the GB-1 well (Pers. Comm. R. Stewart, 2011).

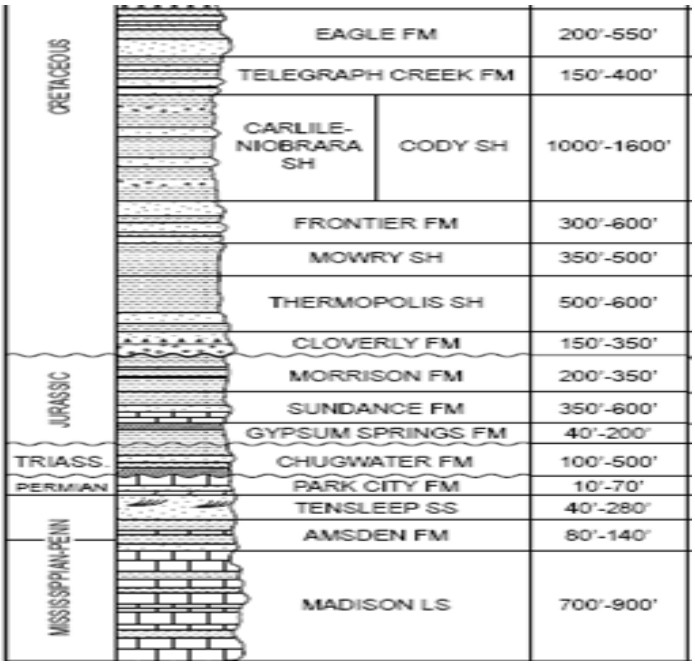

Figure 2-4: General stratigraphic column near Red Lodge, Montana, with regional thicknesses (Kauffman et al., 2008).

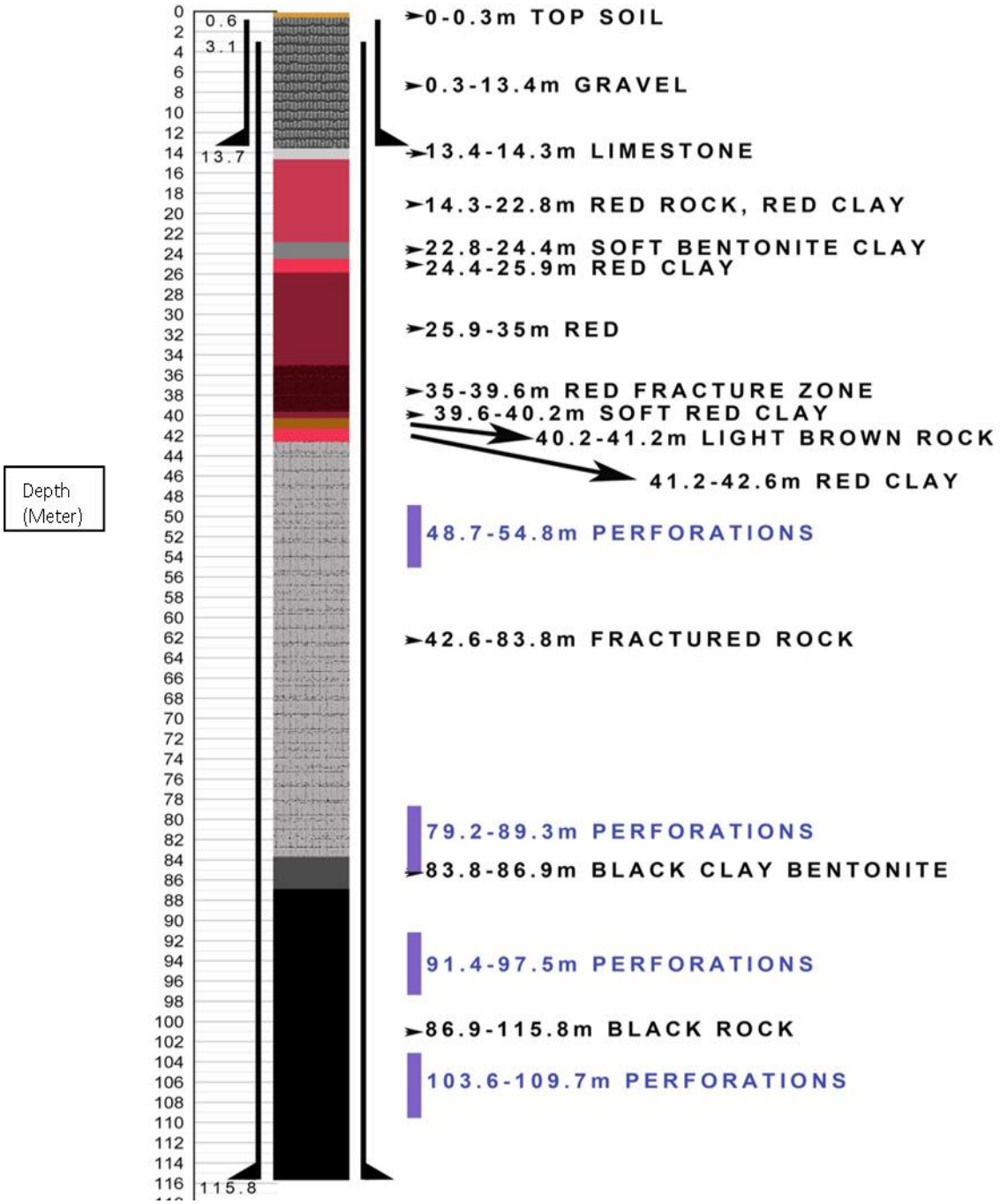

Figure 2-5: Lithology and casing program of the GB-1 well (from B H Drilling Comp. drilling report) (Appendix 2-1). Soft bentonite clay (22.8-24.4m) and soft red clay (39.6-40.2m) indicate the depth of water flow.

2.2 Acquisition equipment

The most important equipment we used in acquiring surface seismic and VSP data are the recording equipment from Geode and the Vibroseis truck. The Geode seismic recorder (from Geometrics Co.) receives the signal from the geophone then transfers it to the computer for recording (Fig. 2-6). One of the advantages of using the Geode was the convenient software provided for recording the seismic signal from geophones. A single Geode box is 8.0lb in weight, and has 24 channels for transmitting seismic signal from 24 geophones to a computer. The Vibroseis truck is a T15000 model from the Network for Earthquake Engineering Simulation laboratory (NEES) at the University of Texas at Austin. It was built by Industrial Vehicles International, INC, with a 6000lb hold-down weight. It can create strong and constant seismic signal, and is connected to the Geode. The truck sends seismic waves into the ground. The vibroseis truck has equipment to control the length and the range of frequency for each sweep. This vibroseis truck was used in the 2D seismic survey in this study. The 3D seismic survey and VSP used an accelerated weight drop (AWD) to create seismic signal. AWD has a 60lb hold-down weight. The field acquisition setup is schematically shown in Figure 2-7.

Figure 2-6: Left: Geode (24-channel seismic recording instrument); Right: Vibroseis truck from the NEES, facility in Austin, Tx.

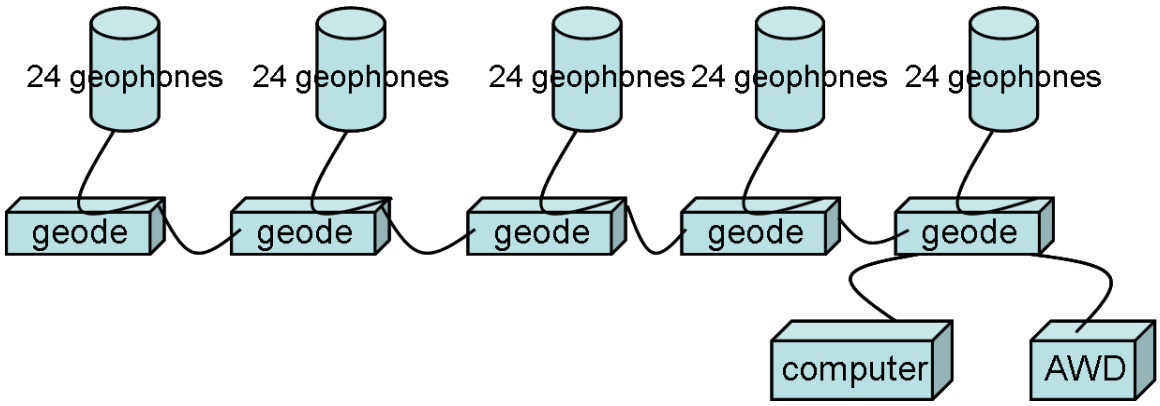

Figure 2-7: a) Schematic diagram of the 2D surface seismic acquisition.

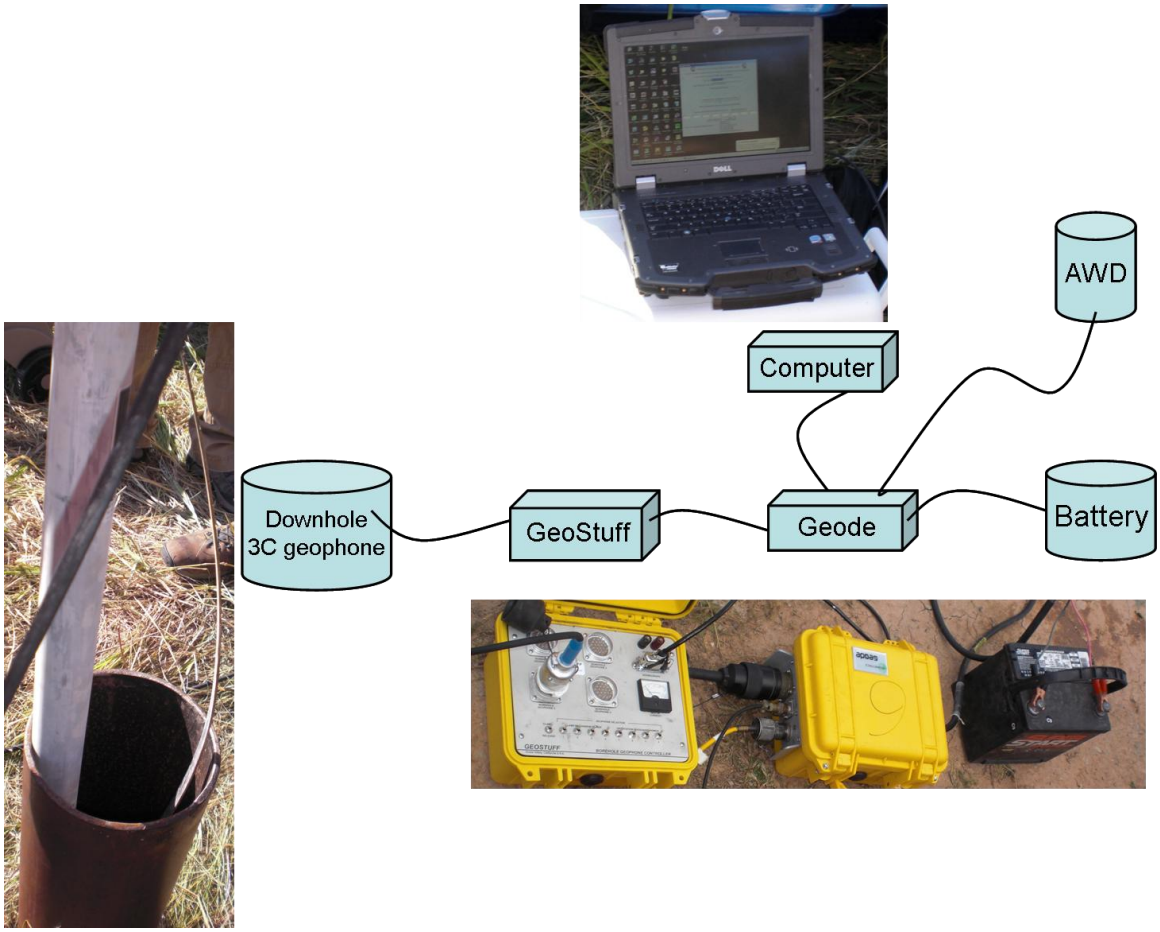

Figure 2-7: b) VSP acquisition equipment (GeoStuff is for operating the clamping of the downhole geophone and its depth).

2.3 Data available

2.3.1 Well logs

The suites of cased-hole geophysical logs (conductivity, gamma, temperature, full wave sonic) were acquired in the GB-1 well through the PVC casing. Gamma ray and resistivity logs delineated the shale/sandstone bedding. The character of the full-waveform sonic first arrival

times bore similarities to the gamma ray log. Different geophysical logs have the same fashion of change at the same depths, which are highlighted by red lines in Figure 2-8.

The metal casing down to 13m, the logs can be interpreted from this depth. The gamma ray, conductivity, resistivity indicate a boundary at 25m. The sonic log is increased from 1500m/s to 2500m/s at 25m depth as well.

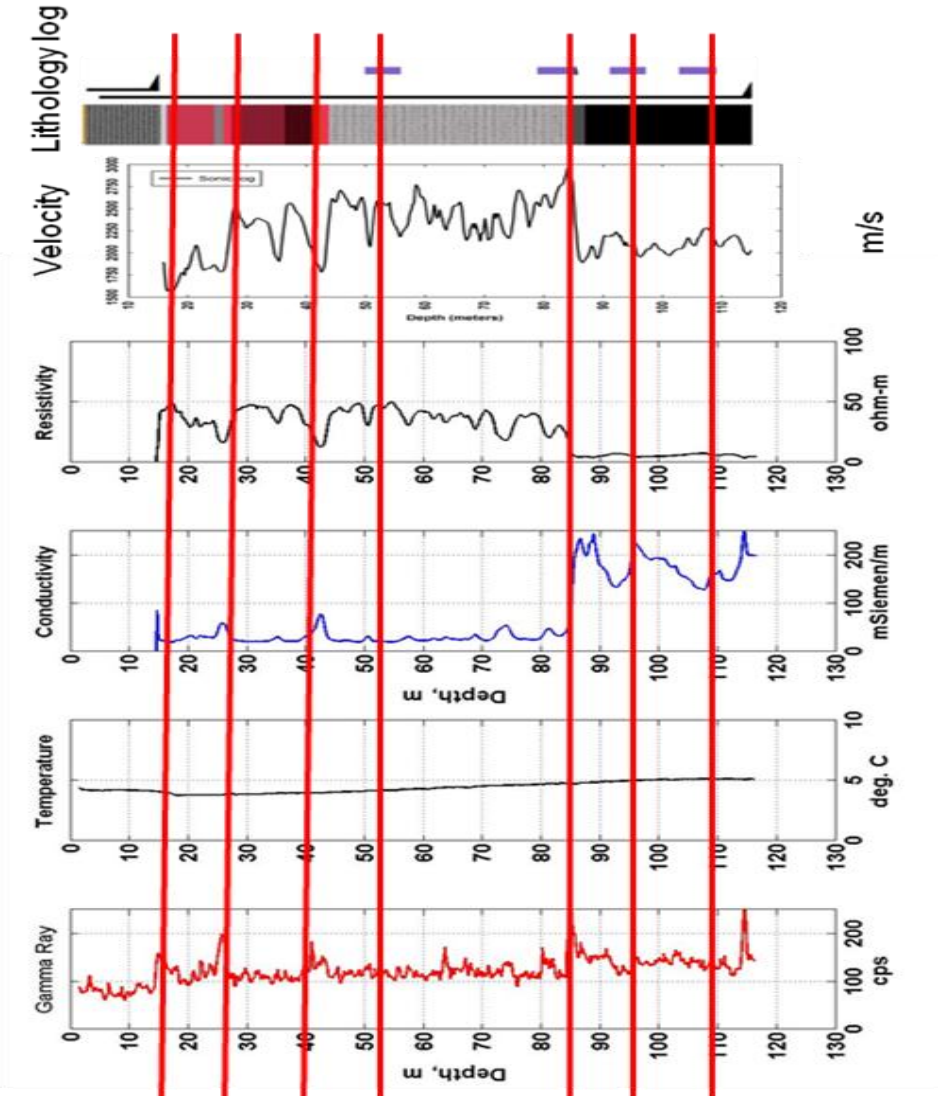

Figure 2-8: Geophysical logs from the GB-1 well as acquired in 2010.

2.3.2 2D seismic refraction analysis

The 2D seismic survey was designed for correlation with the VSP at the end of this study. A 352.5m total grid length (N50E) 2D seismic profile was acquired near the well GB-1. In total, it has 72 receivers at 5m spacing and shots at 5m spacing (Fig. 2-9). We did both AWD and vibroseis truck 2D seismic acquisition. In this study we will talk about vibroseis truck 2D seismic image. For 2D seismic there are three preliminary processing steps including: edit bad traces, edit geometry, and refraction statics. The signal length recorded was 600ms with 0.125ms sample rate (Fig. 2-10). The vibroseis truck sweep was 15-160Hz, with 2-fold source stack. The raw shot gather recorded signal in the frequency band from 15-100Hz (Fig. 2-11). Figure 2-12 shows the near surface three-layer velocity model. After refraction statics, it shows a layer at 25m depth in the near surface velocity model. The velocity is 800m/s in the weathering layer, replaced by the velocity of 1800m/s. From the brute stack result, there is an obvious reflection at the red fracture zone. The brute stack has 352.5m grid length with bin size of 2.5m (Fig. 2-13).

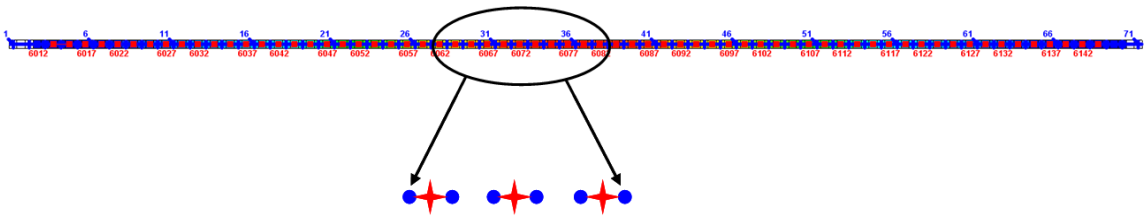

Figure 2-9: 2D seismic survey geometry, the red dots represent shot locations with 5m spacing; the blue dots represent receiver locations with 5m spacing, total 72 receivers.

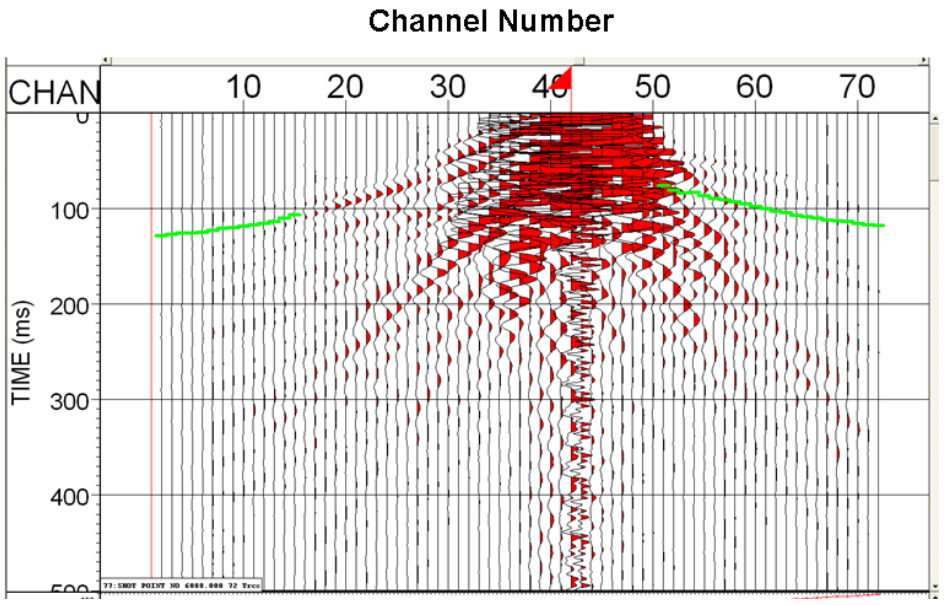

Figure 2-10: Typical shot record from the 2D seismic survey. The first break picks are shown by the blue line. Data is vibroseis, therefore the center of energy pulse have been picked.

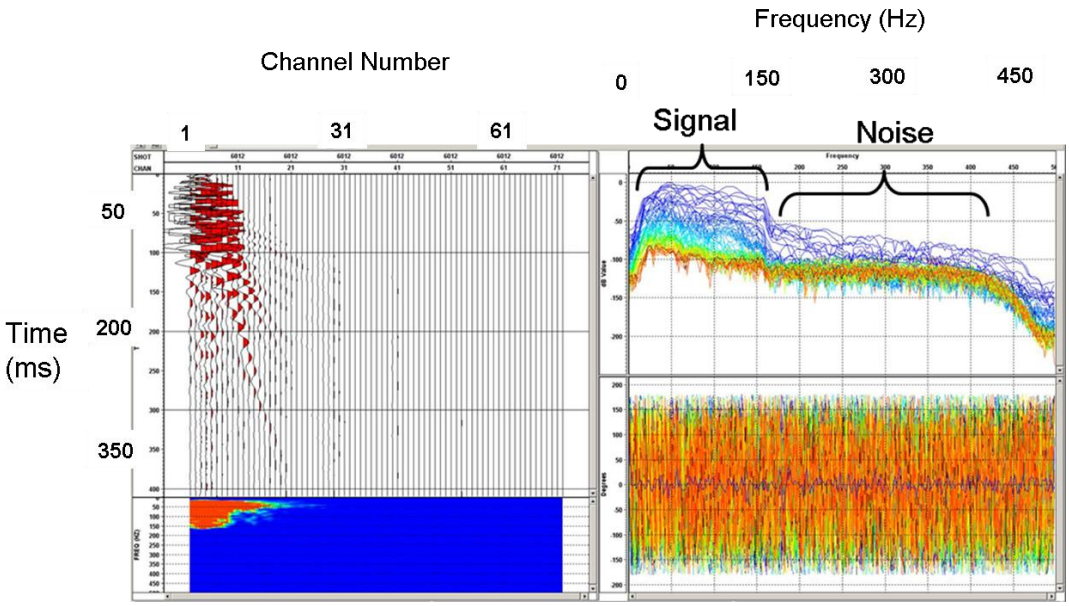

Figure 2-11: 2D seismic frequency, the frequency for each trace is shown by different colors in the figure on the right side (by Vibroseis truck). The signal band is 15-160Hz, which is the same as the Vibroseis sweep.

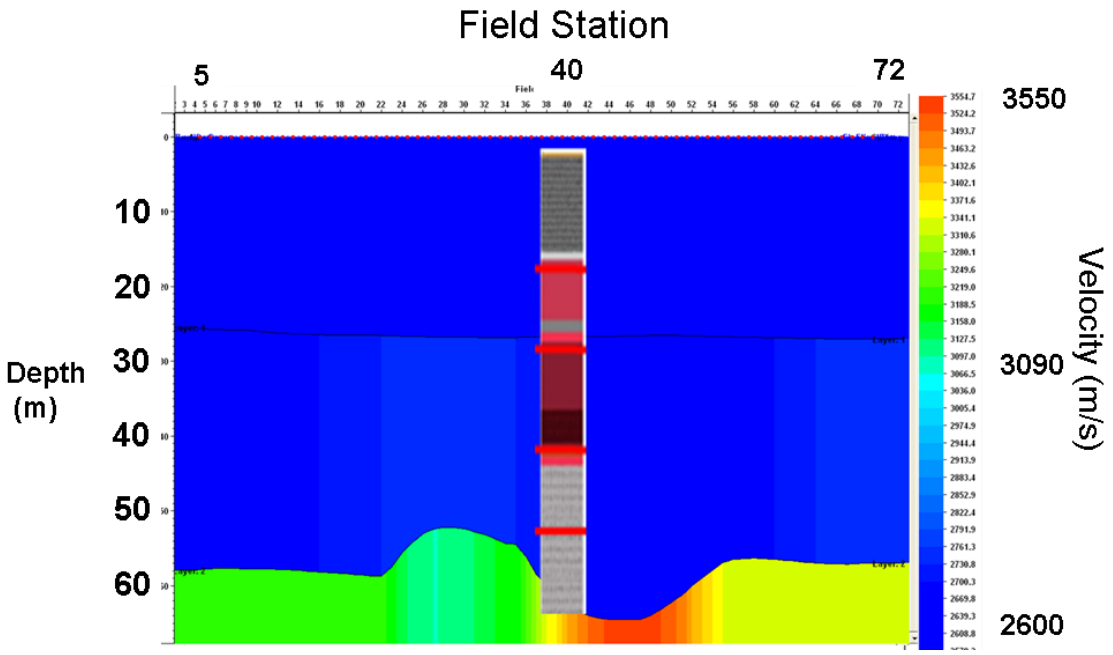

Figure 2-12: Near-surface P wave refraction velocity model from VISTA.

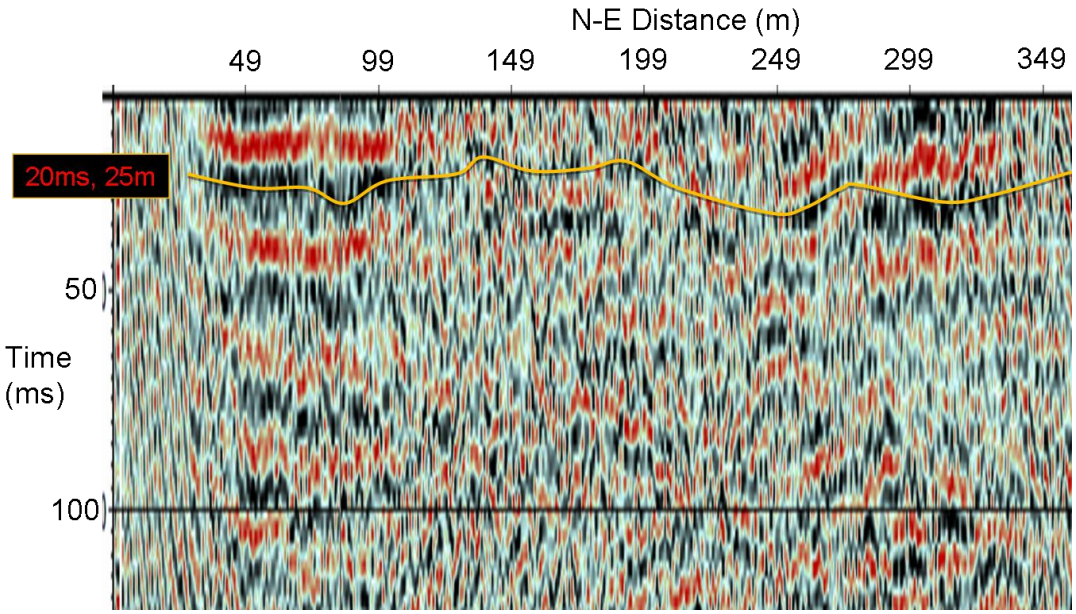

Figure 2-13: 2D seismic brute stack section with 352.5m total grid length (N50E). Data are stacked with constant velocity of 2500m/s. The reflection event at 20ms shows a layer at 25m depth (Pers. Comm. C. Montana, 2010).

2.3.3 3D seismic reflection analysis

To better understand the variation of shallow stratigraphy near the GB-1 well, we also conducted a 3D seismic reflection survey. The source was a 10lb sledgehammer with 5-fold source stack. The survey geometry is rectangular with 8 receiver lines (N50E) and 10 shot lines (N40W) (Fig. 2-14). In total, there were 152 receivers per line at 2m spacing and 9 shots per line at 6m spacing. The raw shot gather recorded signal in the frequency band from 0-14Hz. The signal length recorded was 1024ms with 1ms sample rate.

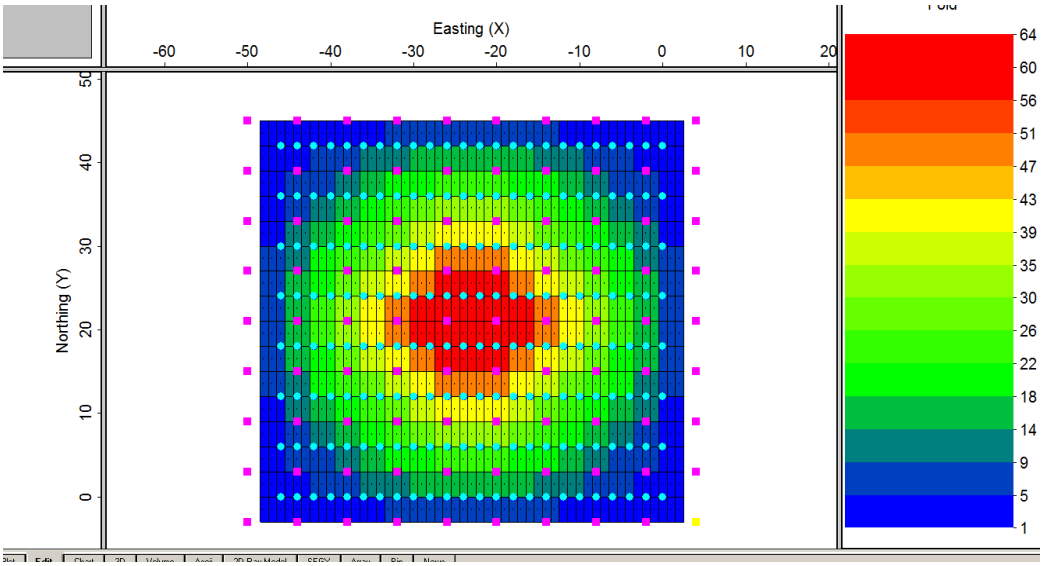

Figure 2-14: 3D seismic survey design using the OMNI program (Pers. Comm. C. Montana, 2010). 8 receiver lines shown by blue dots and 10 shot lines shown by pink dots, the background color shows the fold coverage in the survey.

2.3.4 VSP and acquisition geometry

At the 2010 Geophysical Field Camp, the University of Houston (with help from University of Calgary, GEDCO, and UT-Austin personnel) conducted a VSP in the 115m-deep, PVC-cased water well, GB-1, located on the glacial benches. VSPs were acquired by using an AWD and hammer as sources with a wall-clamping 3-component (3C) geophone and hydrophones as receivers (Fig. 2-15). The wall-clamping 3C geophone was placed at depths ranging from 4m to 114m with half-meter intervals. A hydrophone string covered the depths from 6m to 112m with half-meter intervals. The 3C geophone and hydrophone VSPs with hammer source and AWD source are compared on Figure 2-16. The one with the 3C geophone and the AWD source at 3m east offset, and another one with the hydrophone and the AWD source at 6.7m north offset were selected to process get the final corridor stack in this study. Despite low signal-to-noise ratios characterized by the hammer source walk-away VSP data, it was still processed to get a reasonable AVO curve. The wall-clamping geophone with the AWD source gave data with good signal-to-noise ratios, but the hydrophone results appear unstable, due to the strong effect of tube waves. Automatic gain control (AGC) was applied for display, which takes the root-mean-squared amplitude in a 500ms window to compensate for attenuation. The quality comparison of VSPs by source and receiver types is:

1. From the source type, the AWD has a more constant energy than the sledgehammer. The sledgehammer source VSP has weaker signal and lower signal-to-noise ratio.

2. From the receiver type, the hydrophone shows a strong effect from tube waves, which is the wave that travels through the water along the GB-1 well. The wall-clamping geophone shows more constant signal.

Figure 2-17 shows a section of the walkaway VSPs acquired with the hydrophone array (the western offsets in the survey basemap). The hydrophones are on a down-hole receiver string at 4m interval, placed from 16m to 108m. The frequency of AWD/hydrophone VSP is analyzed shows in figure 2-18. To remove the tube waves from the AWD/hydrophone VSP, a velocity filter (narrow-band f-k reject filter) has been applied to separate the tube waves from the downgoing and upgoing wavefield (Fig. 2-19) Basically, a polygon is drawn around the region of tube wavefield to be rejected in the frequency domain, and then it is transferred back to the time domain. According to Snell's law, refractions occur past the 57m offset, the maximum offset is 72m in this walk-away VSP (Appendix 2-2).

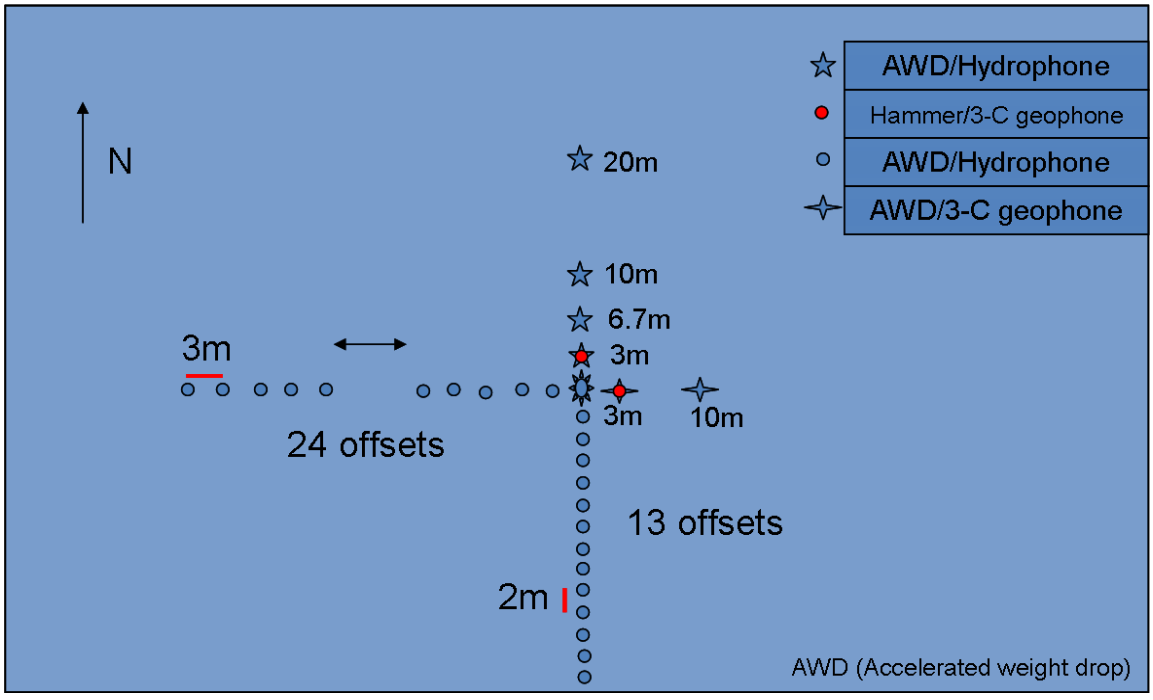

Figure 2-15: Base map of the GB-1 well VSP surveys.

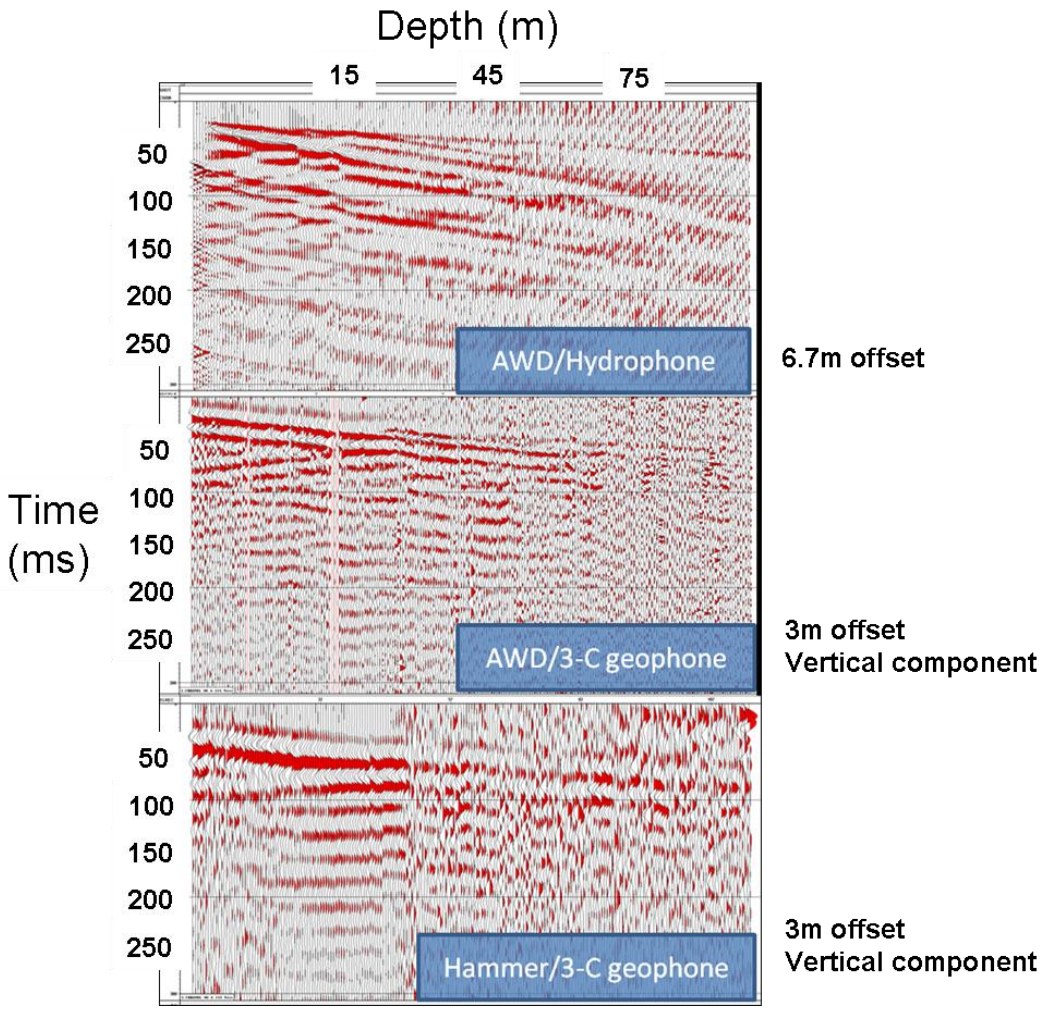

Figure 2-16: AWD/Hydrophone VSP, using a shot point 6.7m north of the GB-1 well; AWD/3-C geophone VSP, using a shot point 3m east of the GB-1 well; Hammer/3-C geophone VSP, using a shot point 3m north of the GB-1 well.

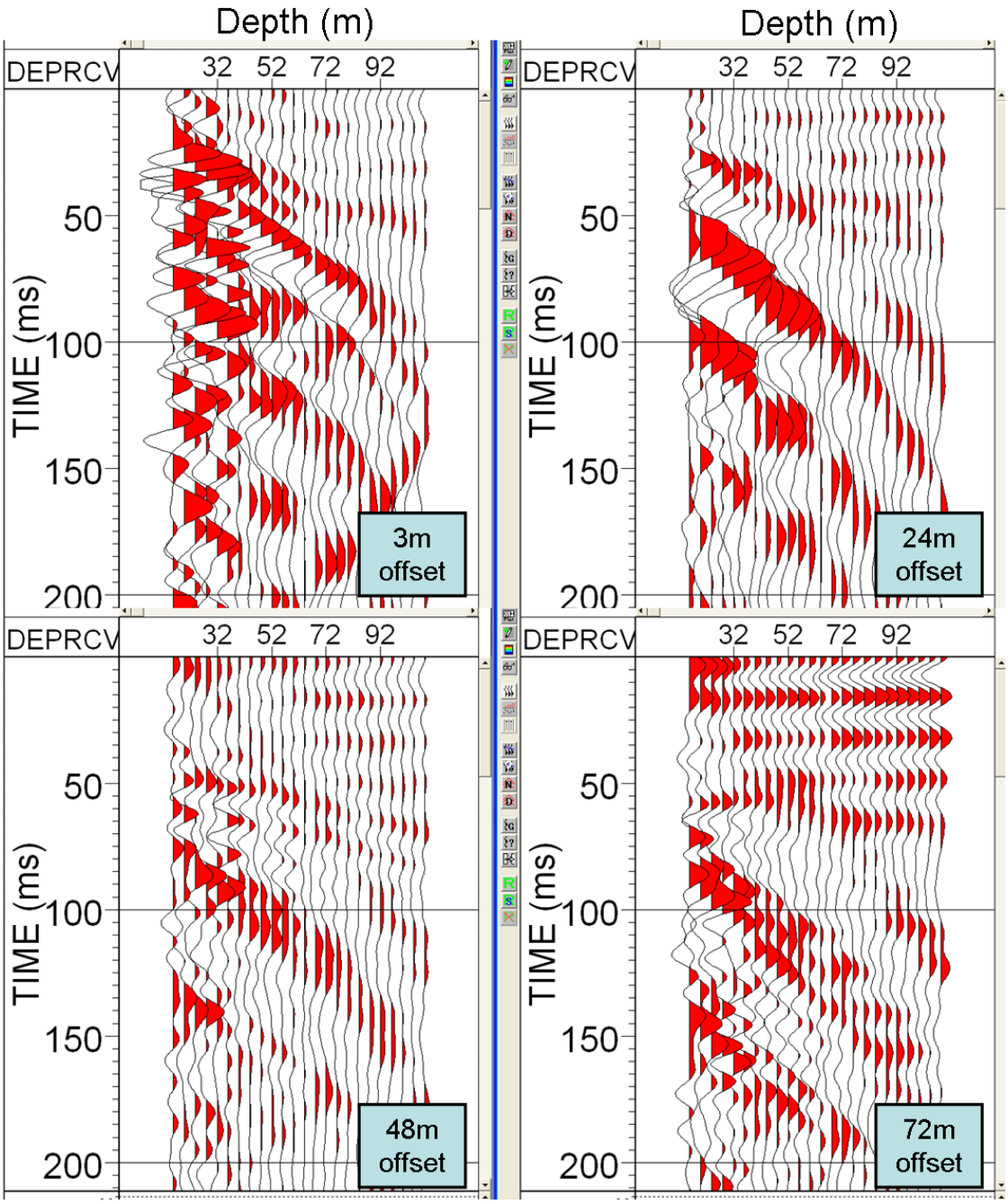

Figure 2-17: AWD/Hydrophone walk-away VSP with 3m offset shot interval west of the GB-1 well, the farthest offset up to 72m, the hydrophone receivers placed from 16m to 108m with 4m interval, displayed with Ormsby filter (5-15-80-100 Hz) and 60Hz notch filter for the power line noise.

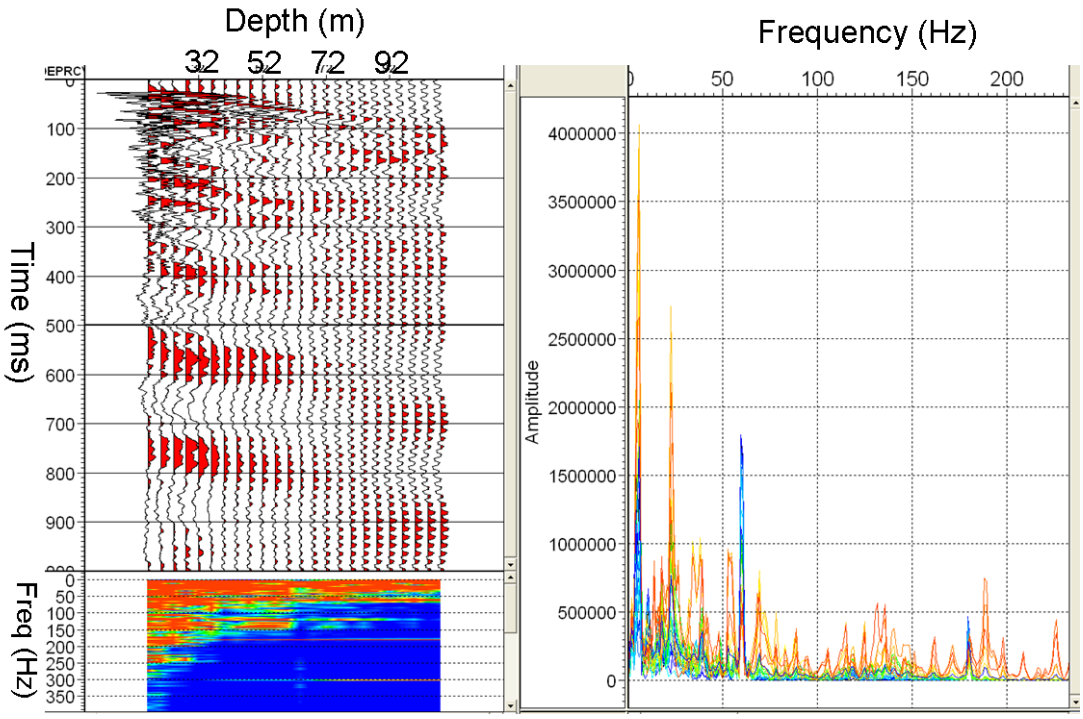

Figure 2-18: Frequency analysis shows the dominant frequency is 55Hz, a 5-15-80-100Hz Ormsby filter designed for displaying AWD/Hydrophone VSP. The nearby power line causes a 60Hz noise.

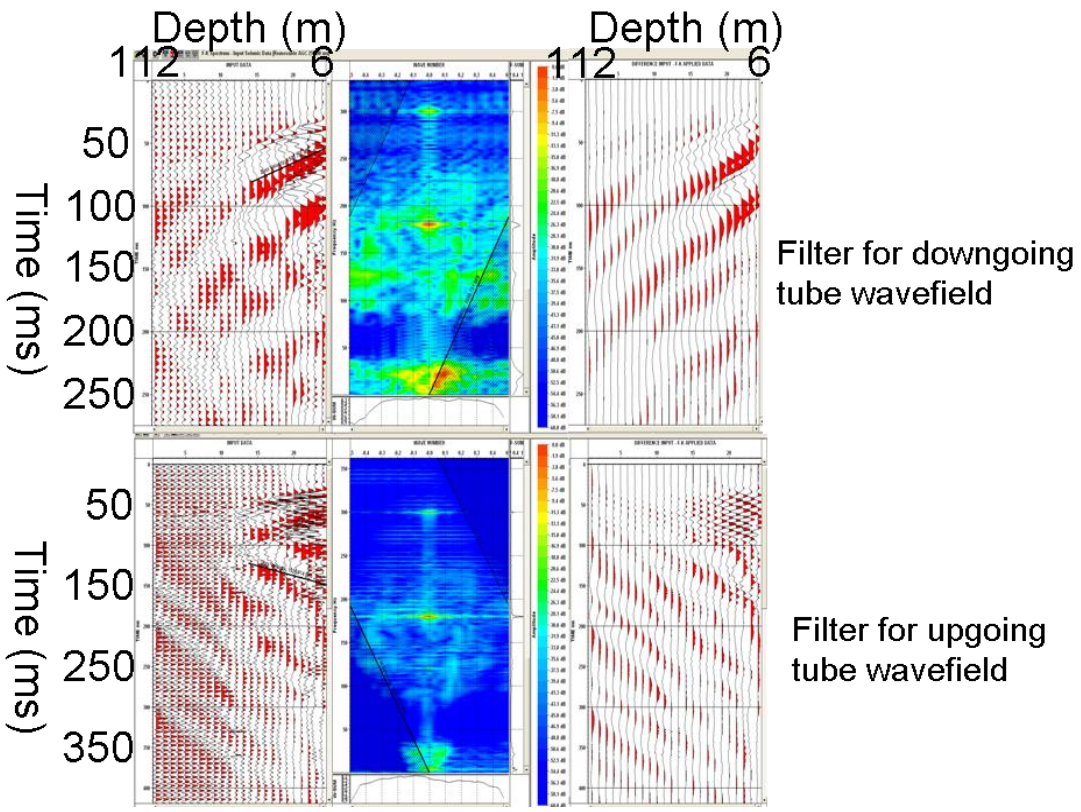

Figure 2-19: a) Velocity filter design for removing the downgoing and upgoing tube wavefield.

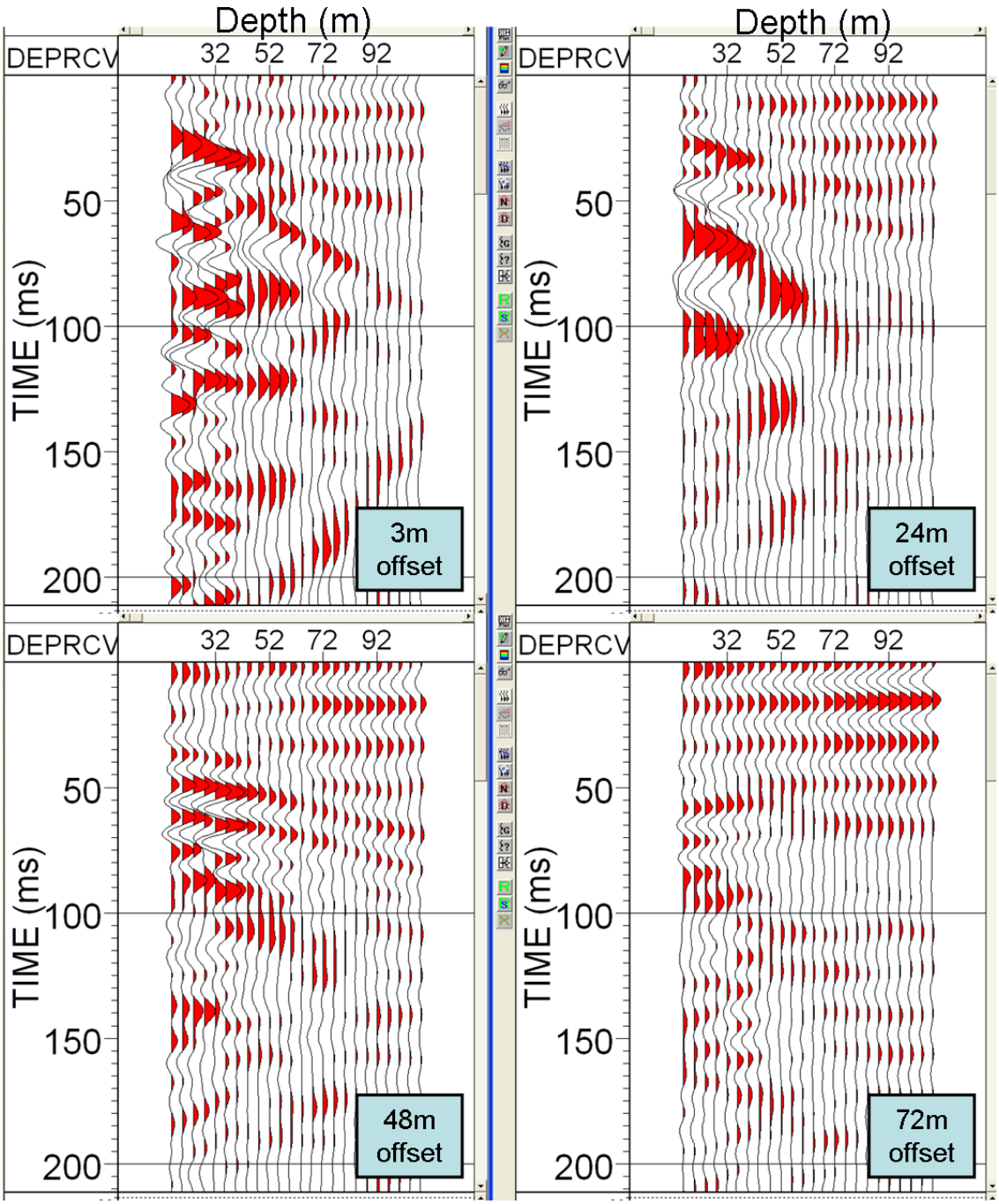

b) AWD/Hydrophone walk-away VSP with 3m offset shot interval west of the GB-1 well, after moving the upgoing and downgoing tube wavefield, displayed with Ormsby filter and 60Hz notch filter.

2.4 Forward modeling and synthetic VSP

A forward model was constructed to simulate the VSP data (Fig. 2-20). Based on the 2D seismic refraction near surface velocity model, and understanding of local geology, a four layer geologic model is built. The initial two-dimensional (2D) finite difference model is 200m wide and 200m deep. The P wave velocity was picked from the sonic log, the S wave velocity was calculated using G. Nottis' equation (Nottis, 2010),

$$Vs = 626.38*D^{.2239},$$

where D is depth in ft, and Vs is in ft/s. In the forward model calculation, depth is the average of each layer, 8m, 30m, and 100m used in this calculation. Density was calculated using Uyanik's equation (Uyanik, 2010),

$$ñ = 16 + 0.002Vp,$$

for weathering layer at 800m/s, density =1.79 g/cc,

for 1800m/s layer, density =2.0 g/cc,

where ñ is in KN/m^3 ($102*KN/m^3=kg/m^3$), and Vp is in m/s. G. Nottis' equation has been employed because it's an empirical equation using glacial deposit data (Appendix 2-3). To simulate the field acquisition, there are 221 receiver positions at 0.5m interval from 4-114m in the GB-1 well. The synthetic VSP parameters are the same as the field VSP, which is 0.001s sample rate with 2s record time. A 100Hz Ricker wavelet has been chosen to generate the synthetic VSP data. After each synthetic model run, it is revised to more closely fit the field VSP data. This iterative process is repeated until the synthetic geologic model produces similar VSP data compared to the field VSP data (Fig. 2-21).

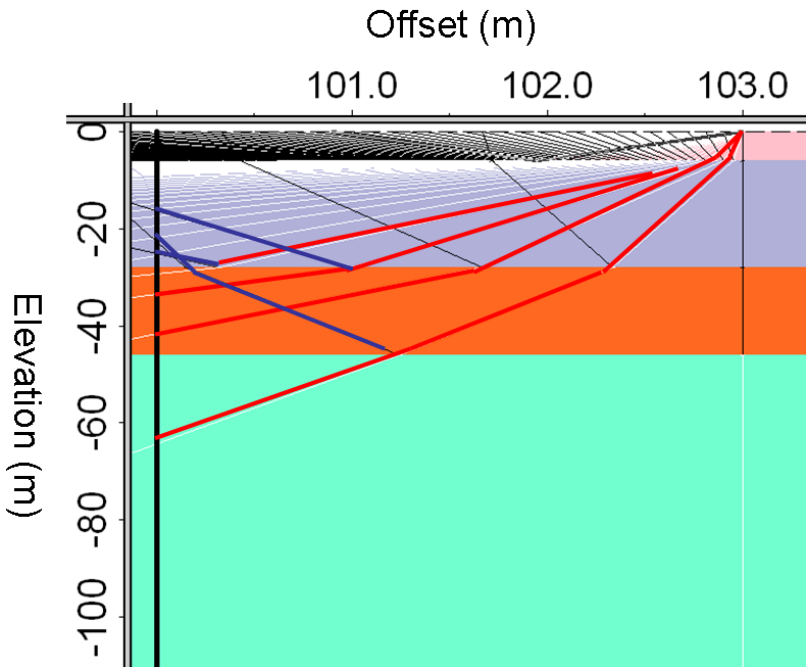

Figure 2-20: The 2D forward model with ray tracing, the primary upgoing wave is highlighted in red lines. The three layer P-wave velocities from top to bottom are 635m/s, 1500m/s, and 3000m/s.

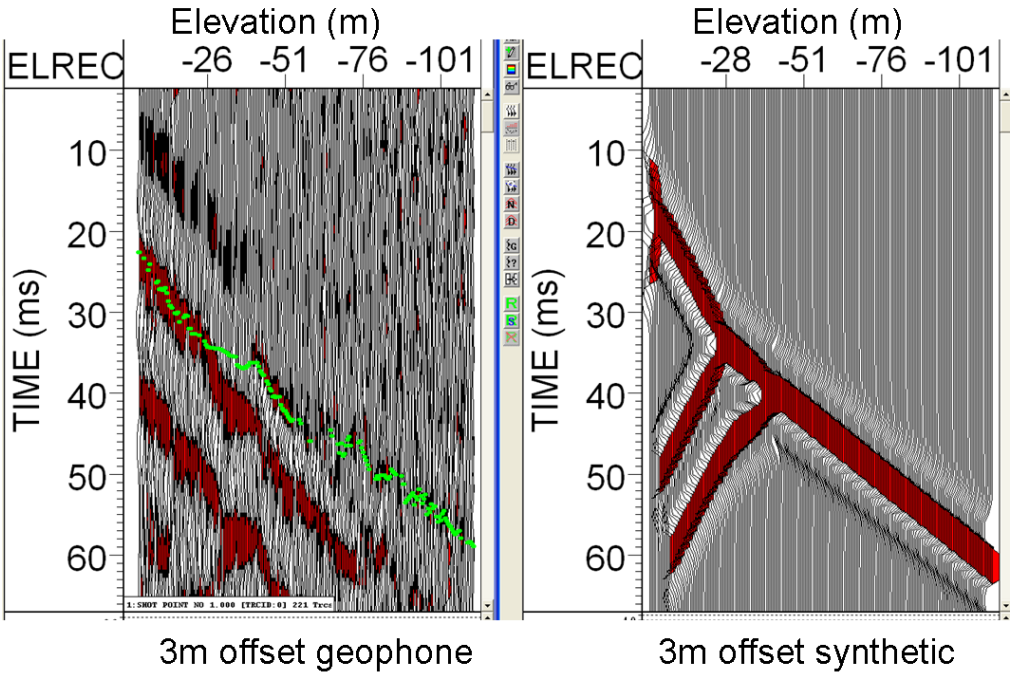

Figure 2-21: Left: Field geophone/AWD VSP vertical component with 3m east offset; Right: Synthetic VSP at 3m offset.

2.5 Hydrophone walk-away VSP tube wave removal

2.5.1 Walk-away VSP shot gathers

The walk-away VSP shot gathers were sorted based on Trace ID code (primary sort) and Depth of the receiver (secondary sort). There are 13 different offsets from 3.2m-27.2m (2m interval) in this walk-away VSP shot south of the GB-1 well. Figure 2-22 shows the data from 0-200ms, displayed with 30-60-150-300Hz Ormsby filter and 500ms automatic gain control (AGC). Similar to the west offset walk-away VSP, the south offset walk-away VSP shows strong effects from tube waves, and the tube wave has similar velocity as the formation. Unlike section 1.3.4 in this study, the fragmented frequency in this VSP results in a lot of random noise when the velocity filter is applied. Instead of a velocity filter, a median filter has been applied to remove the downgoing and upgoing tube waves.

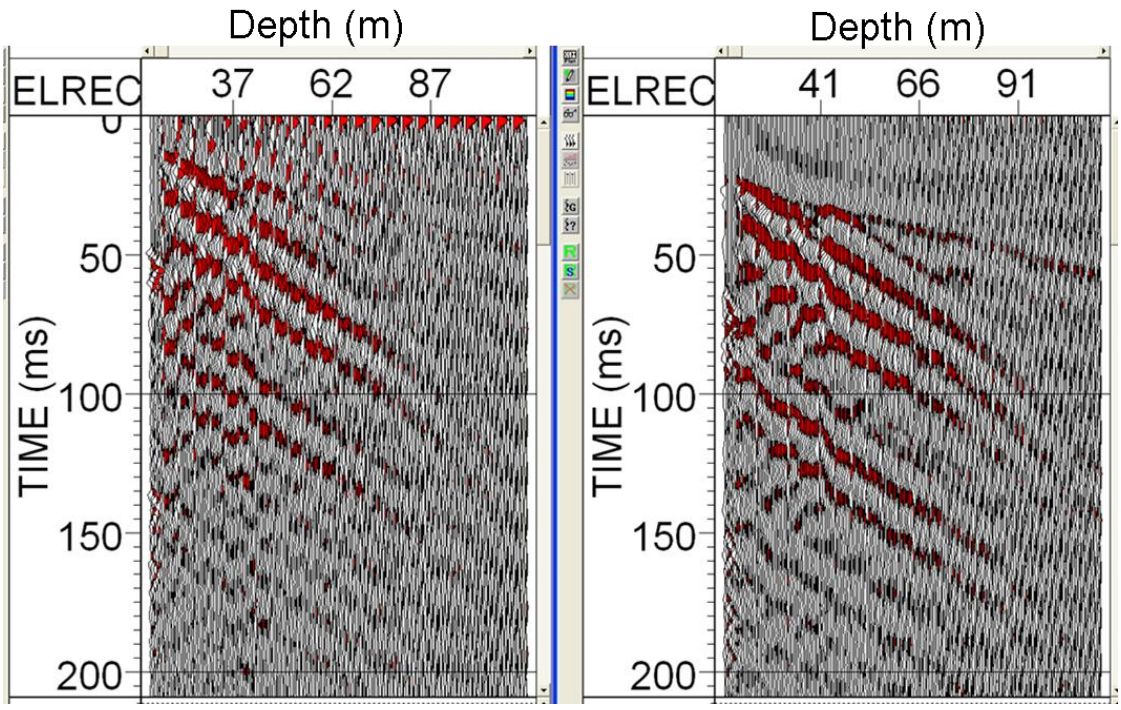

Figure 2-22: a) Left: 3.2m south offset; Right: 5.2m south offset.

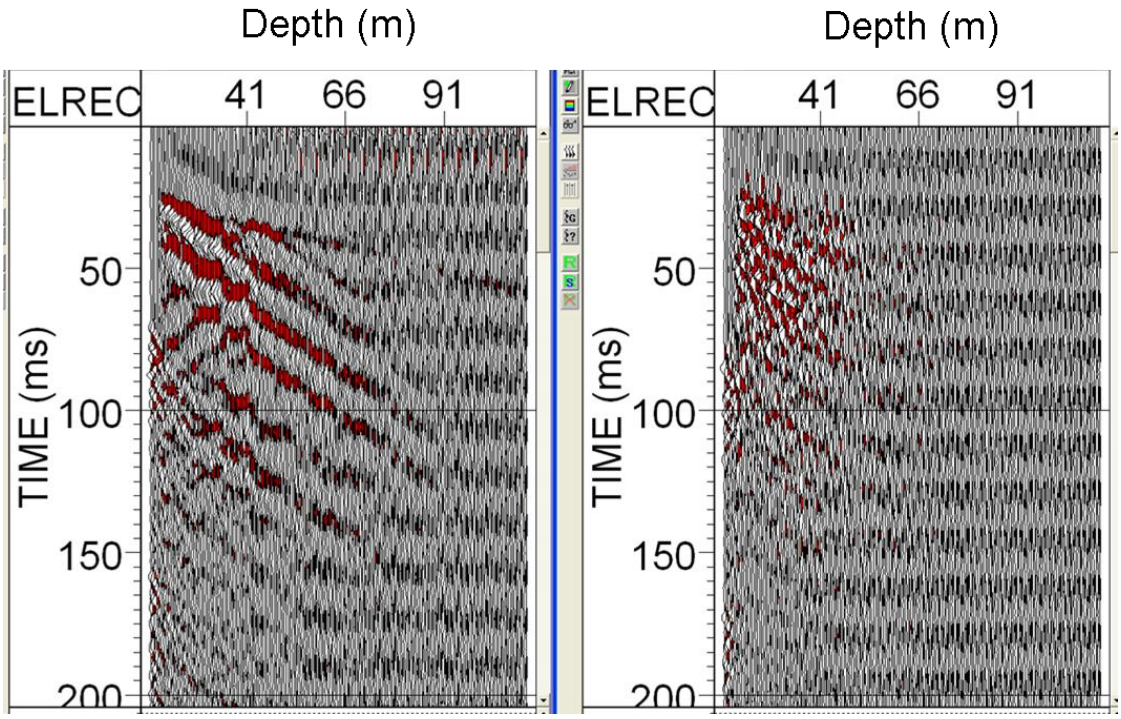

b) Left: 7.2m south offset; Right: 9.2m south offset.

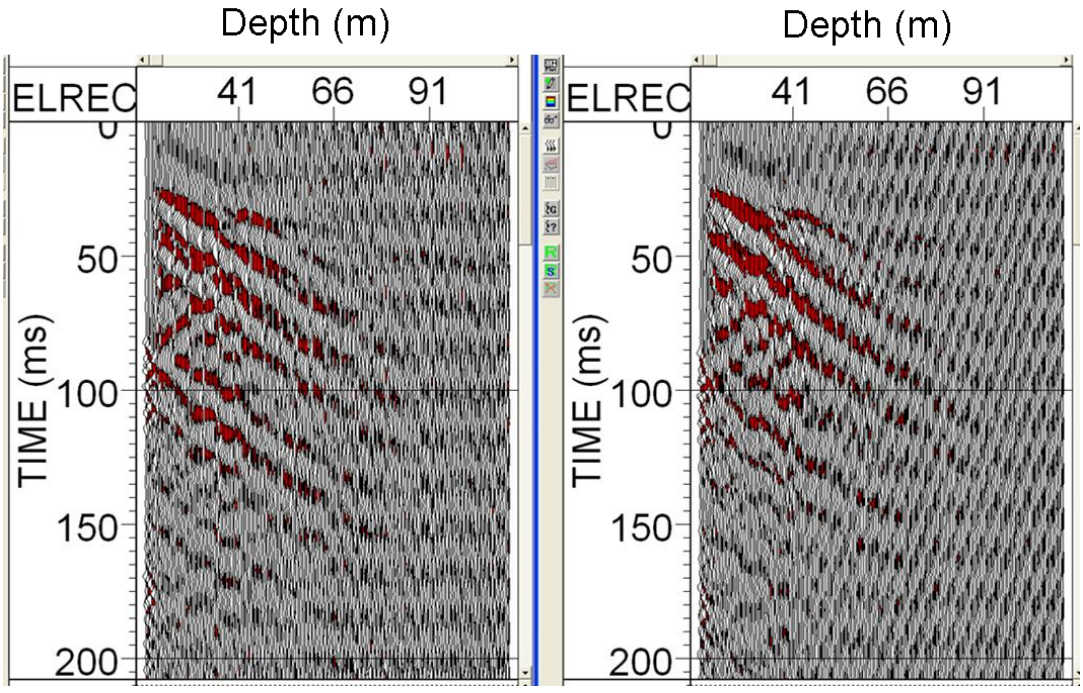

c) Left: 11.2m south offset; Right: 13.2m south offset.

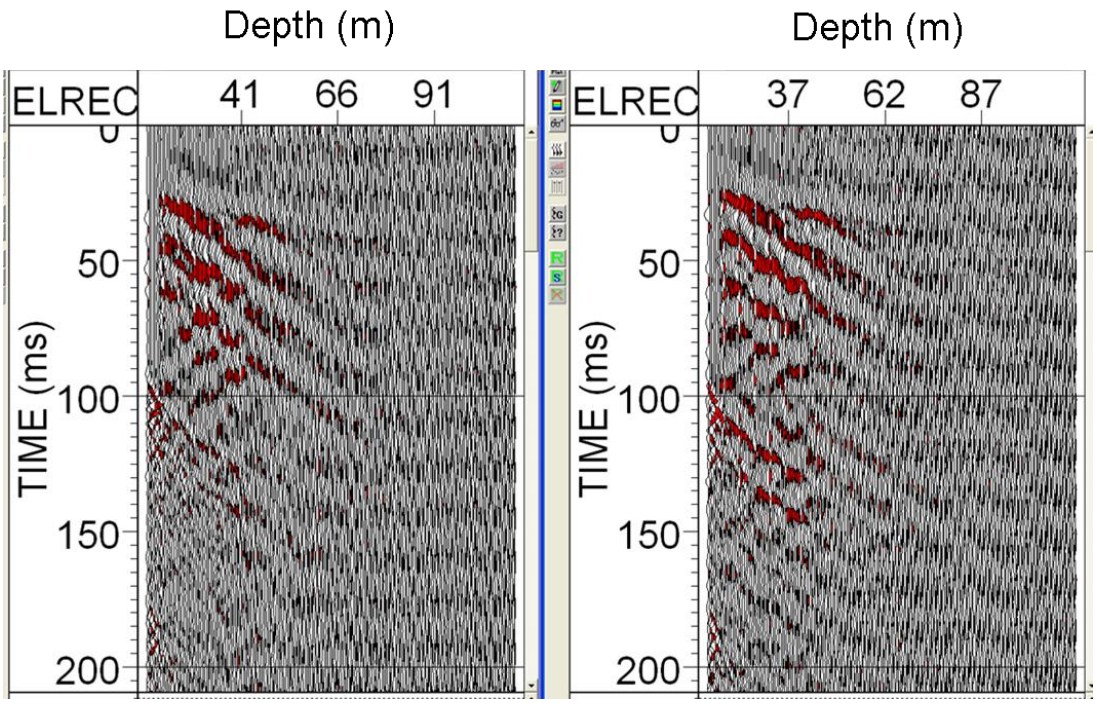

d) Left: 15.2m south offset; Right: 17.2m south offset.

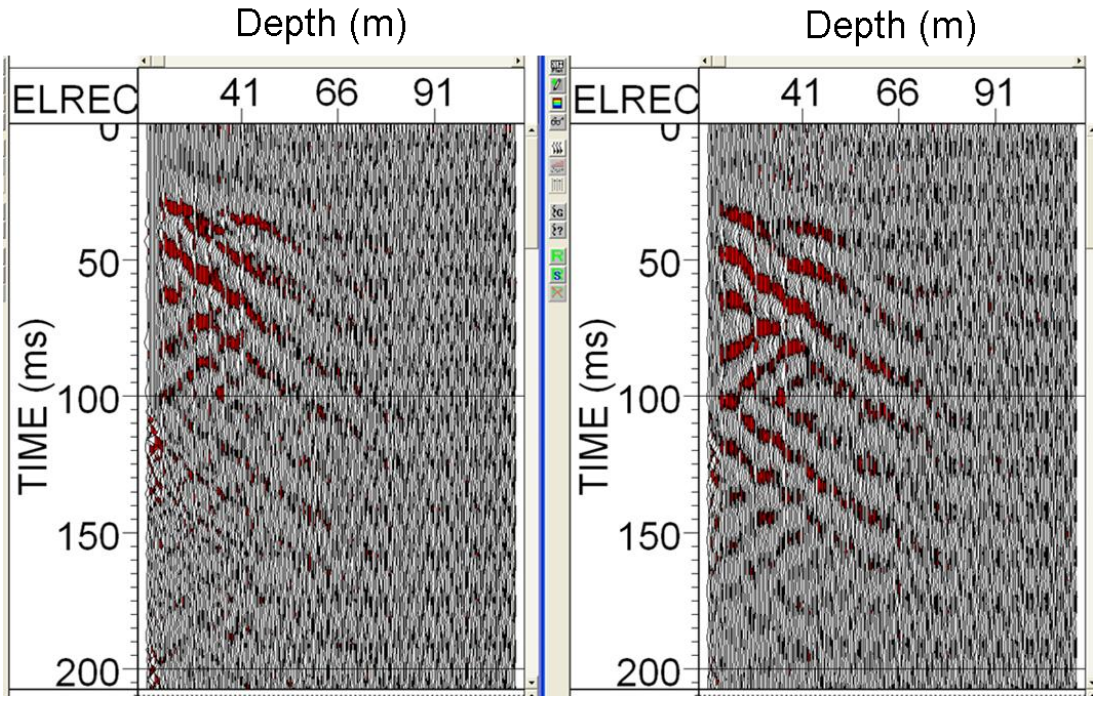

e) Left: 19.2m south offset; Right: 21.2m south offset.

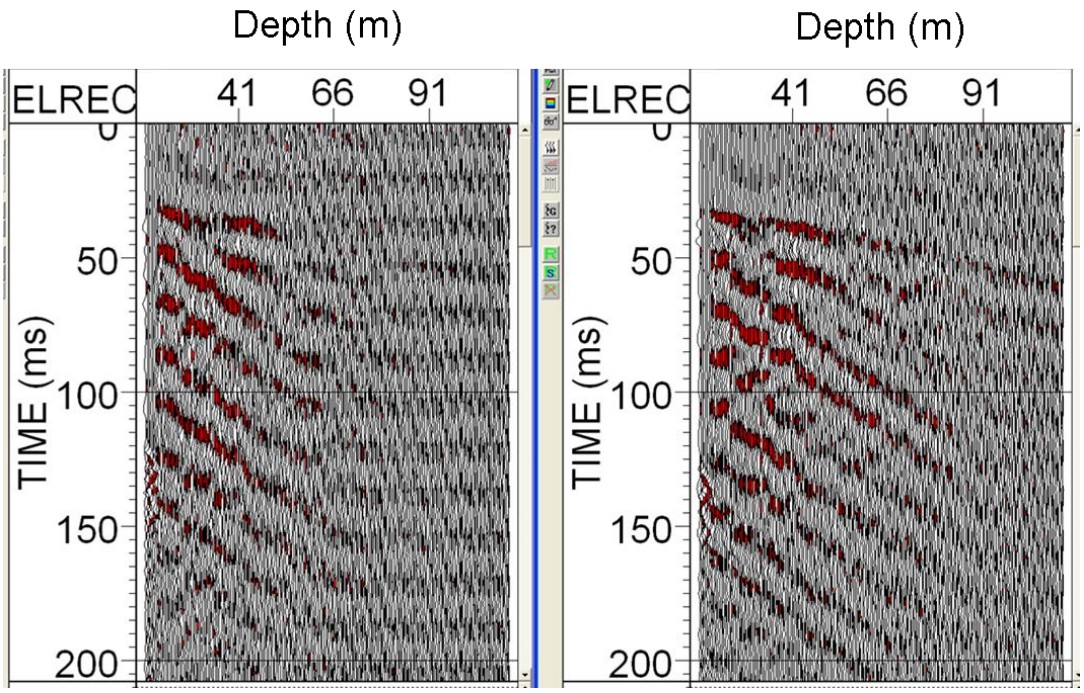

f) Left: 23.2m south offset; Right: 25.2m south offset.

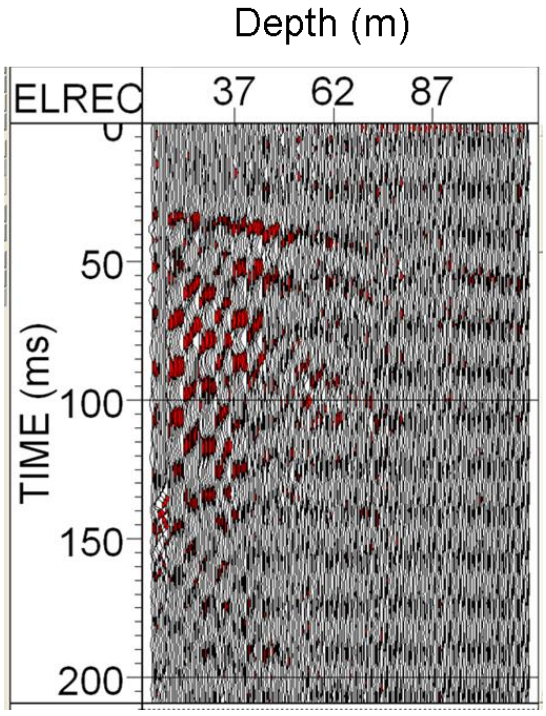

g) 27.2m south offset.

2.5.2 Median filter for tube waves

Tube wave are trapped in the borehole, and propagate through the liquid (Fig. 2-23). High-amplitude upgoing and downgoing tube waves were identified in the hydrophone recordings, but no high-amplitude tube waves were observed in the 3C geophone recordings.

The steps for removing the tube waves by median filter are:

1. First break picked on downgoing tube wave, aligned on 300ms to be subtracted by the median filter (Fig. 2-24).

2. First break picked on upgoing tube wave, aligned on 300ms to be subtracted by the median filter (Fig. 2-25).

The parameters for first break picking are, 60ms search window, and 15ms sliding window (equal to the length of wavelet). The first breaks were picked manually for better accuracy and then interpolated to make sure every trace has a first break time value in the header. Then the data was edited into the corrected VSP geometry for shot location and receiver depth in order to calculate velocity. The parameter for the median filter is 13-trace window length. The comparison of before and after removing the tube waves is shown in Figure 2-26.

From the primary downgoing tube wave first break picks, the velocity changes at around 90m depth. From the lithology log, there are perforations at that depth, so the wave energy is trapped in the well causing the tube wave velocity change.

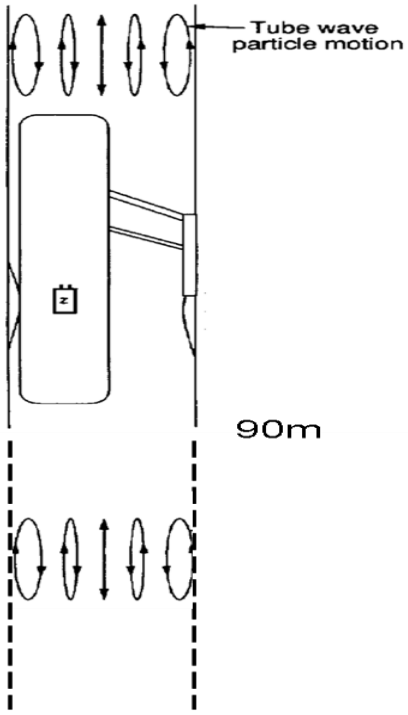

Figure 2-23: Illustration of tube wave propagation, the perforation zone is shown by the dashed line (adapted from Kramer, 1991).

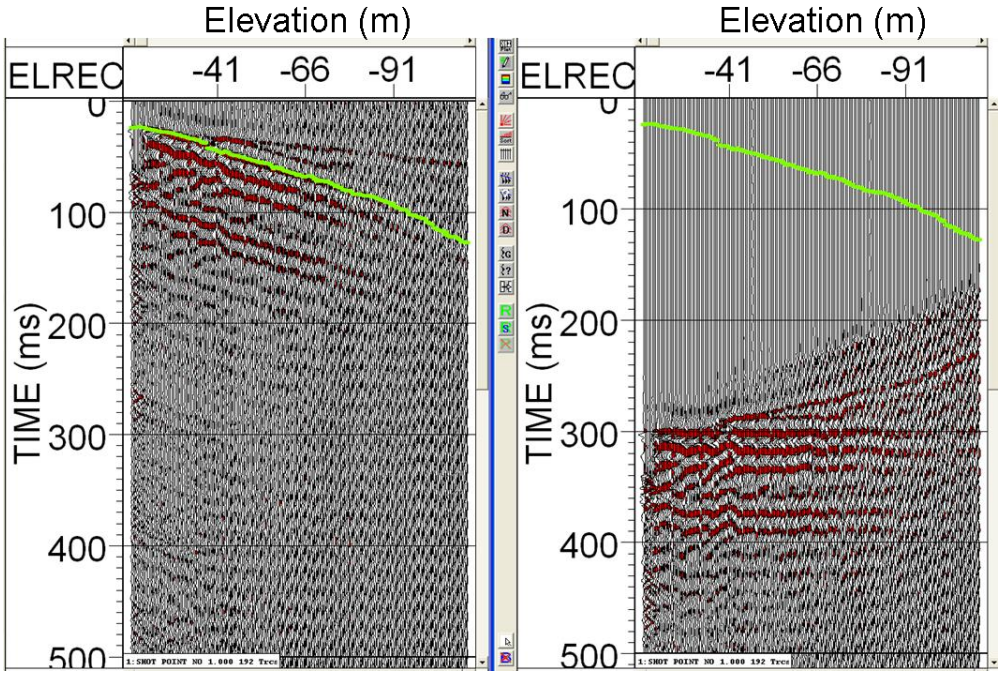

Figure 2-24: a) Left: 5.2m south offset with primary downgoing tube wave highlighted by the green line. Right: The downgoing tube wavefield flattened at 300ms, displayed with Ormsby filter and AGC).

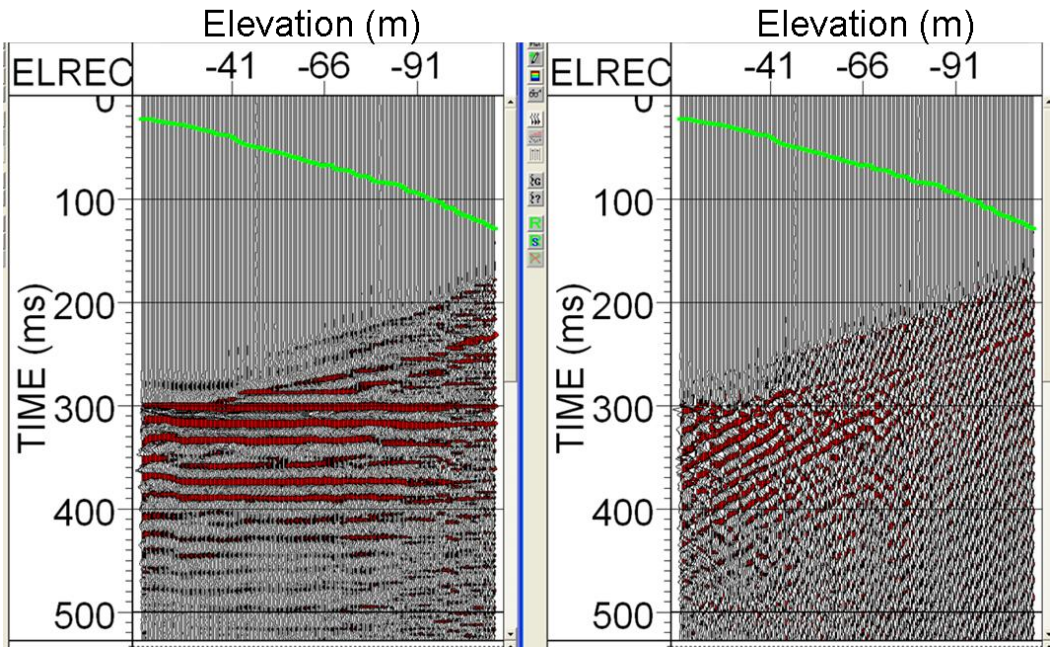

Figure 2-24: b) Left: Enhanced downgoing tube wavefield flattened at 300ms. Right: The wave field after subtracting the enhanced downgoing tube wavefield (displayed with Ormsby filter and AGC).

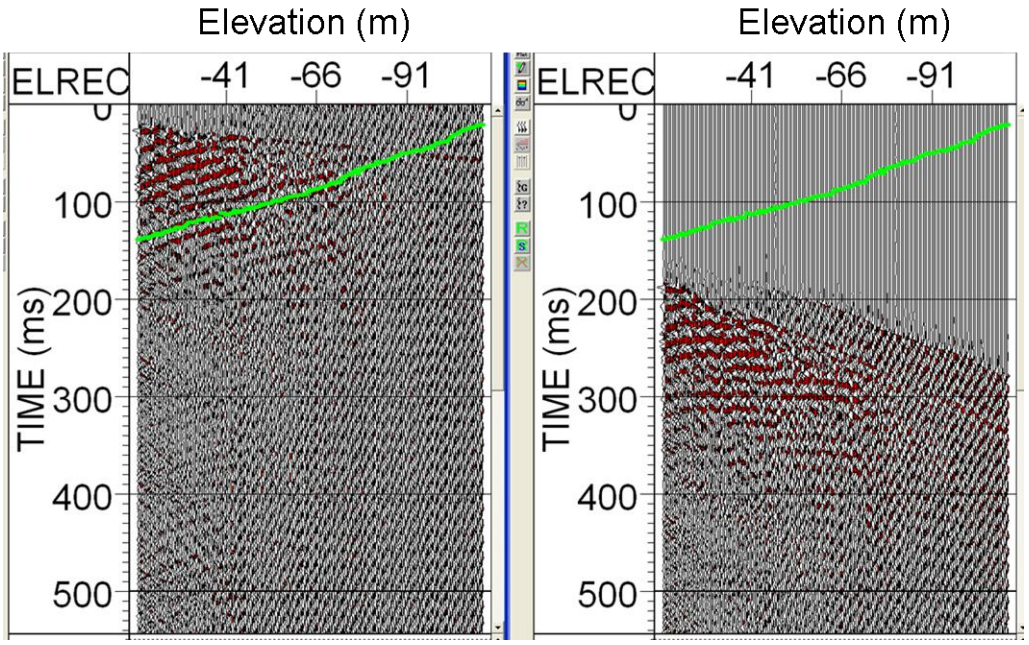

Figure 2-25: a) Left: Primary upgoing tube wave highlighted by the green line (FRT). Right: Flattened at 300ms (displayed with Ormsby filter and AGC).

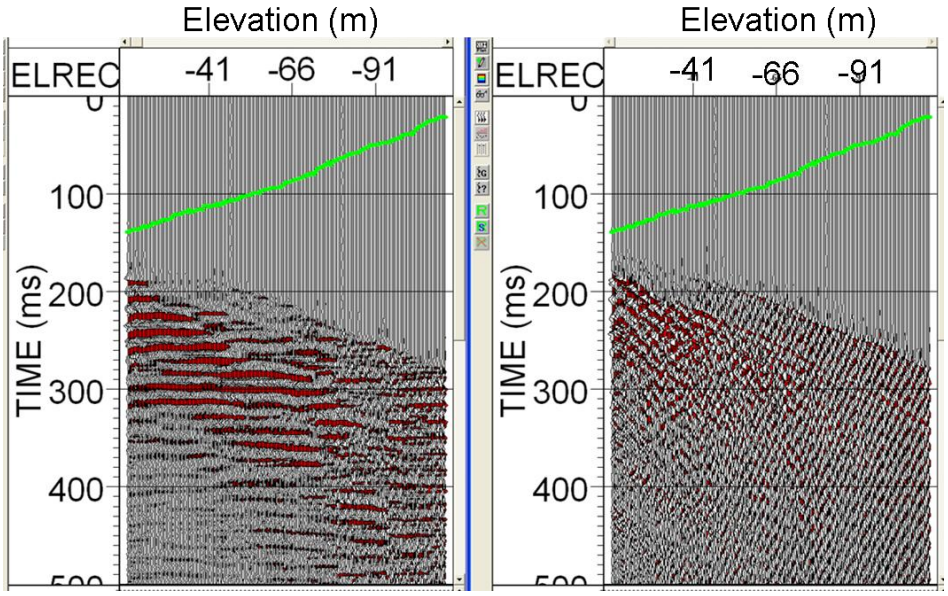

Figure 2-25: b) Left: Enhanced upgoing tube wavefield flattened at 300ms. Right: The wave field after subtracting the enhanced upgoing tube wavefield (displayed with Ormsby filter and AGC).

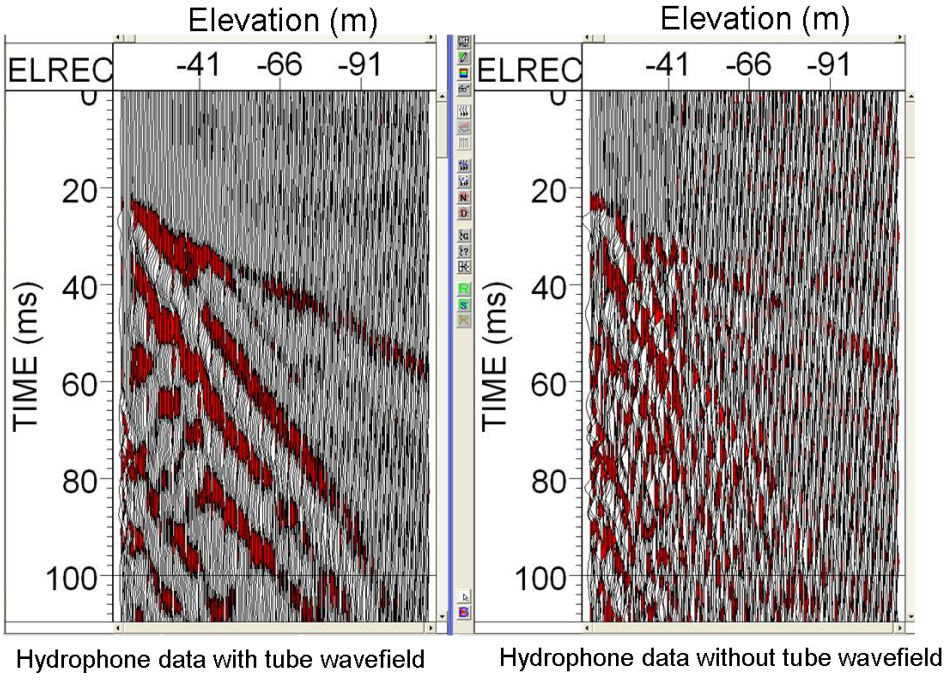

Figure 2-26: Left: hydrophone data before removing the tube wavefield. Right: After removing the tube wavefield, displayed with Ormsbyfilter (20-40-150-300 Hz) and AGC (500ms length window).

2.6 Hydrophone VSP signal processing

The VISTA seismic processing package was employed for analyzing and processing the VSP data. The 5.2m south offset hydrophone/AWD VSP with half-meter receiver interval and 0.5ms sampling rate is processed in this section. The hydrophone receiver contains only pressure component. The frequency analysis shows the dominant frequency of the data is 80Hz (Fig. 2-27). The VSP was performed close to a power line, so to get better signal to noise ratio, a 60Hz notch filter was applied. A 500ms AGC was applied to the hydrophone VSP for display in the following processing steps.

2.6.1 Acquisition geometry and first break picking

An essential step in VSP processing is the geometry input. This was done by sorting the data according to Channel Number (primary sort) and Depth of Receiver (secondary sort) to create proper trace headers. The first break picked on the peak of primary downoing wave. The interval velocity is calculated by dividing the straight-line distance from two nearby receivers by the picked first arrival time difference (Fig. 2-28).

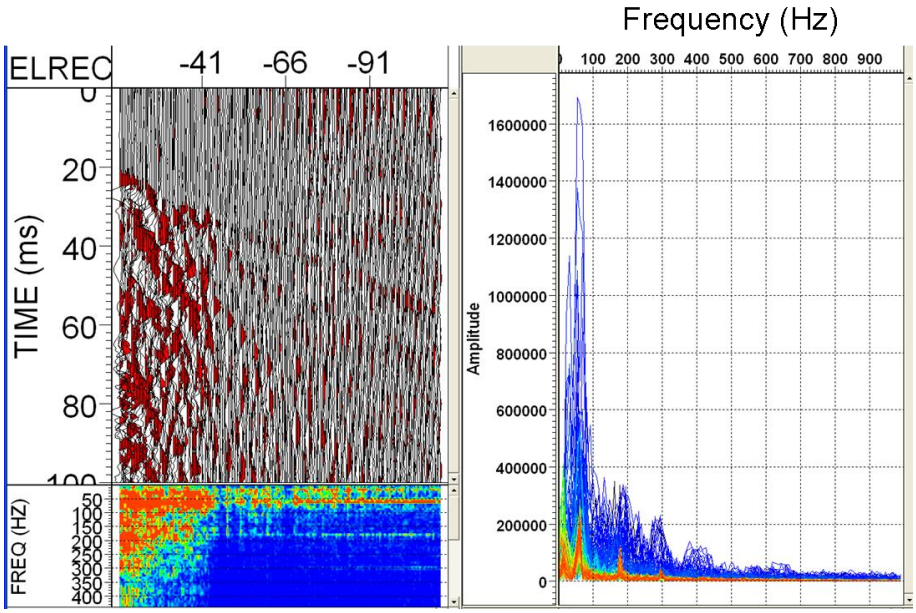

Figure 2-27: Hydrophone VSP after removing the tube wavefield frequency analysis.

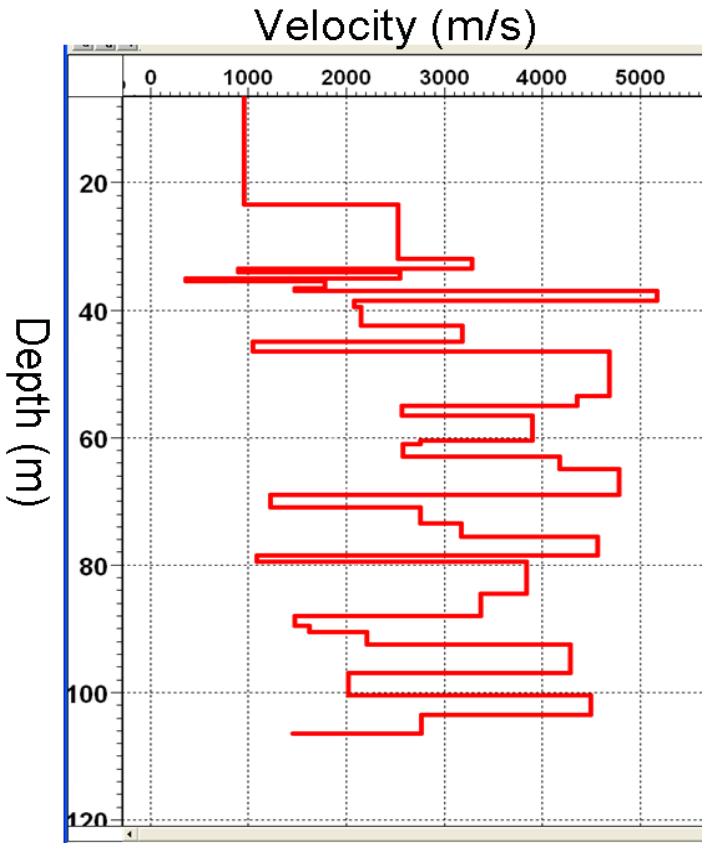

Figure 2-28: Interval velocity calculated from the first arrival time of primary downgoing P wave.

2.6.2 Wavefield separation using median filter

The next major processing step was to separate the downgoing from the total wavefield to get the upgoing wavefield. Median filtering was chosen to separate the wavefields. The total wavefield was flattened to a 100ms datum by subtracting the first break times from each trace (Hinds, 1996). Muting was then applied to the 100ms datum. We tested different lengths of 9, 11, 13, 17, and 21 points in the median filter. The traces of a selected window were organized by ascending amplitude, and the middle value of the sequence was picked as the filtered value (Stewart, 1985). After repeating many times, the median filter can separate the flattened downgoing wave from the total wavefield, obtaining the upgoing wavefield. To get wavefield separation, a 13-point median filter was applied to the flattened downgoing wavefield to get the upgoing wavefield (Fig. 2-29, 2-30).

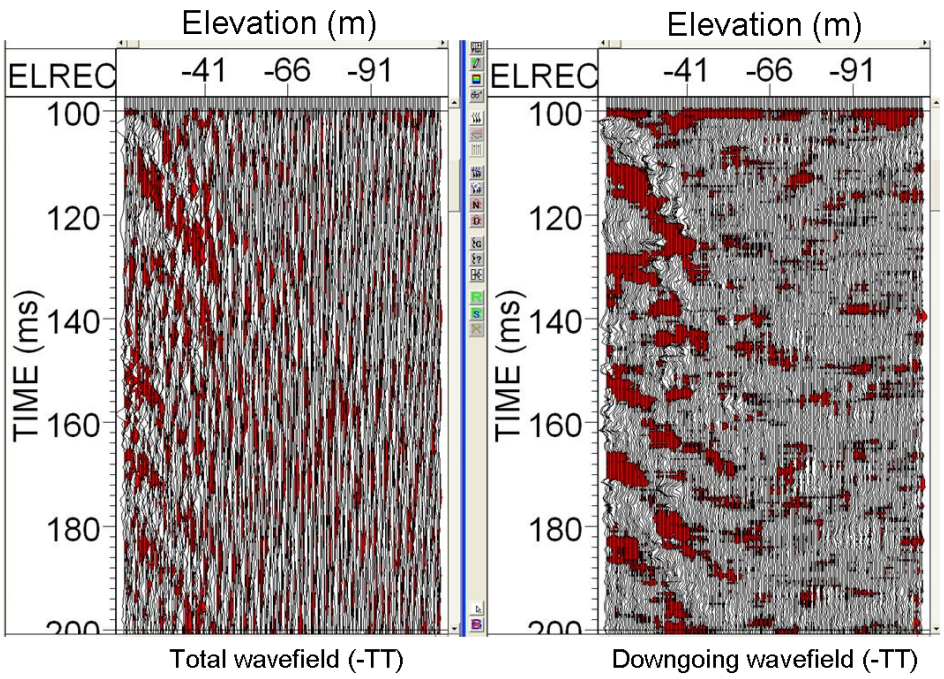

Figure 2-29: Wave field separation, both displayed with AGC (500ms length window).

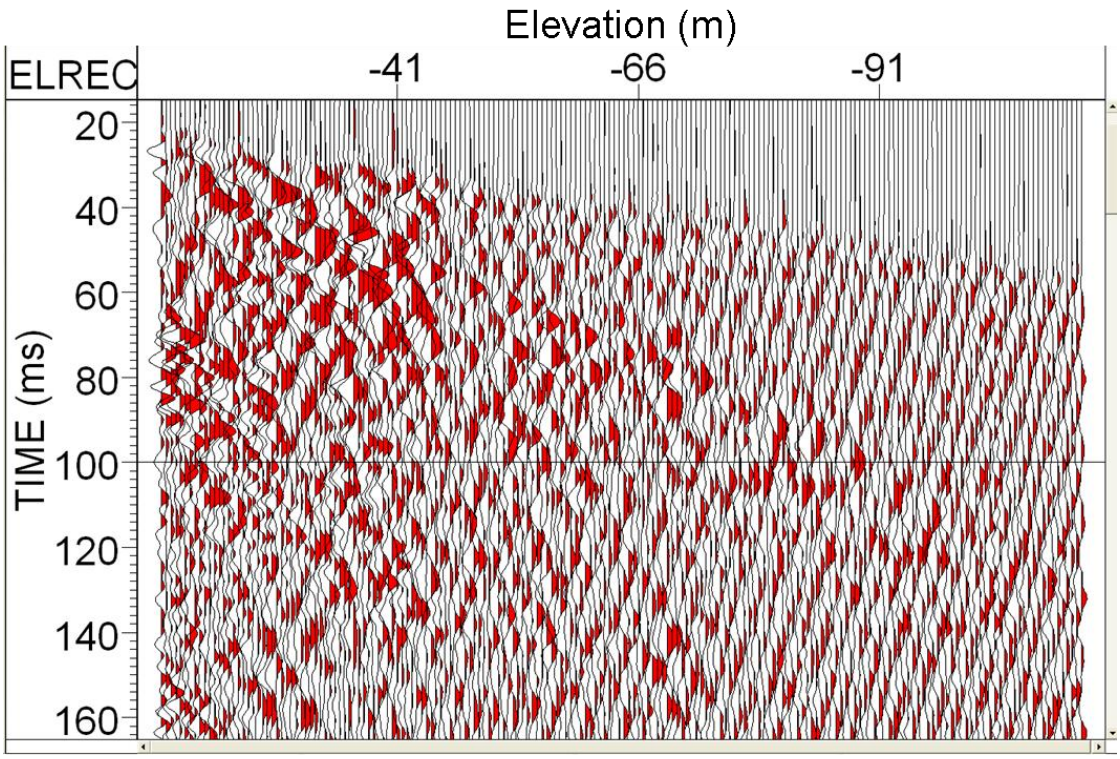

Figure 2-30: Upgoing wavefield (FRT), displayed with Ormsby filter (20-40-150-300 Hz) and AGC (500ms length window).

2.6.3 Deconvolution

The next step was to deconvolve the data using the downgoing direct wavefield to estimate the source signature. First, a deconvolution operator with optimized parameters was generated using the flattened downgoing traces. The deconvolution window started at 0ms and extended to 50ms. This wide window was chosen because the data was found to not contain significant multiples within it. The deconvolution operator designed using the downgoing wavefield was then applied to the upgoing wavefield to get an estimated reflectivity series. After deconvolution, both upgoing and downgoing events appear to be sharper and better defined. (Fig. 2-31).

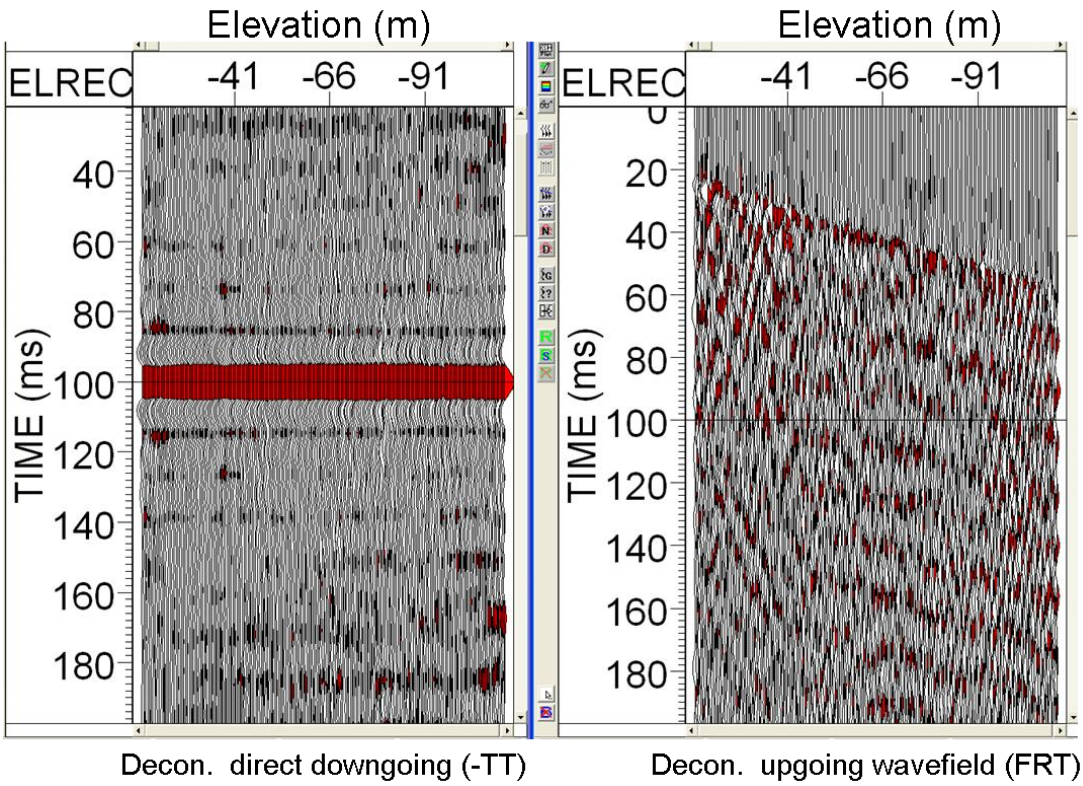

Figure 2-31: Right: Deconvolution of direct downgoing wavefield (-TT), displayed with Ormsby filter (20-40-150-300 Hz) and AGC (500ms window length); Left: Deconvolution of upgoing wavefield (FRT).

2.6.4 Corridor stack

The upgoing wavefield was converted into Two-Way Time (TWT) by adding the first break time to every flattened trace twice. This step produced the final estimate for the reflection coefficient series. In this case, the signal is more continues inside of the corridor. The inside 20ms corridor stack to get the final reflection series, the final reflection series was used in the final L-plot interpretation (Fig. 2-32).

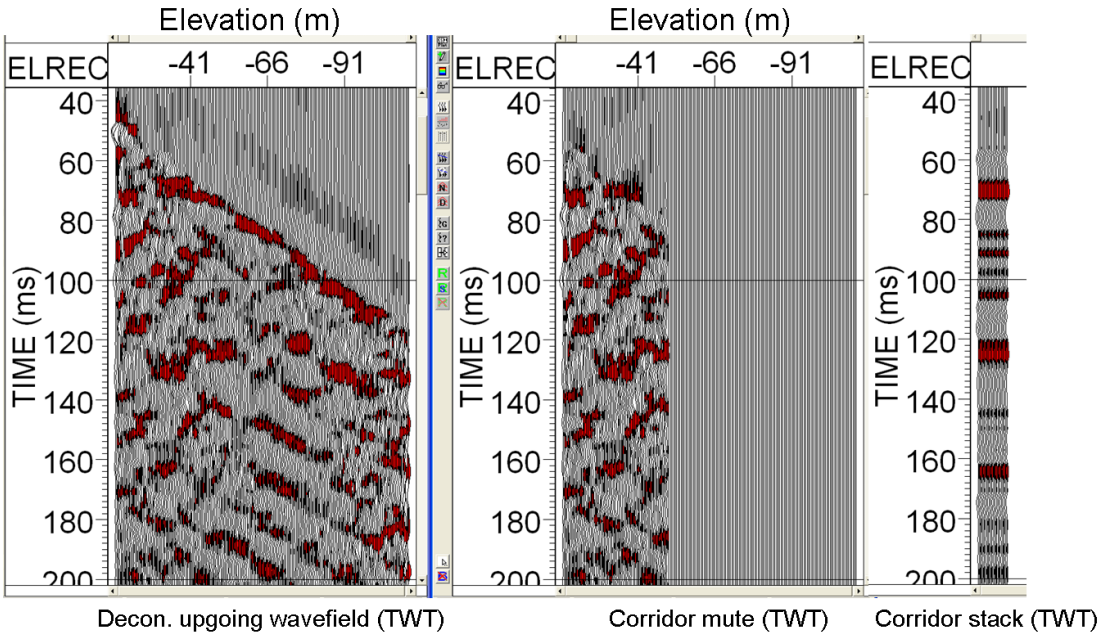

Figure 2-32: Corridor stack, all displayed with Ormsby filter (20-40-150-300 Hz) and AGC (500ms length window)

2.7 Hydrophone walk-away VSP-AVO analysis

The south 13 offsets at 2m offset intervals have been processed to get an AVO curve. After processing all 13 offsets of the walk-away VSP, using the processing workflow above, the 36m Common Receiver Gather (CRG) shows a reflection event at 40ms (Fig. 2-33). The theoretically predicted AVO curve has been calculated using the Zoeppritz equation (Fig. 2-34). The amplitude from the CRG event at 40ms has been plotted with the 13 different offsets to get the AVO curve (Fig. 2-35).

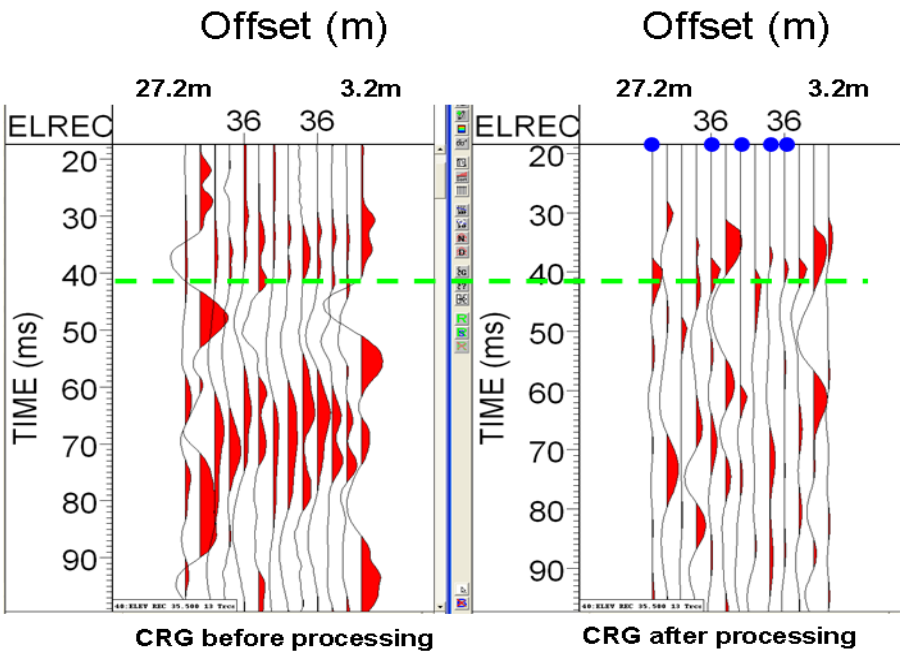

Figure 2-33: Left: 36m deep CRG before processing. Right: 36m deep CRG after processing. Displayed without Ormsby filter and AGC (Appendix 2-4).

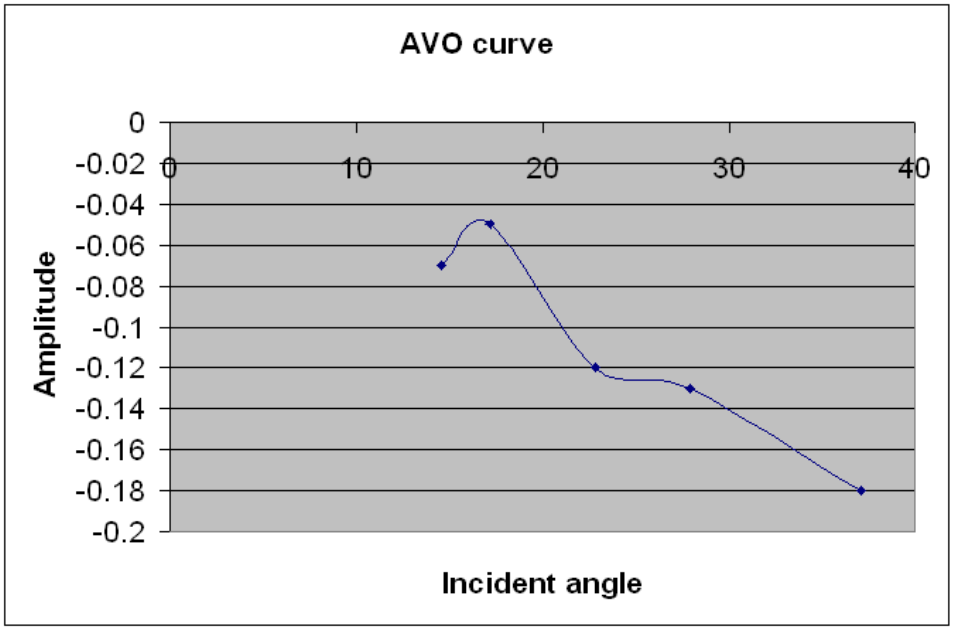

Figure 2-34: Practical AVO curve from the 36m depth CRG, the amplitudes are selected for reliable AVO curve highlighted in blue dots in Figure 2-33.

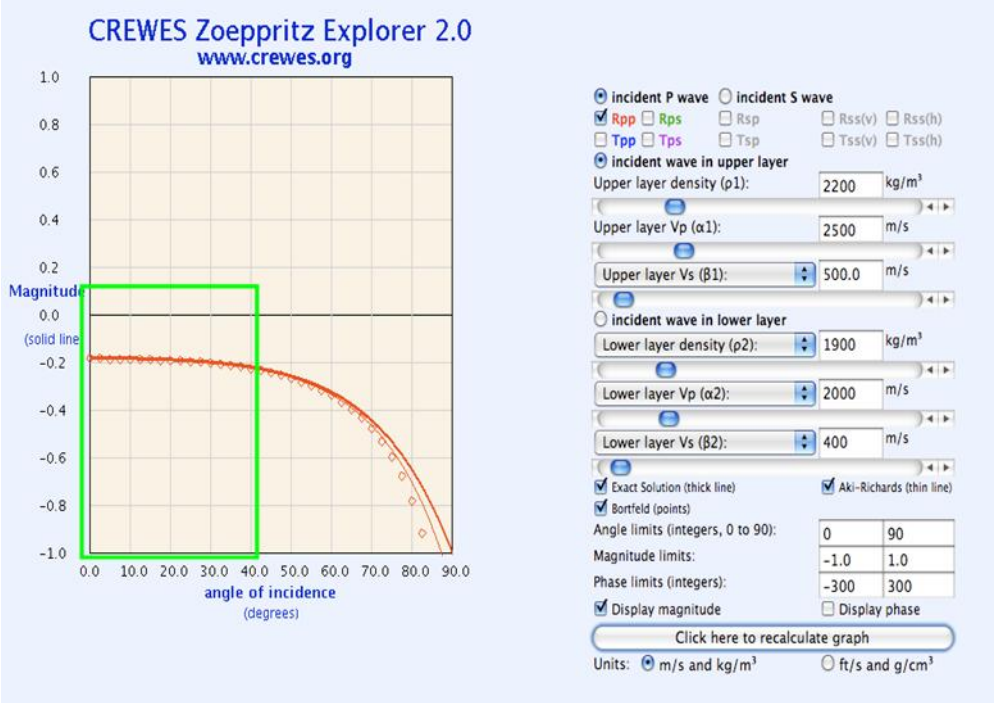

Figure 2-35: Zoeppritz theory predicted AVO curve (using the CREWES Explorer), the input velocity in the program are reading from sonic logging data above and below 40ms event.

2.8 Hydrophone VSP tube wavefield processing

2.8.1 Acquisition geometry and first break picking

The 5.2m offset hydrophone tube wavefield choosen for tube wavefield processing (Fig. 2-36). The interval velocity has been calculated by dividing the straight-line distance from source to receiver by the picked first arrival time (Fig. 2-37).

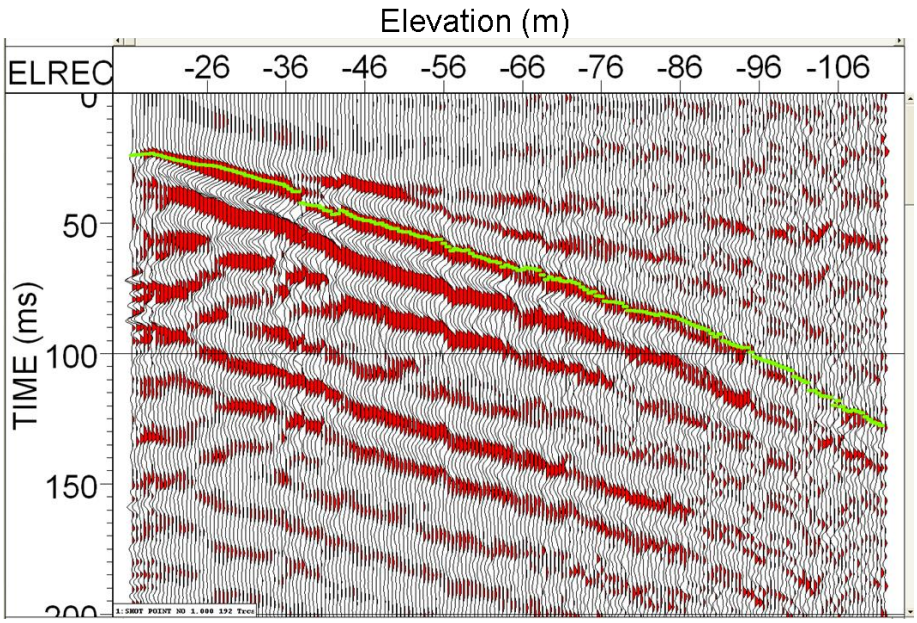

Figure 2-36: The 5.2m offset hydrophone tube wave field, after subtract reflection wavefield from figure 2-26, displayed with AGC only.

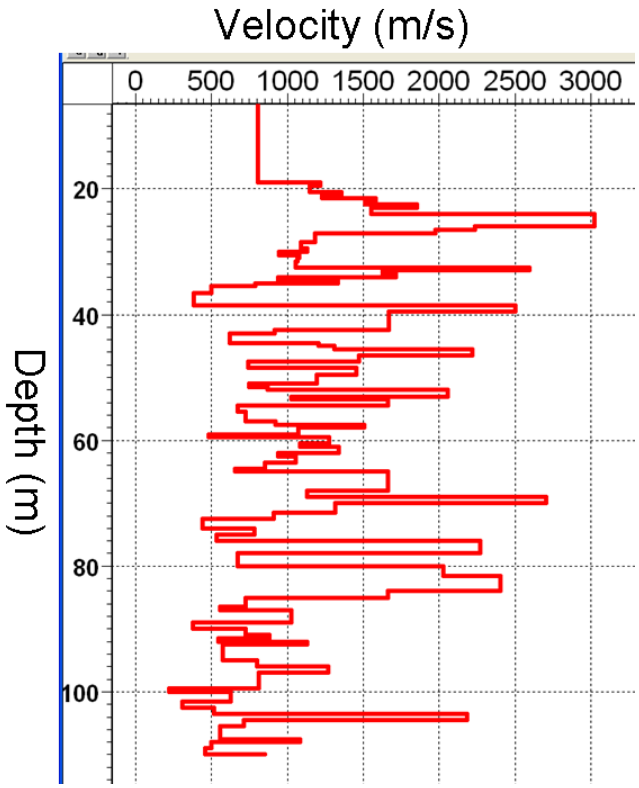

Figure 2-37: The 5.2m offset hydrophone tubewave field, Velocity curve of downgoing tube wave from the green color picked first break.

2.8.2 Wavefield separation using median filter

To get wavefield separation, a 17-point median filter was applied to the flattened downgoing wavefield to get the upgoing wavefield (Fig. 2-38, 2-39).

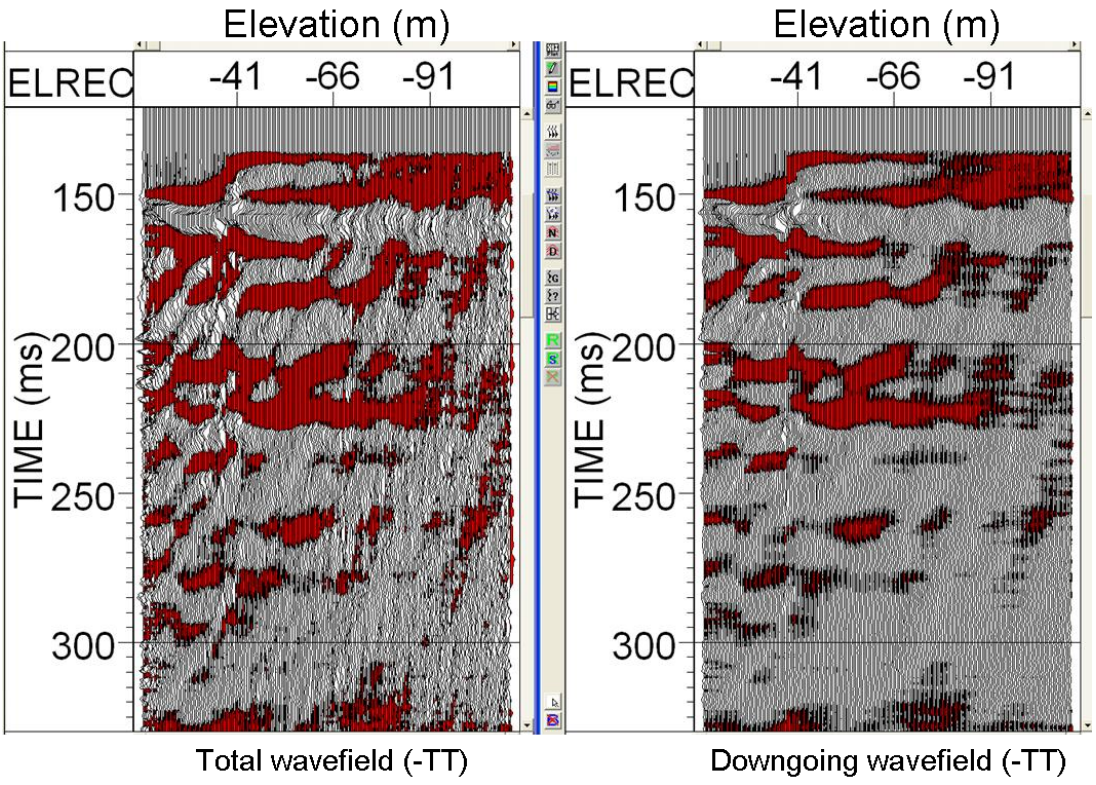

Figure 2-38: 5.2m offset hydrophone tube wavefield. Left: Total wavefield (-tt). Right: Downgoing wavefield (-tt). Displayed with AGC only.

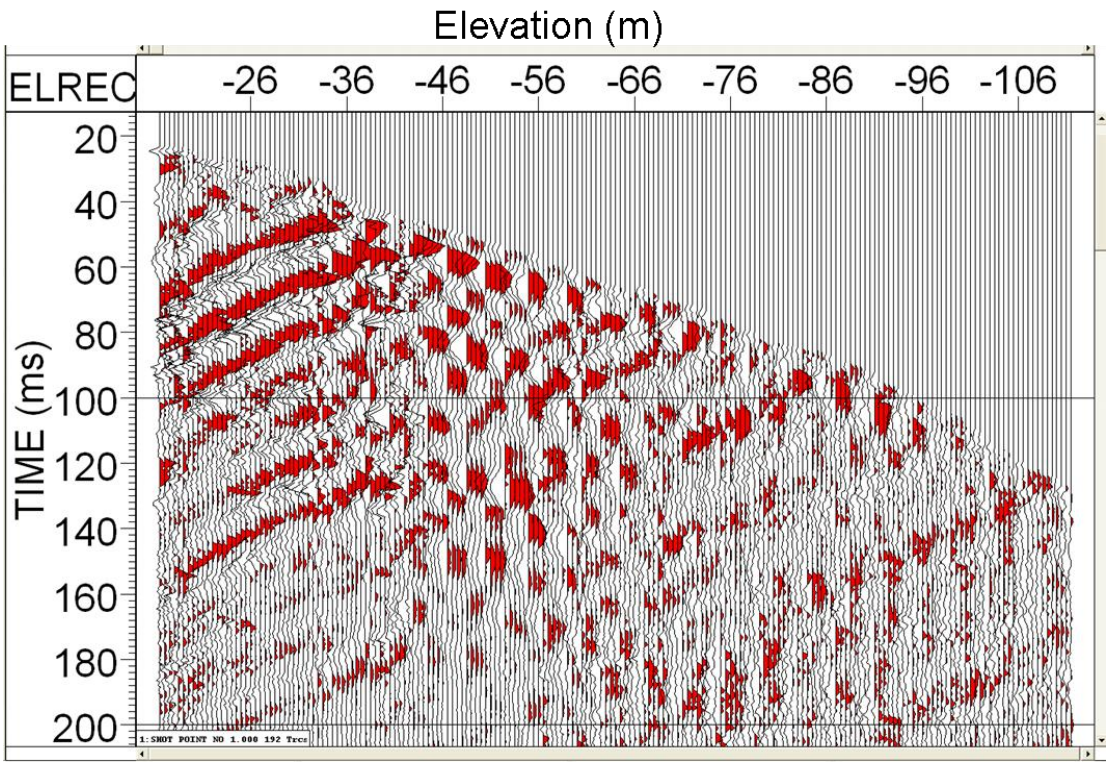

Figure 2-39: 5.2m offset hydrophone tube upgoing wavefield (FRT).

2.8.3 Deconvolution

A deconvolution with 100ms operation window produces sharper and better-defined reflection events (Fig. 2-40, 2-41).

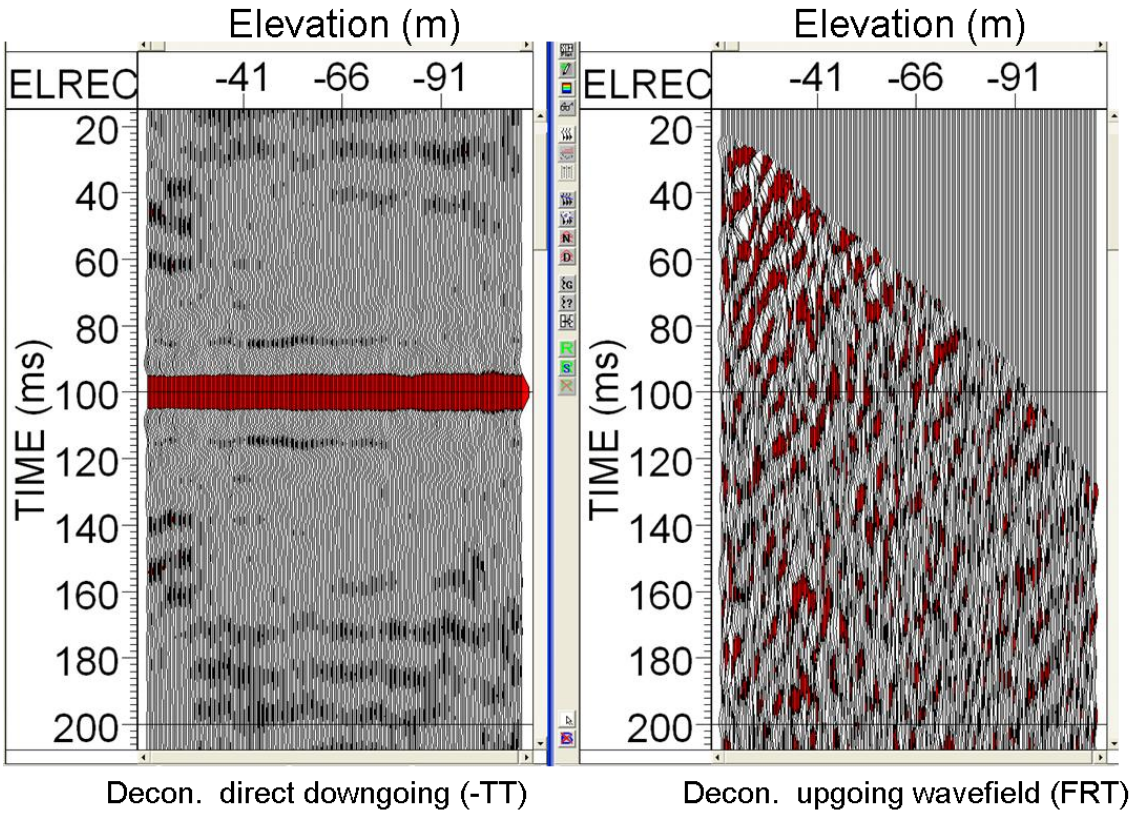

Figure 2-40: 5.2m offset dydrophone tube wavefield. Left: Deconvolution downgoing wavefield (-TT). Right: Deconvolution of upgoing wavefield (FRT).

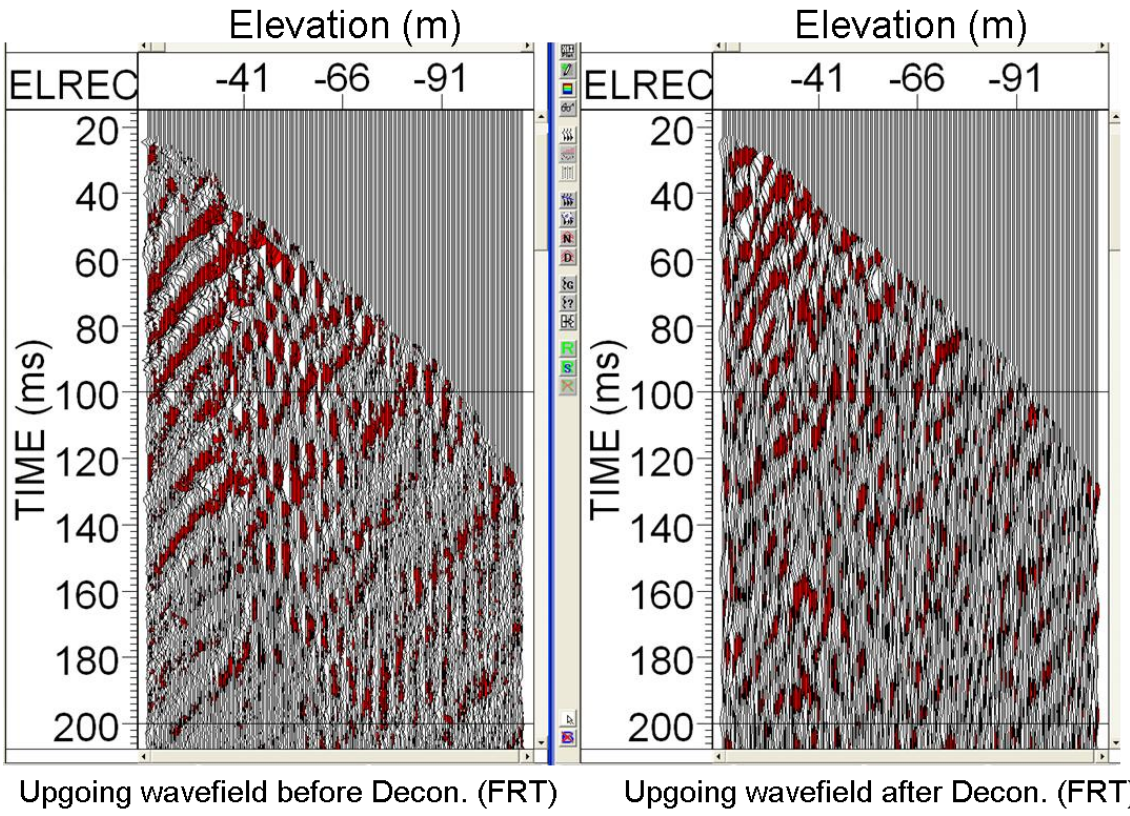

Figure 2-41: 5.2m offset hydrophone tube wavefield. Left: upgoing wavefield before deconvolution (FRT). Right: upgoing wavefield after deconvolution (FRT).

2.8.4 Corridor stack

The last processing step was the outside 100ms corridor stack to get the final reflection series (Fig. 2-42, 2-43).

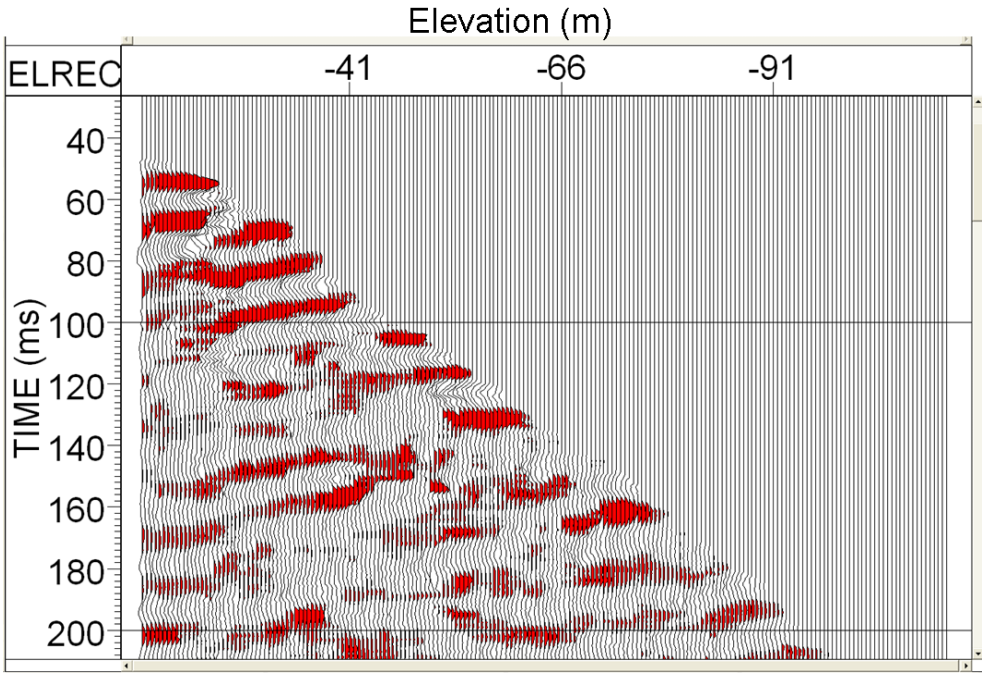

Figure 2-42: Deconvolution upgoing wavefield (TWT).

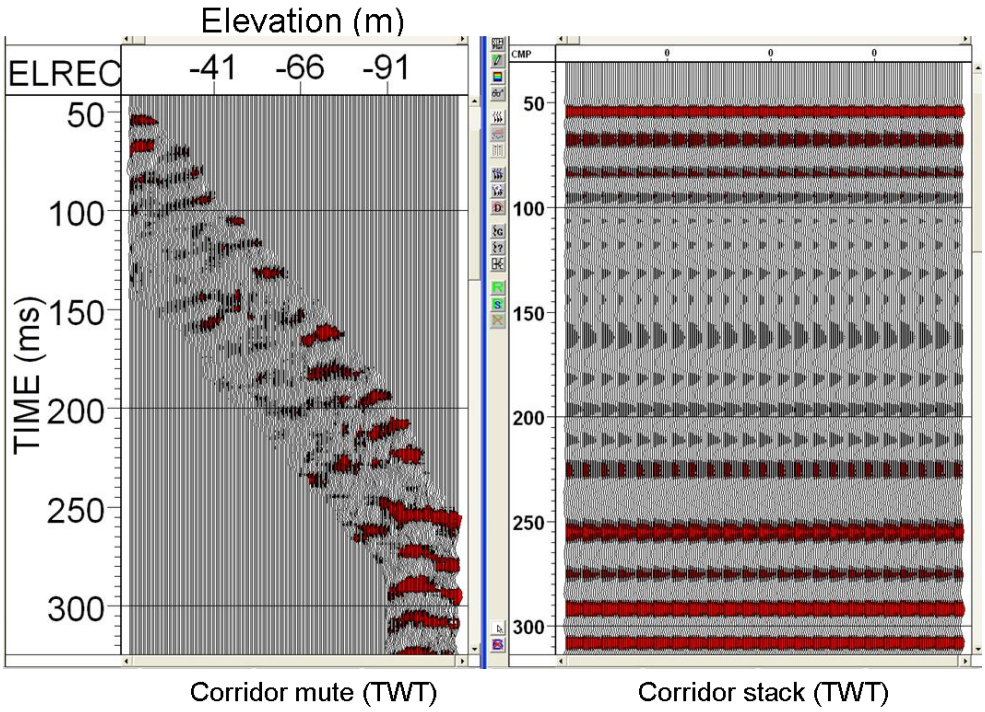

Figure 2-43: Left: 100ms window fatten deconvolution upgoing wavefield (TWT) length corridor. Right: Corridor stack.

2.9 Near-Offset geophone VSP Processing

The 3m south offset geophone/AWD VSP with half-meter receiver interval and 0.5ms sampling rate is processed in this section. The borehole geophone contains two horizontal components and one vertical component. The two horizontal components are named X and Y while the vertical component is named the Z component. The reflected upgoing P-waves were much stronger and clearer on the Z component compared to those on the X and Y components. There was not enough upgoing energy in the X and Y components to be processed, so only the vertical Z component has been processed. The 3C geophone VSP has higher frequency band and higher signal to noise ratio than the hydrophone VSP. The 3C geophone VSP has better consistency of upgoing P wave events. The VSP was performed close to a power line, so to get better signal to noise ratio, a 60Hz notch filter was applied. The coupling between the 3C geophone and well GB-1 is better than the hydrophone, since the 3C geophone has an arm to push it onto the wellbore, whereas the hydrophone does not. The 3C geophone VSP has a dominant frequency of 100Hz from the frequency analysis. An Ormsby band pass filter with corners at 30-60-150-300Hz and 500ms AGC were applied to the Z component VSP for display in the following processing steps.

2.9.1 Acquisition geometry and first break picking

As mention in 2.6.1, the essential step in VSP processing is the geometry input. This was done by sorting the data according to Channel Number (primary sort) and Depth of Receiver (secondary sort) to create proper trace headers. The first break times were picked on the raw vertical Z component, which is easier from hydrophone VSP since the 3C geophone VSP

contains some lower frequency signal. The first break picks were picked on the primary downgoing wavefield with a search window of 60ms and sliding window of 20ms that is equal to the length of the wavelet, and were adjusted manually for better accuracy. The top 10m of casing in the GB-1 well is not grouted, this is visible on 3C geophone VSP (Fig. 2-44). The interval velocity is calculated by dividing the straight-line distance from two nearby receivers by the picked first arrival time difference. The resulting interval velocities show that P-wave velocities are in the range of 200-3500m/s. Figure 2-45 shows that the VSP interval velocities increase at 25m depth, same as sonic log.

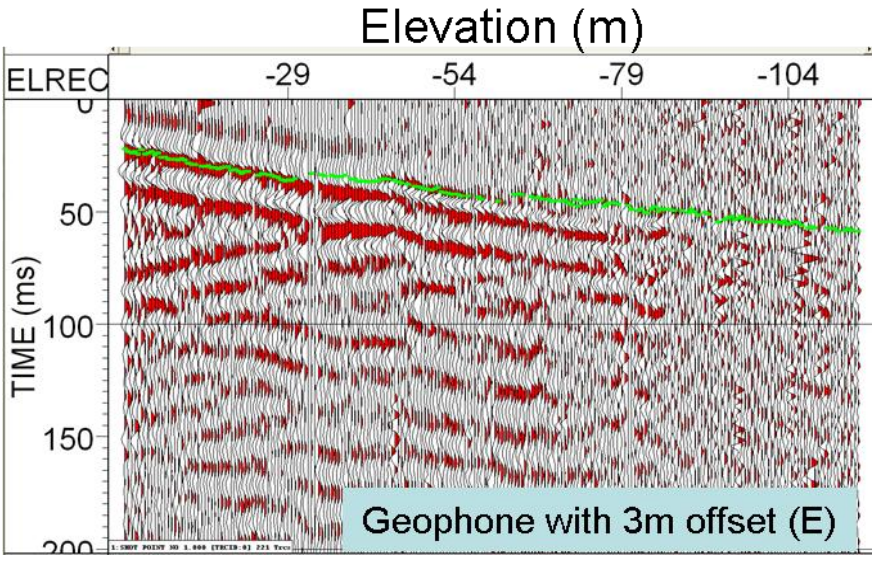

Figure 2-44: First break picks (green lines) from the 3m east offset geophone Z component data, displayed with Ormsby filter and AGC.

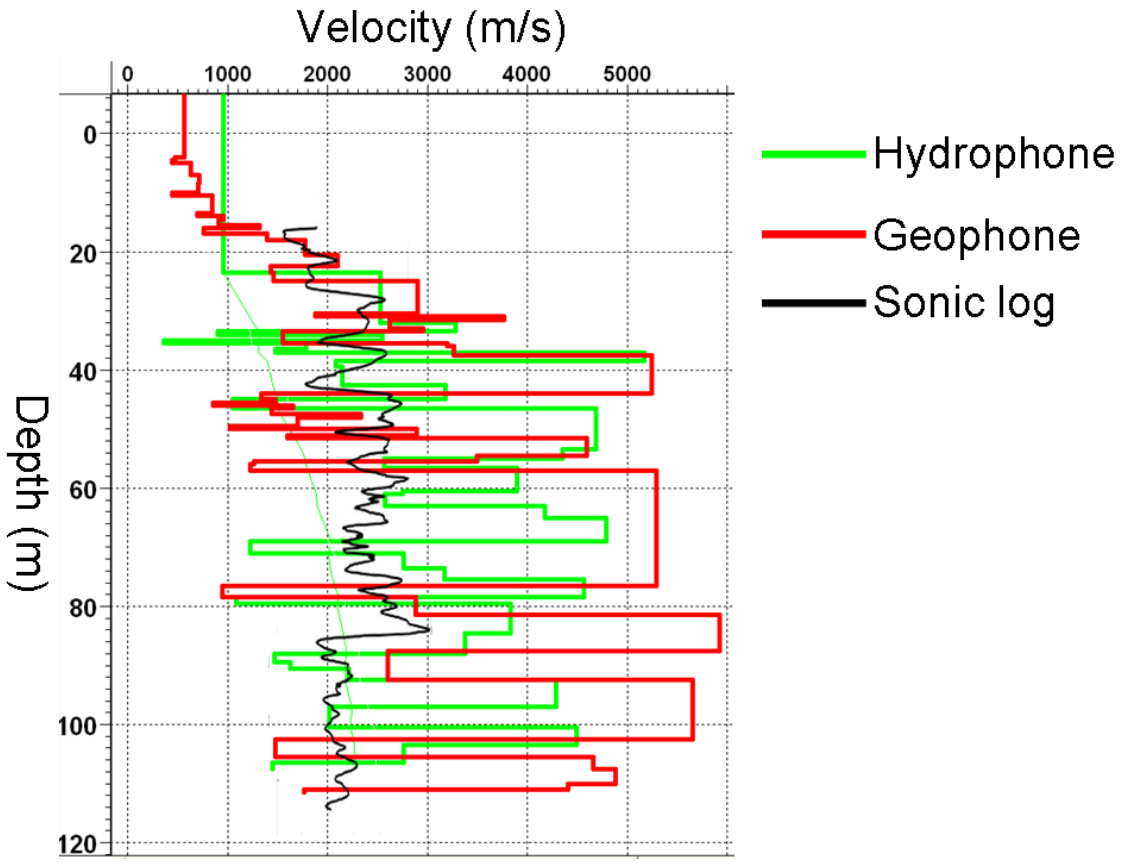

Figure 2-45: Comparison of sonic log and VSP interval velocity from the GB-1 well. VSP travel times are measured at frequencies from 10 to few 500Hz, sonic logging traveltimes are measured at frequencies from 2 to 20KHz. So VSP P-wave interval velocity bigger than sonic velocity, the drift will be applied to sonic velocity before the synthetic seismogram generated.

2.9.2 Wavefield separation using median filter

A 21-point median filter proved best at isolating the downgoing events and, after subtraction, produced the most continuous and coherent upgoing events (Fig. 2-46).

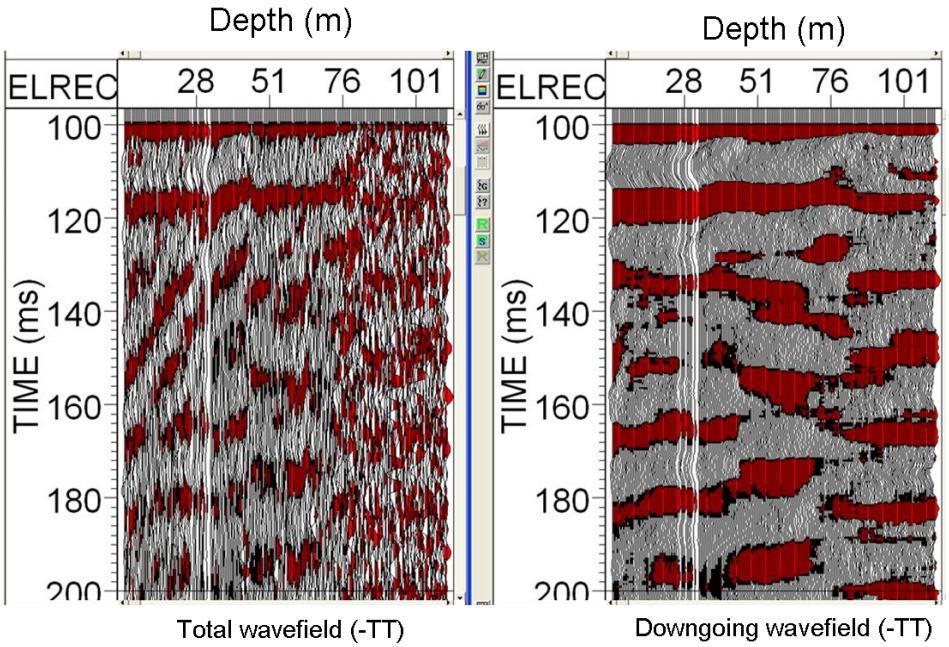

Figure 2-46: a) Wavefield separation of the Z component geophone VSP (-tt), displayed with Ormsby filter and AGC.

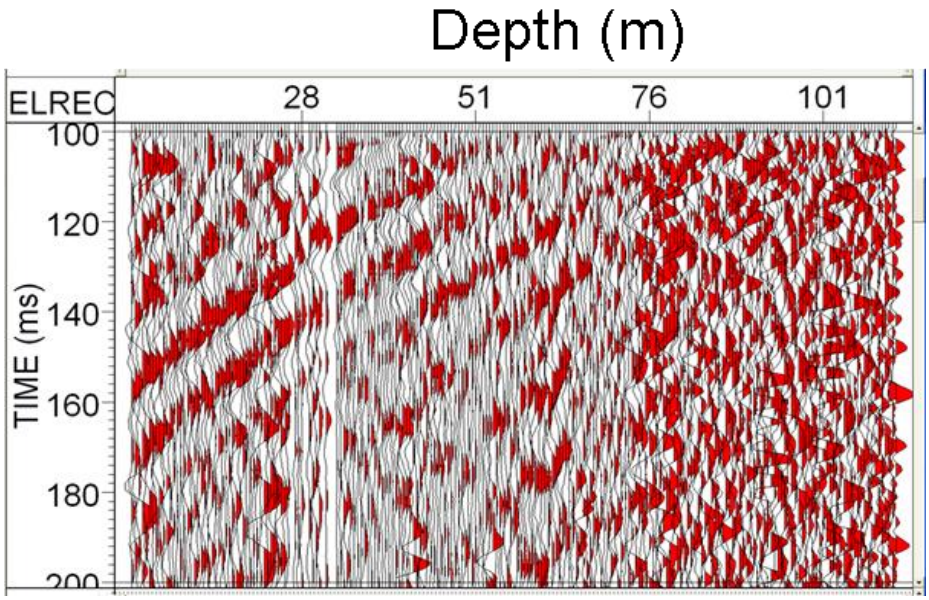

Figure 2-46: b) Upgoing wavefield of the Z component geophone VSP (-tt), displayed with Ormsby filter and AGC.

2.9.3 Deconvolution

A deconvolution with 30ms operation window produces sharper and better-defined reflection events. A 21 trace median filter was then applied to the deconvolved upgoing reflection events to flatten and enhance the deconvolved upgoing wavefield (Fig. 2-47).

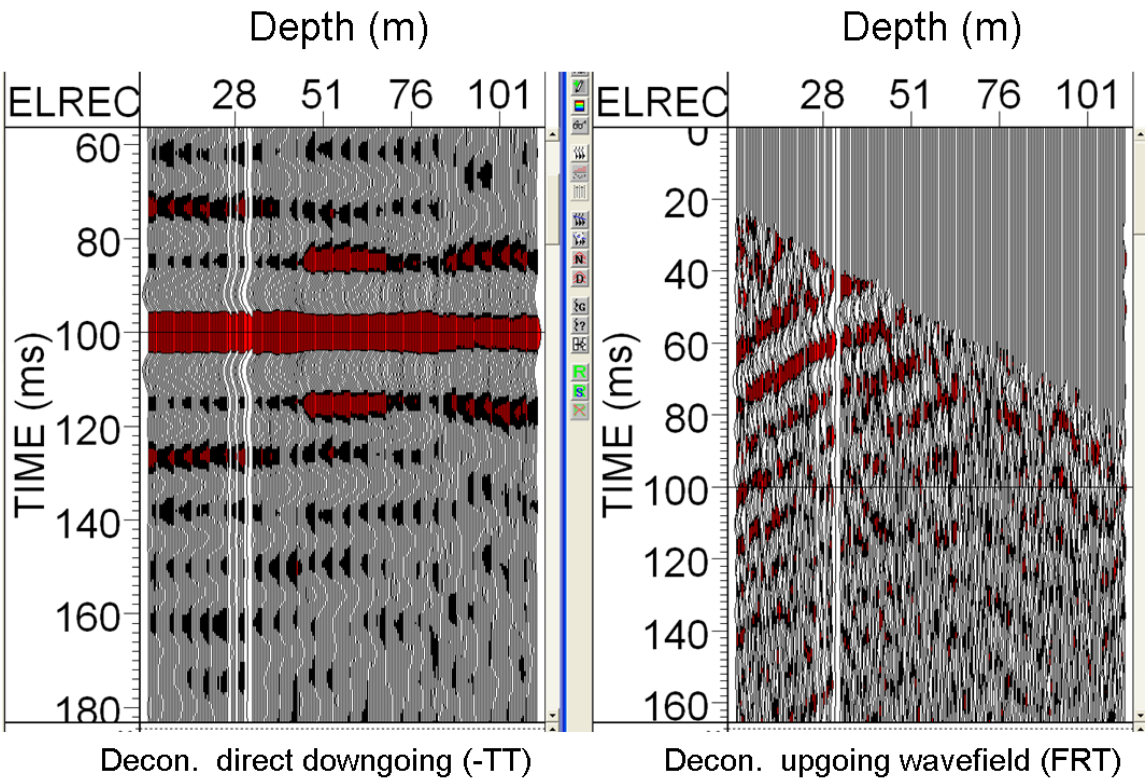

Figure 2-47: Left: Decon. of Z component geophone downgoing wavefield (-tt), displayed with Ormsby filter and AGC; Right: Decon. of geophone upgoing wavefield (FRT), displayed with Ormsby filter and AGC.

2.9.4 Corridor stack

In the field data, there is a lot of noise in the pre-stack profile. A corridor is windowed along the edge, which does not include any multiples, avoiding noise from the whole data profile. In this case, 50ms windowed edge was applied to the data. Then the data were stacked across the corridor into one trace (Fig. 2-48).

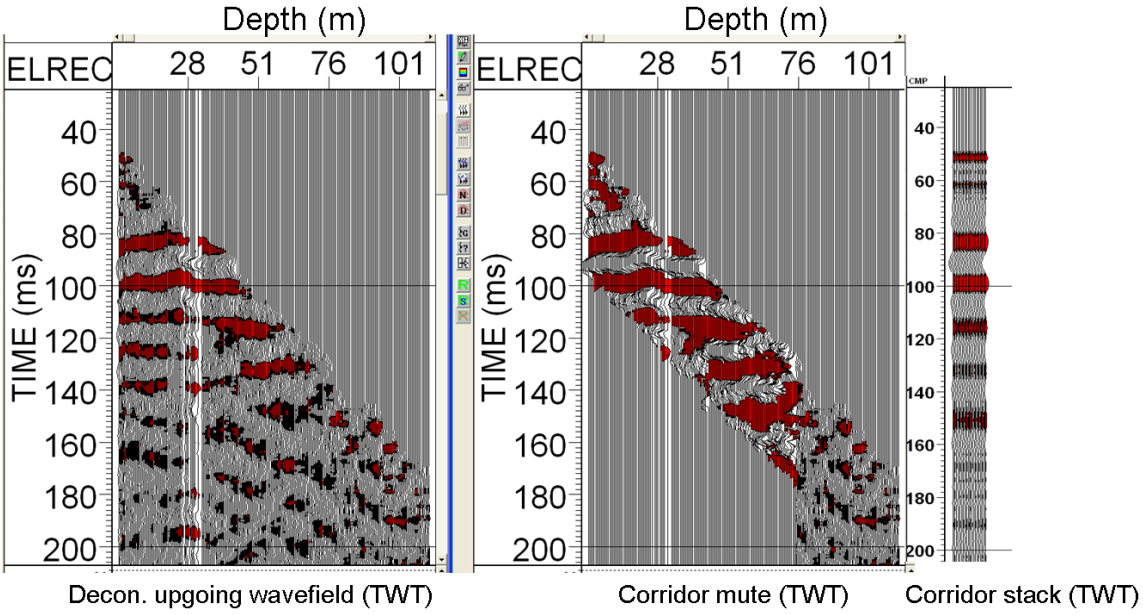

Figure 2-48: Geophone 50ms corridor stacks, repeated 20 times for display, displayed with AGC (500ms length window) only.

2.10 Wireline logs, 2D seismic, and VSP comparison

From the first break time, the two-way time and depth curve have been calculated for time-depth relation (Fig. 2-49), since the sonic log and gamma ray log, acquired at depths of 4m to 115m, are shown with the processed VSP, which is in time. Also shown are the processed

geophone and hydrophone VSPs (Fig. 2-50).

The figure shows that prominent events on the VSP corridor stack correlate fairly well with the features on the geophysical logs. Three events can be identified on the L-plot. 40m depth event, shows on geophone Z component stack, and hydrophone stack. Also gamma ray log increases, velocity decrease at 40m depth.

A 50m depth event is shown on geophone Z component stack, and hydrophone tubewave field stack. Also conductivity increases, velocity decreases at 50m depth. A 65m depth event shows on geophone Z component stack. Also gamma ray log and velocity increases at 65m depth.

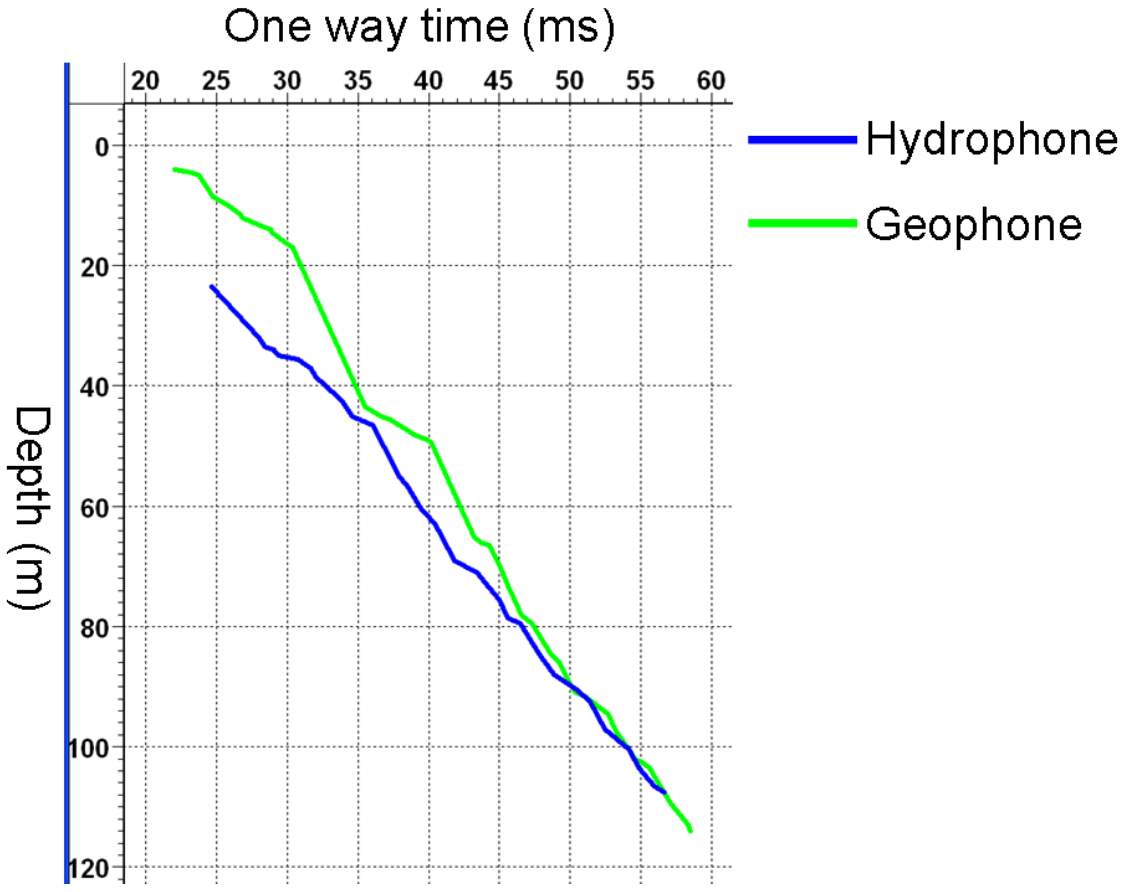

Figure 2-49: One way time to depth curve from the geophone and hydrophone.

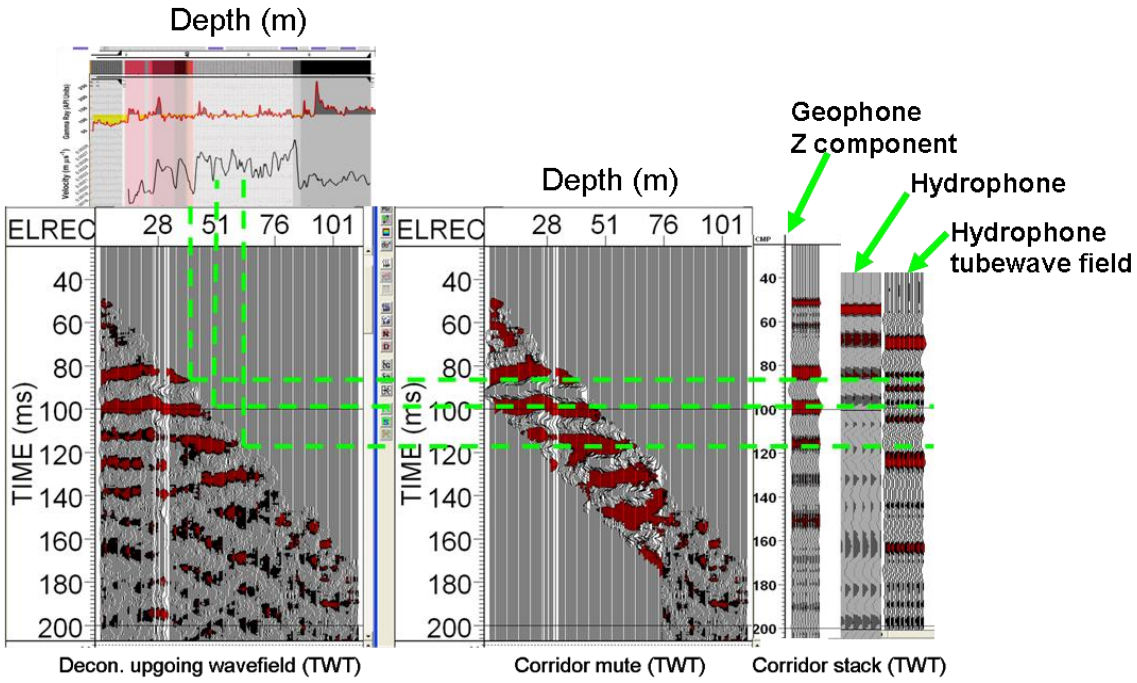

Figure 2-50: L-plot of VSP (TWT), sonic & gamma logs, and VSP corridor stack.

2.11 Discussion and conclusions

The purpose of this study was to interpret the VSP, surface seismic, and well log data, in order to tie them to glacial deposit thickness. Different data types correlated reasonably well with geophysical logs and the driller's report from the GB-1 well.

2D seismic brute stack section shows a layer at 25m depth. The gamma ray, conductivity, resistivity indicate a boundary at 25m depth. The sonic log is increased from 1500m/s to 2500m/s at 25m depth as well.

The VSP survey, conducted with a wall-clamping 3C geophone with an AWD source and hydrophone with an AWD source, proved successful in providing coherent data. The interval velocity from the VSP first break picks matches with the sonic velocity log trend.

For hydrophone/AWD 5.2m south offset VSP processing, a 13-point median filter was applied to separate the wavefields. A 0-50ms window was chosen for designing the deconvolution operator. A inside 20ms corridor stack was applied to get the final reflection series.

For hydrophone/AWD 5.2m south offset tube wavefield VSP processing, a 17-point median filter was applied to the flattened total tube wavefield to get the upgoing tube wavefield. A deconvolution with 100ms operation window produces sharper and better-defined reflection events. A outside 100ms corridor stack to get the final reflection seriers.

For geophone/AWD 3m east offset VSP processing, a 21-point median filter was applied to the flattened downgoing wavefield to get the upgoing wavefield. Deconvolution was performed to produce sharper and better defined reflection events, and a median filter was applied to enhance the reflection series. The last processing step was the outside corridor stack to get the final reflection series at each geologic layer.

The VSP velocities shows a velocity 25m depth, same fashtion changes are also detected from geophysical logs, which is interpreted as the total glacial deposits in this study.

An AVO curve has been calculated from the 36m depth CRG from the walk-away hydrophone VSP for analysis the 40ms reflection event. The AVO slope and intercept attributes can be further analyzed for pore-fluid and lithology prediction (Hilterman, 2001).

Hydrophone was used to enhance the recording of tube waves that reflect from perforation zones (aquifer features). The L-plot shows a 50m depth event on geophone Z component stack, and hydrophone tubewave field stack, but not a strong reflection event on hydrophone (removed tubewave field) stack. Also conductivity and velocity decreases at 50m depth. The driller's report shows a water perforation zones at 50m depth as well.

Chapter 3 VSP analysis Garden Banks, Gulf of Mexico

3.1 Geology and motivation

The study area is located on the Louisiana slope, Gulf of Mexico (GOM), known as the Garden Banks block (Fig. 3-1). Throughout the northern Gulf, thick sediments are being sculpted by deep salt layers. Salt movement influences the chemistry and geology of the slope, locally called the Sigsbee escarpment. Garden Banks has a discontinuous primary basin section with deeper secondary minibasins across bucket welds (Pilcher et al., 2011). The complex velocity structure is caused by the complexity of the bucket welds, which are defined by the steeply dipping salt geometries. The well analyzed here is about 150 miles (240km) from the Louisiana coast, named Bushwood, located in a water depth of approximately 2,800ft (850m) in the Garden Banks block. The total depth of the Bushwood well is 24,947ft (7600m), of which 24,812ft (7500m) was logged. The depth is the measured depth refers to the ocean bottom. Bushwood is located near the Sigsbee escarpment, where the water depth increases from 650ft (200m) at the shelf break to 9800ft (3000m) in the deep-water basin. For local geologic background, Pilcher et al. (2011) provides a general stratigraphic column at the Garden banks block. The generalized stratigraphy suggests that the reservoir rock is probably located in the Oligocene rocks, so generally the source rock should be older (Fig. 3-2). Well log analysis from Bushwood indicates more than 260ft (80m) of net gas pay in multiple sand layers at 18,700ft (5700m) depth, with more than 150ft (45m) of net gas pay found in the deeper portions, which are considered conventional deepwater reservoirs (Apache Comp. online news). The seismic image has poor quality because of the complex salt geometry, as mentioned before. VSP has been applied to this challenge; the goal is to get a basic time-to-depth conversion to calibrate surface seismic anomalies and in situ velocities were the main motivation. The amplitude

versus offset (AVO) information from the VSP dataset has also been tested in this study. The angle range of the reflection coefficient from the VSP is the main factor in AVO investigation.

The target stratigraphy of the Bushwood well was the Miocene and Oligocene, which are separated by an unconformity. The Bushwood well encountered multiple shaly gas sands in shallower formations.

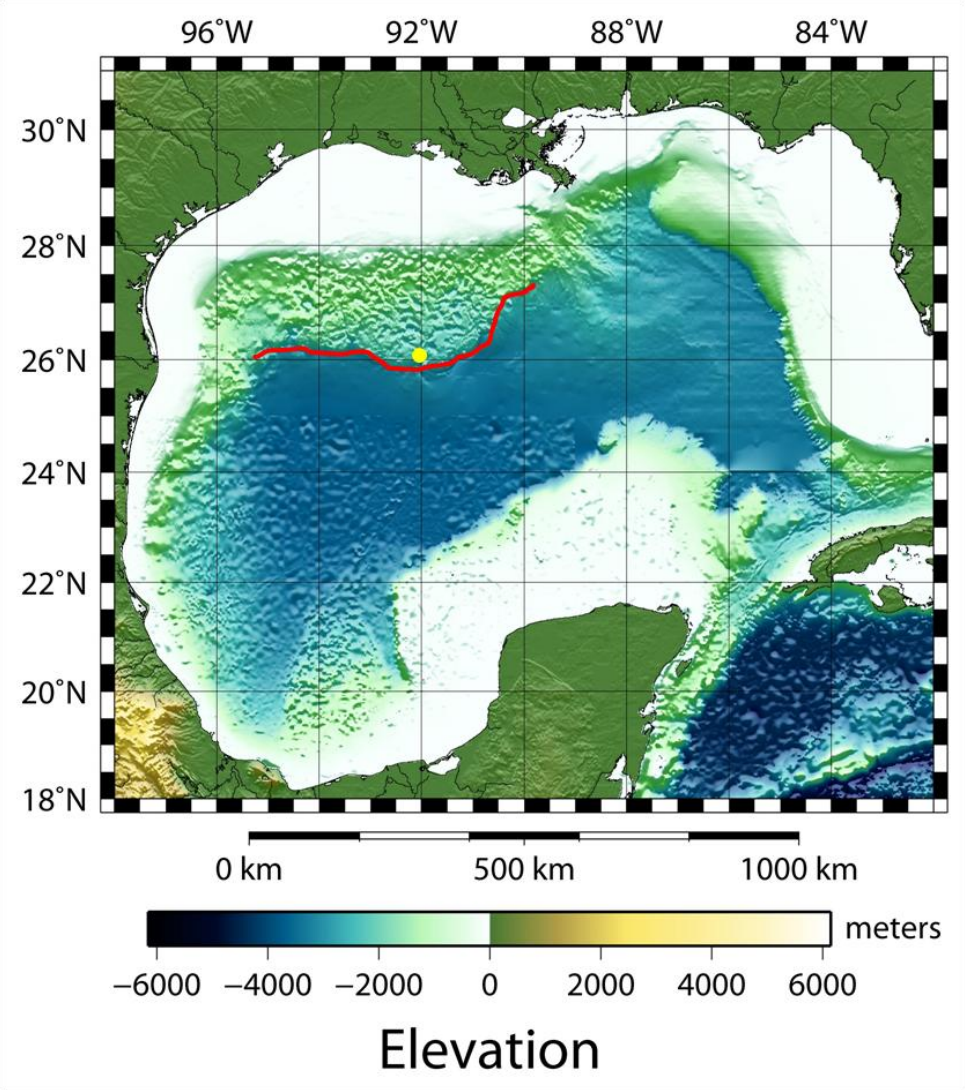

Figure 3-1: Map of the study area in the Gulf of Mexico, using the Generic Mapping tools (GMT). The Bushwood well location is shown by the yellow dot and the Sigsbee escarpment is highlighted by the red line.

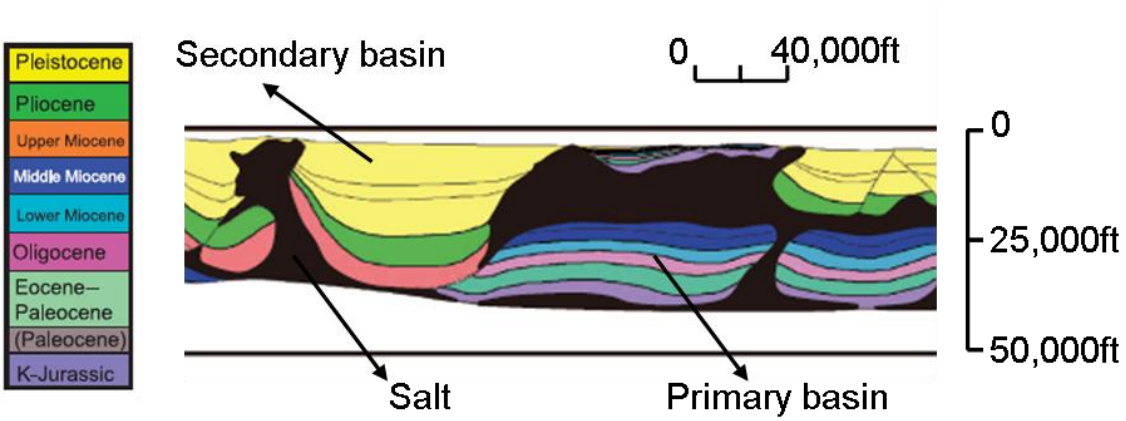

Figure 3-2: General stratigraphic column in the Garden Banks block, Gulf of Mexico (Pilcher et al., 2011).

3.2 Target Description

The sedimentary section dips along 136-degree azimuth. Bedding dips more steeply with depth and ranges from an apparent dip of 13 degrees in the shallow section to 45 degrees at basement. The depth of the section of interest is around 23,000ft (7000m).

To test the VSP-AVO potential in the deeper gas target area, a 3D geologic model has been built for incident angle analysis using OMNI software (Fig. 3-3). The model was based on the field grid, which from N-S (Y) covers 9970000-9990000ft (3038800-3044900m), and from E-W (X) covers 1685000-1705000ft (513600-519700m). To simulate the survey, the bin size is 100×100ft (30×30m), so there are 200 Inlines (0-199), and 200 Crosslines (0-199). Bin size ideally should be equal to or less than the resolution. Based on the resolution of field survey, nine layers have been built in the geologic model. The layer parameters here are the same as the 2D model (Appendix 3-2).

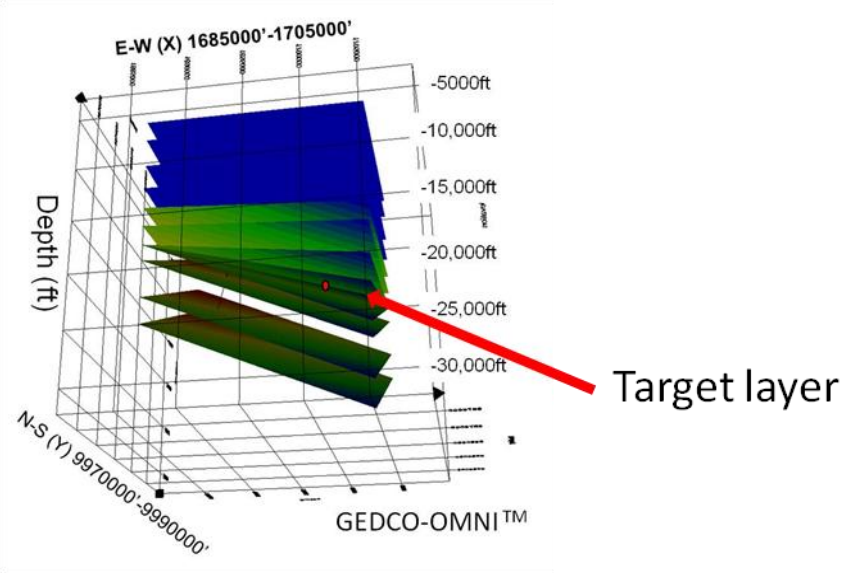

Figure 3-3: 3D geologic model, the target layer is shown by the red arrow, the AVO target is shown by the red dot.

3.3 Data available

Logging data available in this study includes sonic, density, conductivity, resistivity, gamma, and temperature. Logging data has been used to gain a better understanding of the lithology (Fig. 3-4). From the logs, the average density is estimated to be around 2.25 g/cc.

Two different VSP profiles were acquired: a Vertical Incidence VSP (VIVSP), and an offset VSP (OVSP) (Appendix 3-1). The VSPs were used for several objectives: the VIVSP to tie surface seismic with well logs and the OVSP to map the lateral character of the target shaley sand. Field data acquisition parameters are shown in table 3-1. The VIVSP survey includes receiver depth from 14,900ft (4500m) to 24,700ft (7500m), with 99 depth points at 100ft (30m) intervals. The OVSP, with a 20,000ft (6100m) offset source, has receivers over 8000ft (2400m) to 24,570ft (7500m), with 113 depth points at 100ft (30m) intervals (from 8000ft (2400m) to 14500ft (4400m) the depth interval is 500ft (150m)) (Fig. 3-5).

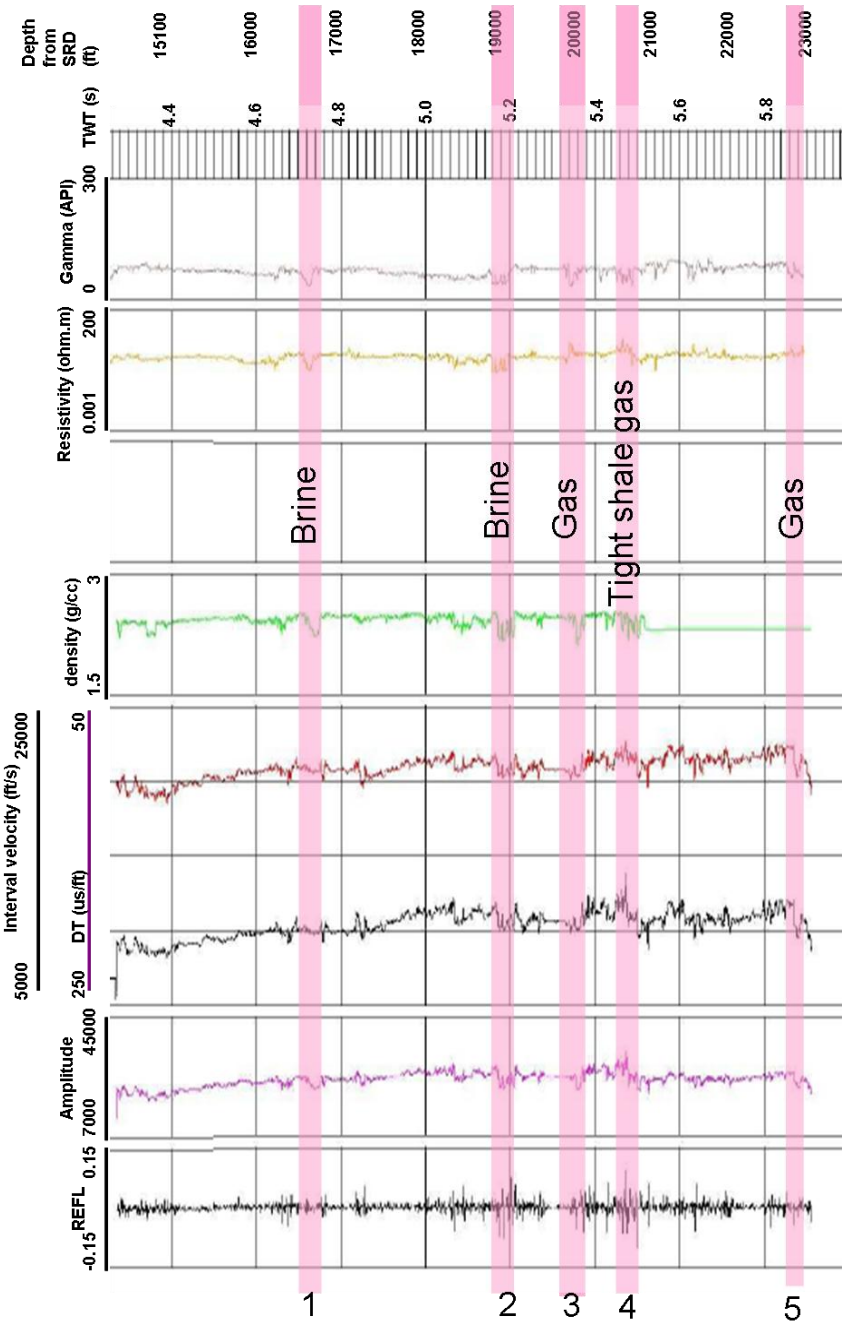

Figure 3-4: Geophysical logs from the Bushwood well (reflectivity, amplitude (impedance amplitude), interval velocity, slowness, density, resistivity, gamma ray, two way time). The average interval velocity is around 10,000ft/s (3000m/s), and at depth of 17,000ft (5200m), there is a velocity increase layer.

Acquisition Parameters	VIVSP/OVSP
Source	Air gun
Source offset	0-20,000ft (0-6096m) Azimuth=136deg.
Receiver tool	9 shuttle tool with 3C receivers
Receiver separation	100ft (30m)
Acquisition depths	VIVSP 14,900-24,700ft (4540-7528m) OVSP 8,000-24,570ft (2438-7489m)
Kelly Bushing elevation	86ft (26m)
Ground level	-2823ft (860m)
Sample rate	1ms
Time length	VIVSP 9sec OVSP 12sec

Table 3-1: VSP acquisition parameters.

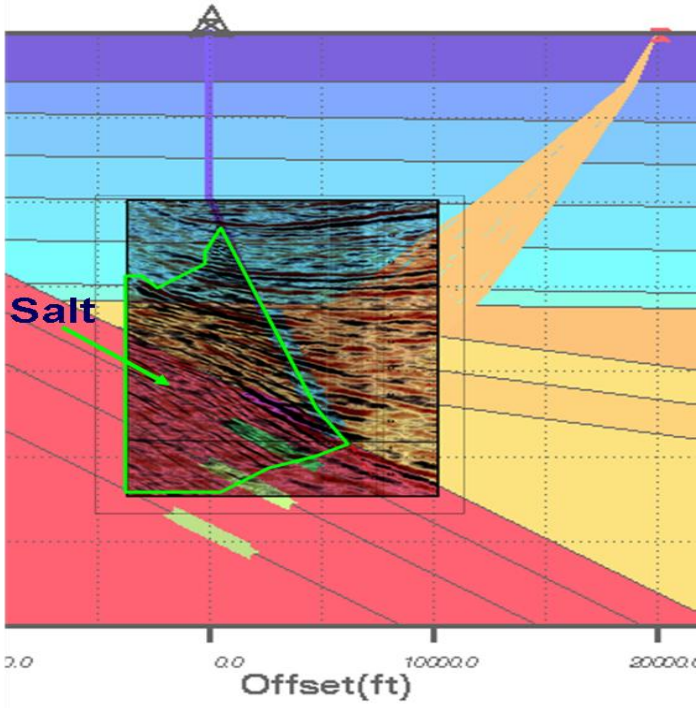

Figure 3-5: Seismic section and processed VIVSP section overlaying the 2D forward model, there is good correlation at the dipping layer imaging by surface seismic and VIVSP (Schlumberger processing report, 2010).

3.4 VIVSP synthetic and processing

3.4.1 VIVSP acquisition geometry and first break picking

There are three components in this VIVSP dataset, the two horizontal components are X and Y, and the vertical component is Z. Each shot location has been repeated more than once, so a stack was applied to make sure each shot location just has one shot. Also each fixed VSP receiver tool (9 receiver shutter) location, the shot moves three different locations in order to record the vertical incidences angle out of the 9 receivers shutter location (Fig. 3-6).

Some traces had reversed polarity in the X and Y components, but not the Z component. This was caused by the lack of rotation control for the down-hole geophone. The sorting of the data was by channel number (primary) and elevation of receiver (secondary) in order to edit the geometry. An Ormsby filter (5-10-45-55Hz) was designed for display after the frequency analysis (Fig. 3-7). A 500ms window length AGC was applied for display as well (Fig. 3-8).

The dominance of the downgoing P wavefield is clear on the Z component compared to the X and Y components. So the first break was picked on the primary downgoing wave on the Z component then transfered to the X and Y components. The parameters for picking the first break include a 200ms search window and 50ms sliding window, which is equal to the length of the primary downgoing wavelet. The first break was picked manually for better accuracy, which was used to calculate the average velocity at each true vertical depth (Fig. 3-9).

a)

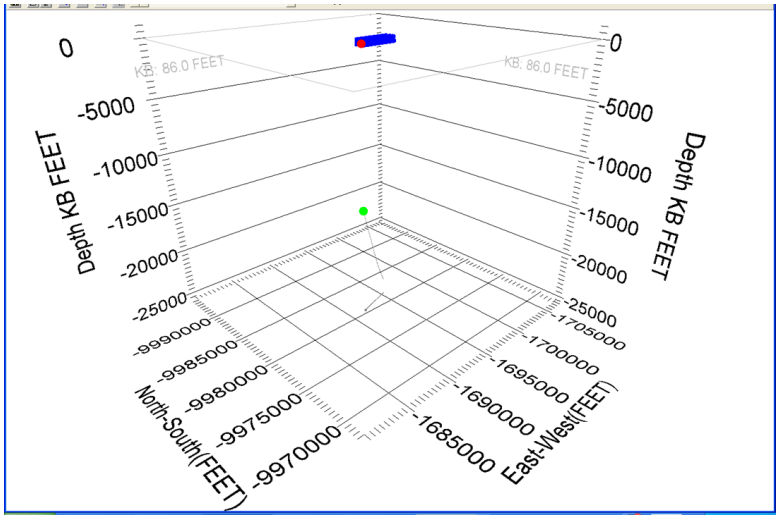

b)

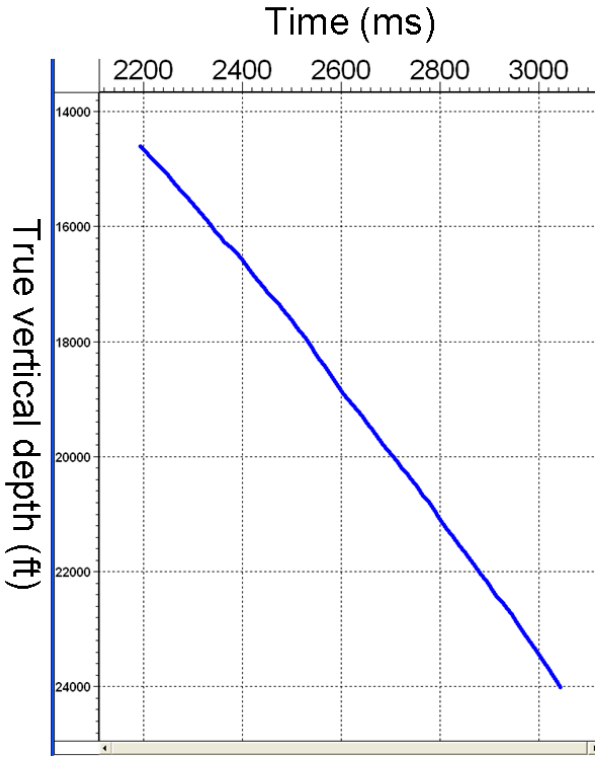

Figure 3-6: a) VIVSP acquisition geometry, the first shot location is shown by the red dot, the first receiver location is shown by the green dot, this VIVSP geometry give the average velocity to each depth from the first break time; b) True vertical depth versus the first arrival time.

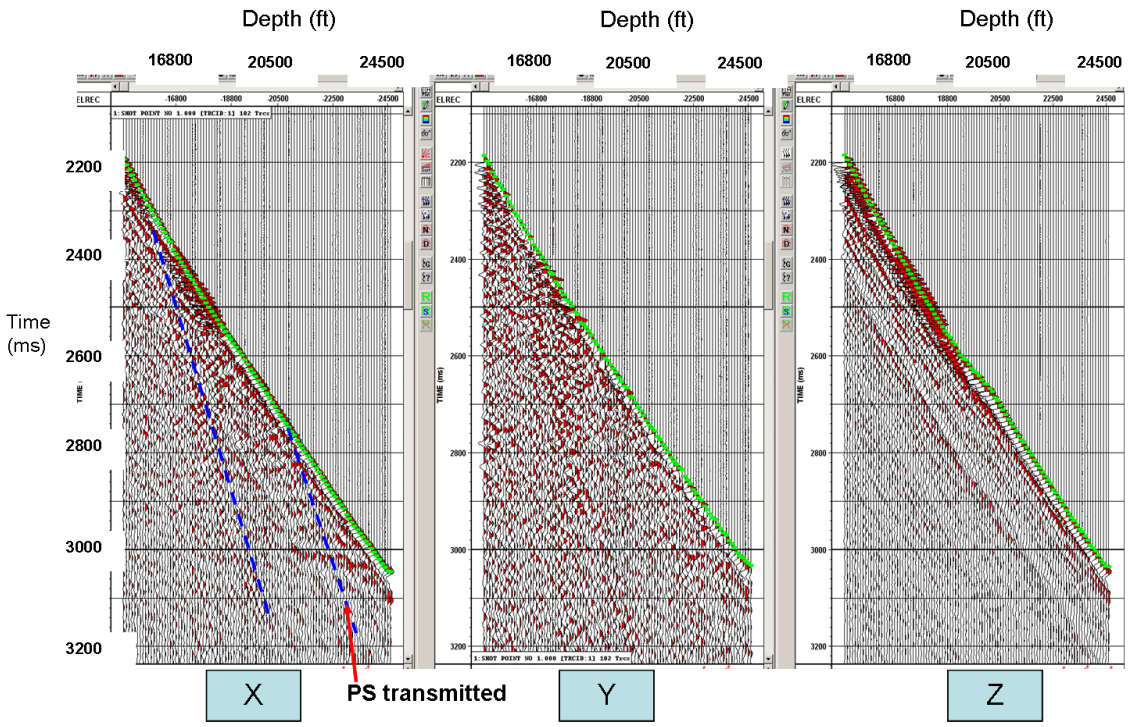

Figure 3-7: Three components of the raw VIVSP data, the PS transmitted wave are illustrated by the blue lines, displayed with Ormsby filter and AGC.

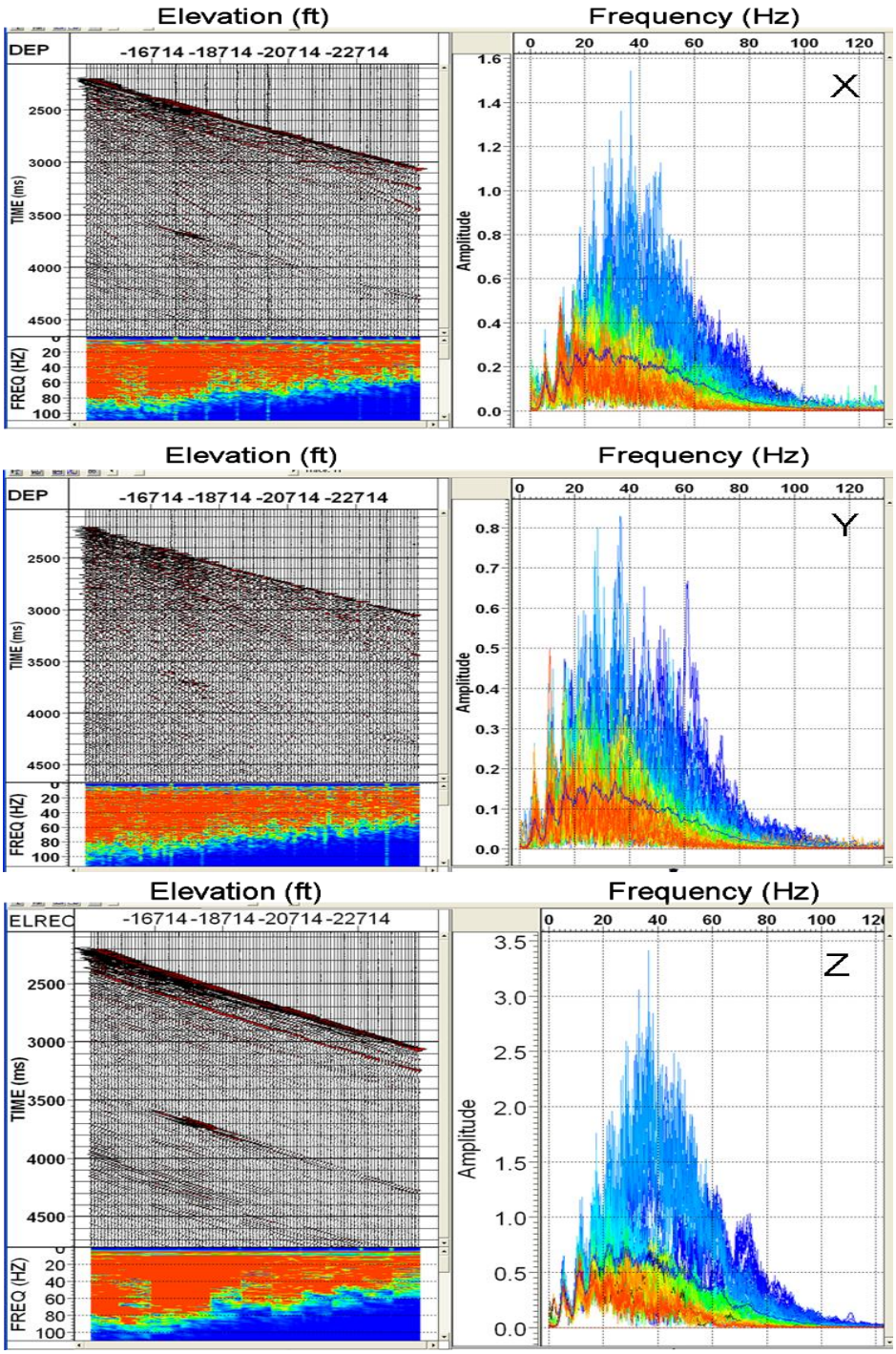

Figure 3-8: VIVSP three components frequency analysis. The frequency is analyzed for the seismic in the time window shows in the picture. It shows they have similar frequency band of 10-100Hz. The Z component frequency analysis indicates the dominant frequency is 40Hz.

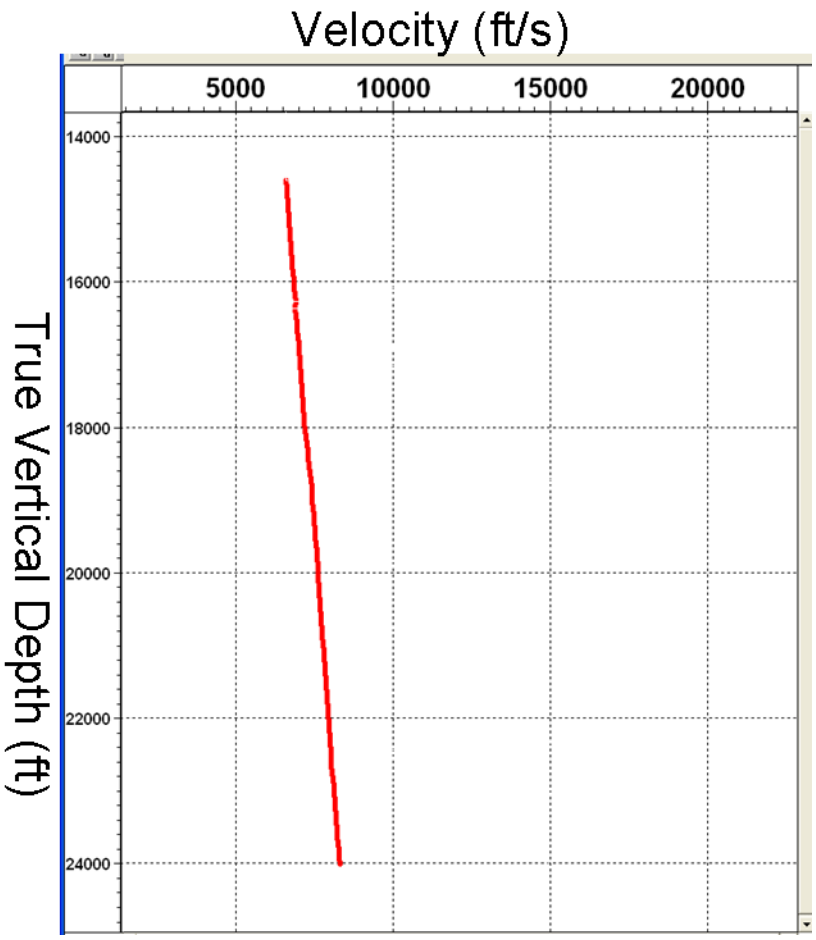

Figure 3-9: The average velocity curve, which was calculated by dividing the straight-line distance from source to receiver by the picked first arrival time at that depth.

3.4.2 Forward modeling and synthetic VSP

A 2D model has been built for synthetic VSP analysis to better understand the reflectivity from the existing VSP geometry. The dip angle of the formation has been provided by 2D surface seismic (Fig. 3-10). The sonic log was used to get the velocity information (Appendix 3-2). The density was read from the density log and the S-wave velocity was calculated using the

Castagna equation,

$$V_s = \frac{(V_p - 1360)}{1.16}, \text{ in m/s}$$

A synthetic VIVSP was generated by using the ray tracing method and convolved with a 55Hz Ricker wavelet, which is equivalent to the primary downgoing wavefield from the field VIVSP (Fig. 3-11). This synthetic data can also be used to test the VSP processing workflow to troubleshoot any processing problems. The two high amplitude peaks at the beginning of 200ms of the downgoing wavefield, it caused by bubble effect of air gun, the shot elevation is -13ft.

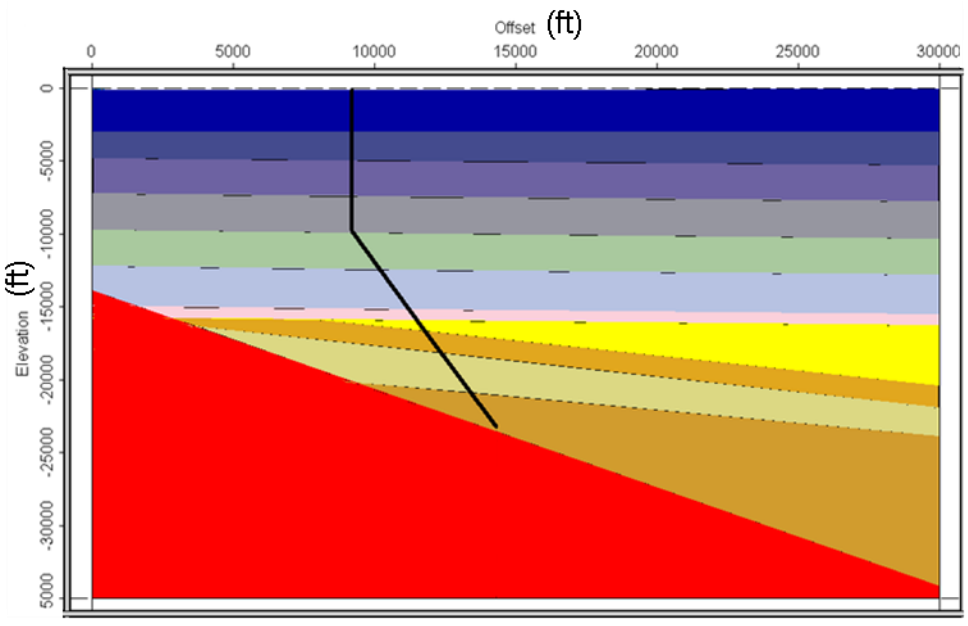

Figure 3-10: 2D geologic model for synthetic VSPs.

a)

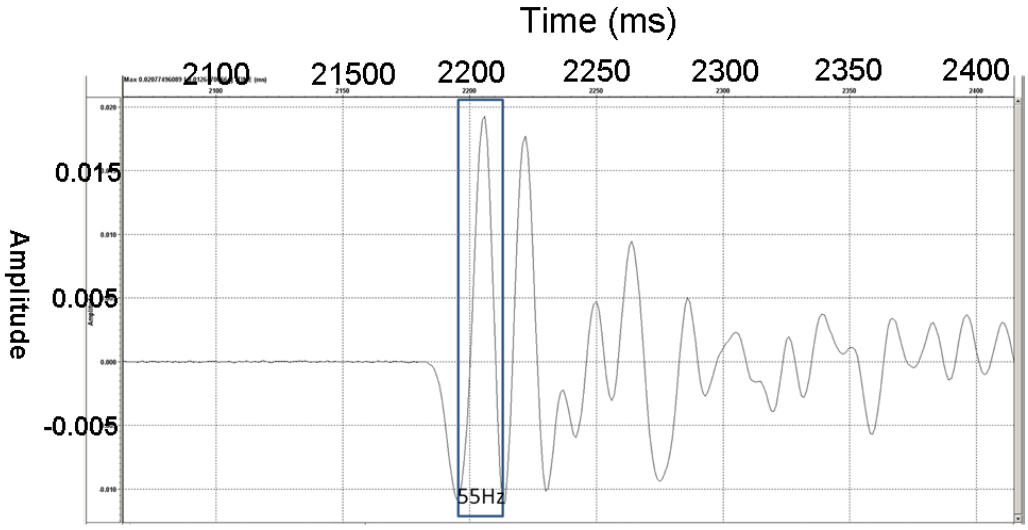

b)

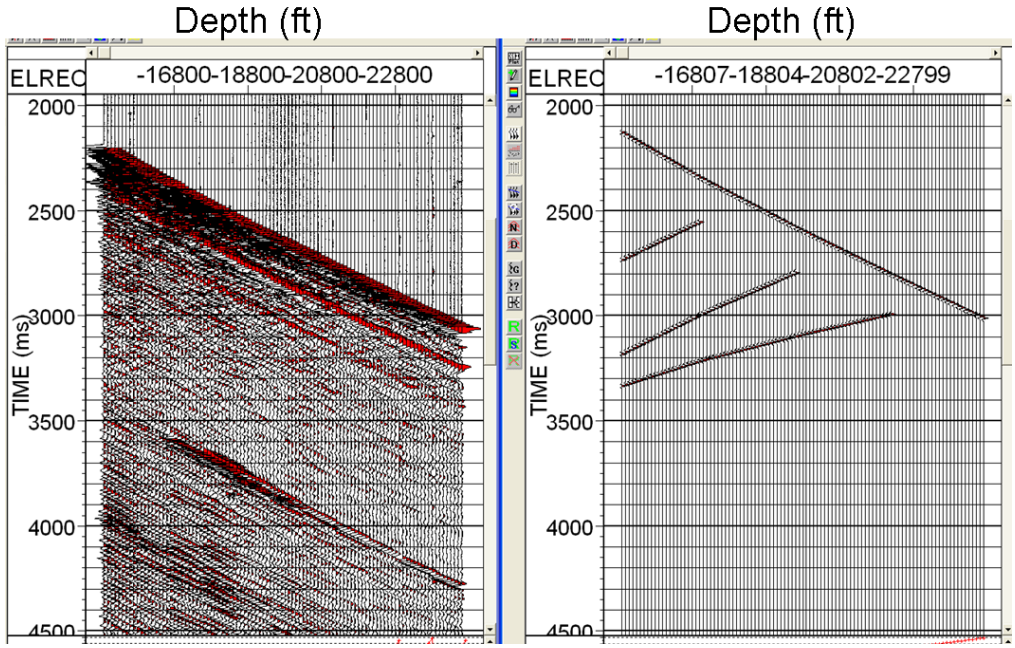

Figure 3-11: a) Wavelet extracted from the VIVSP downgoing wave. b) Synthetic VIVSP (left) compared with the field VIVSP vertical component data (right), displayed with AGC. Synthetic based on P wave only wavefield.

3.4.3 VIVSP Z component wavefield separation by median filter

After subtracting the time delay on each downgoing wave trace, the downgoing waves were flattened at 100ms datum. A median filter was applied to extract the downgoing wavefield using a 21-point window. After subtracting the continuous downgoing wavefield from the total wavefield, the upgoing wavefield has been assessed (Fig. 3-12). There are significant 9 traces step in the figure, because of the 9 shuttle acquisition tool effects. Based on this 9 shuttle step effects, 5-point window will have better wavefield separation result compare to 21-point window. In this step, the 9 shuttle step effects has not been considered.

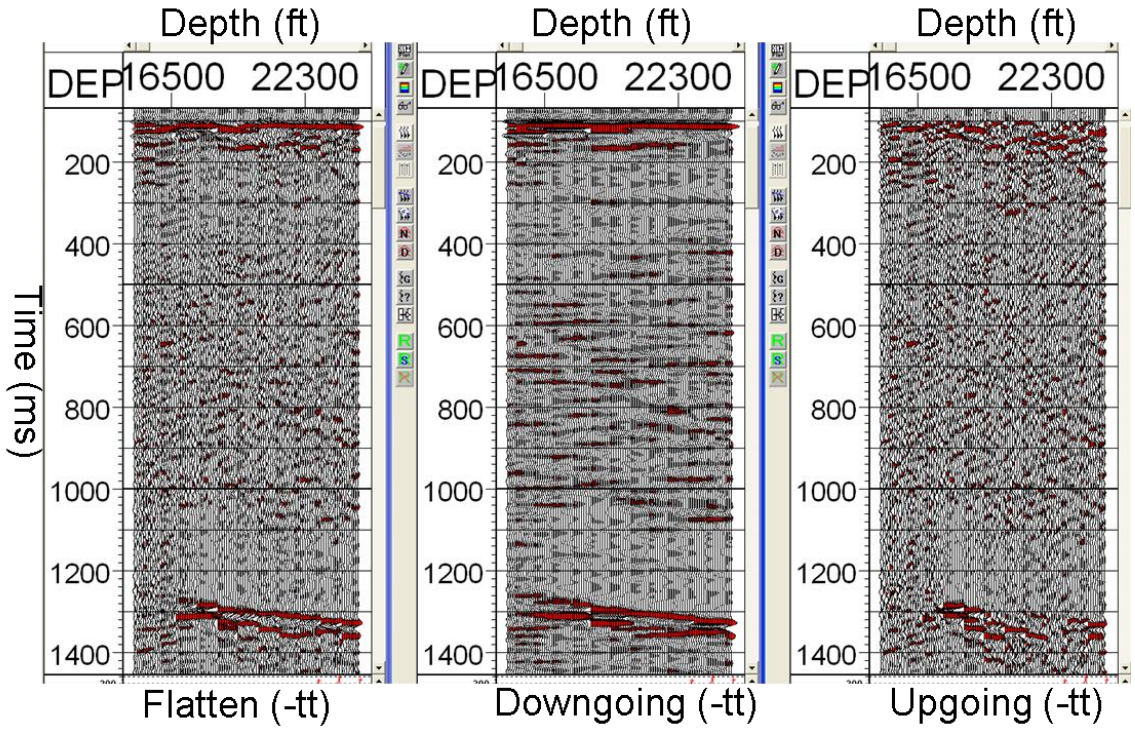

Figure 3-12: VIVSP Z component wavefield separation, displayed with Ormsby filter and AGC.

3.4.4 VIVSP Z component deconvolution

The next step was to deconvolve the data using the downgoing direct wavefield, that represents the source signature, and applying it to the upgoing wavefield to create a zero phase wavefield (Hinds et al., 1999). The deconvolution windows started at 0 ms and extended to 300ms. The deconvolution process appears successful because no significant multiples are apparent in the upgoing wavefield after the deconvolution has been applied (Fig. 3-13).

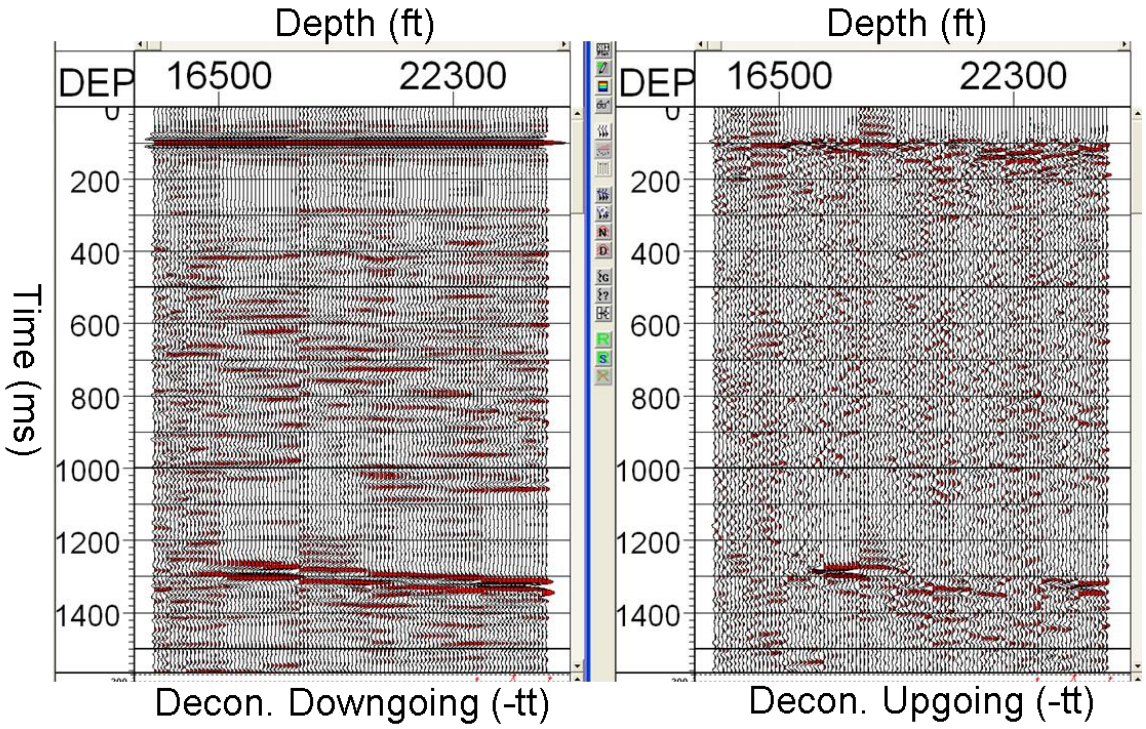

Figure 3-13: a) VIVSP Z component of the upgoing wavefield (FRT) used as input for 300 ms window length Deconvolution; Z component after Deconvolution (FRT), displayed with Ormsby filter and AGC;

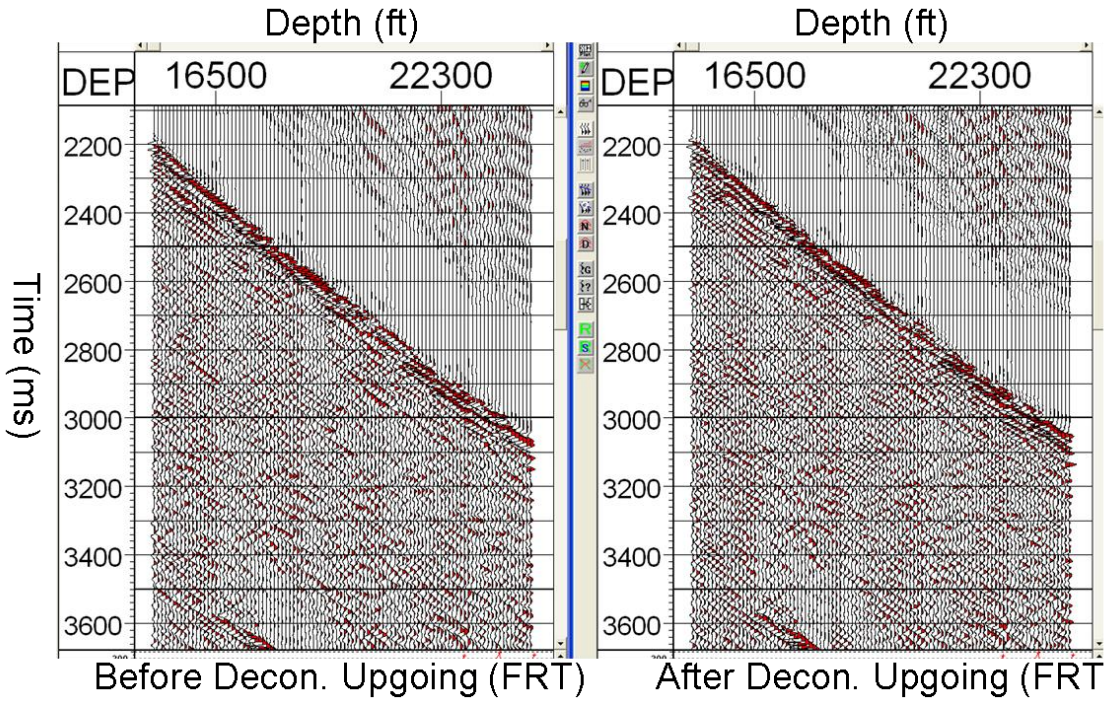

Figure 3-13: b) Z component after Deconvolution (TWT), displayed with Ormsby filter and AGC. Static shift (+) trace by First break time is Two Way Time (TWT), static shift (-) trace by First break time is (-tt). FRT is Field Record Time.

3.4.5 VIVSP CDP mapping

A 40ft bin size has been chosen in this VSP-CDP calculation. This CDP Mapping considers the deviated well geometry, so the dipping structure has been resolved from the CDP Mapping result. The deconvolved Z upgoing wavefield (FRT) is the input, which carries most P wave energy (Fig. 3-14).

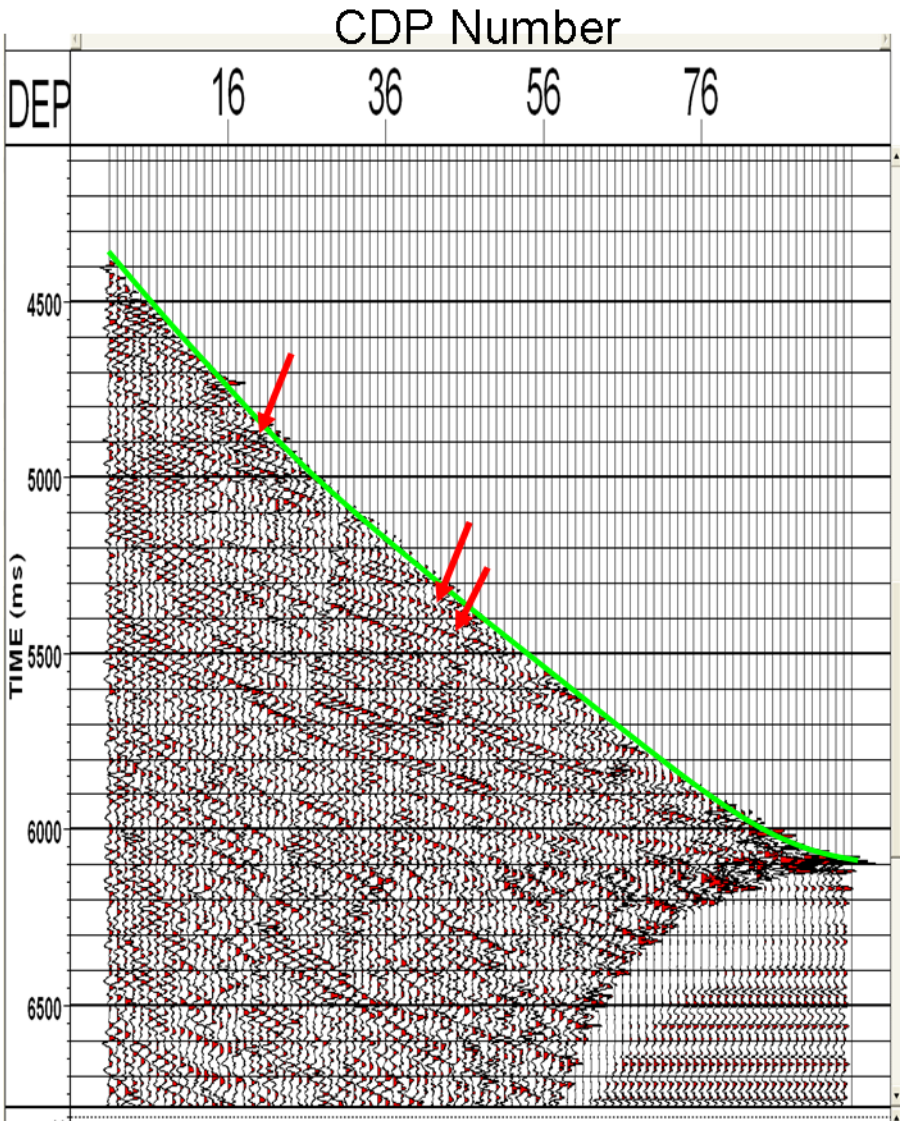

Figure 3-14: 40ft (12m) bin size CDP Mapping shows in two-way time. The well track is highlighted by the green line, there are dipping two reflectors encountered with the well at 17,000ft (5200m) (4.8s), which is the low velocity layer, and it also resolves the events at 20,000ft (6100m) (5.35s) and 20,500ft (6200m) (5.45s) are two different reflection events, which agrees with the schlumberger depth migration result (Appendix 3-1). The three events illustrated by the red arrows. The 20,000ft (6100m) event was interpreted as a gas layer and 20,500ft (6200m) event was interpreted as a tight gas layer from the logging data.

3.5 OVSP synthetic and processing

3.5.1 OVSP acquisition geometry and first break picking (time to depth)

Compared with VIVSP, editing the OVSP geometry is much simpler. The shot location was fixed at 20,000ft (6100m) offset, and sorting for the OVSP data was by shot point number (primary) and elevation of receiver (secondary) (Fig. 3-15). The first break time was picked from each individual component. From the first break of the OVSP data, refractions caused by two layers due to the velocity increase with depth (Fig. 3-16).

If the sediments behave with vertical transverse isotropic, the velocity value from the OVSP should be larger than the VIVSP, since the wave path travels more horizontally in OVSP, compared to the VIVSP wave path, which travels largely vertically through all layers (Fig. 3-17). The OVSP interval velocity curve calculated based on the assumption, when ΔZ is small enough, è does not change (Fig. 3-18),

$$\tan\theta \approx \frac{X_{off}}{Z}$$

$$V_{\text{int}} = \frac{Z_2 - Z_1}{t_2 - t_1}(\cos\theta)$$

The OVSP interval velocity curve from the vertical component shows the velocity increase at 17,000ft (5200m) depth, which agrees with the sonic logging interpretation (Fig. 3-19).

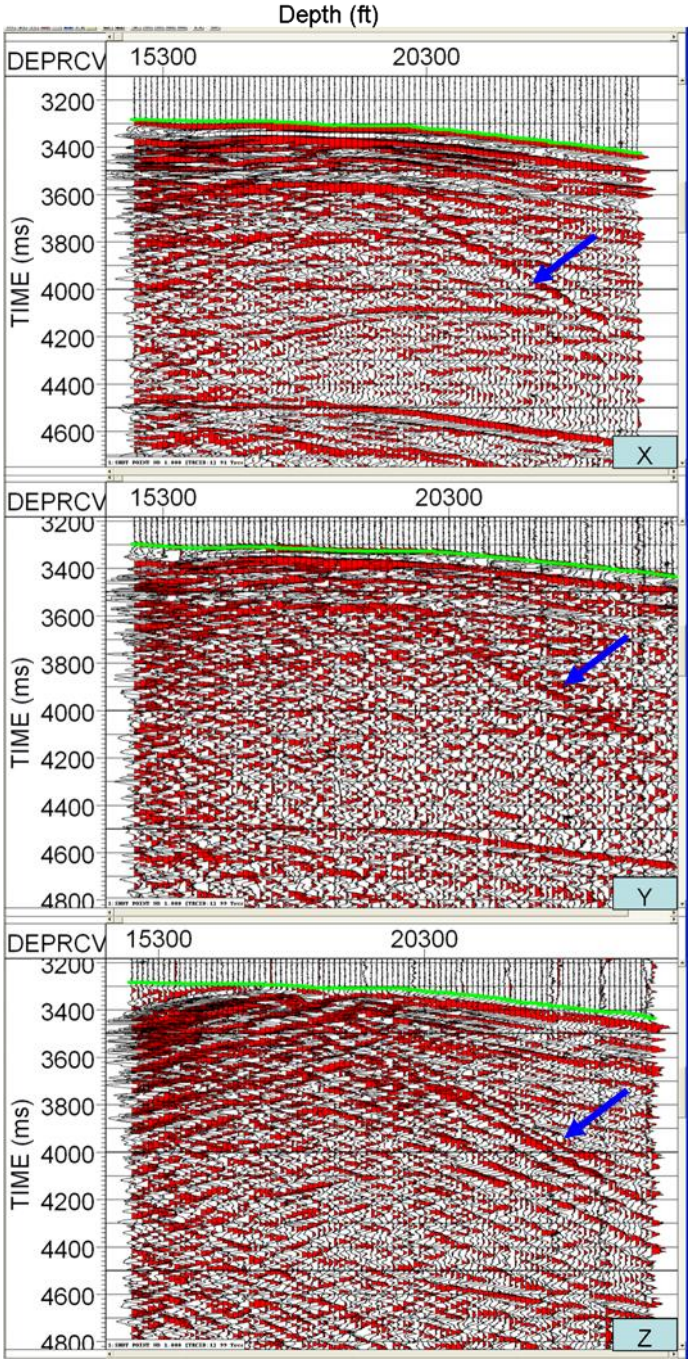

Figure 3-15: Three component OVSP data with first break times, displayed with AGC. The Z component shows stronger downgoing converted waves (PS) than the others, PS-waves are caused by the velocity increase around 17,000ft (5200m). The blue arrows illustrate the PS-transmitted wave.

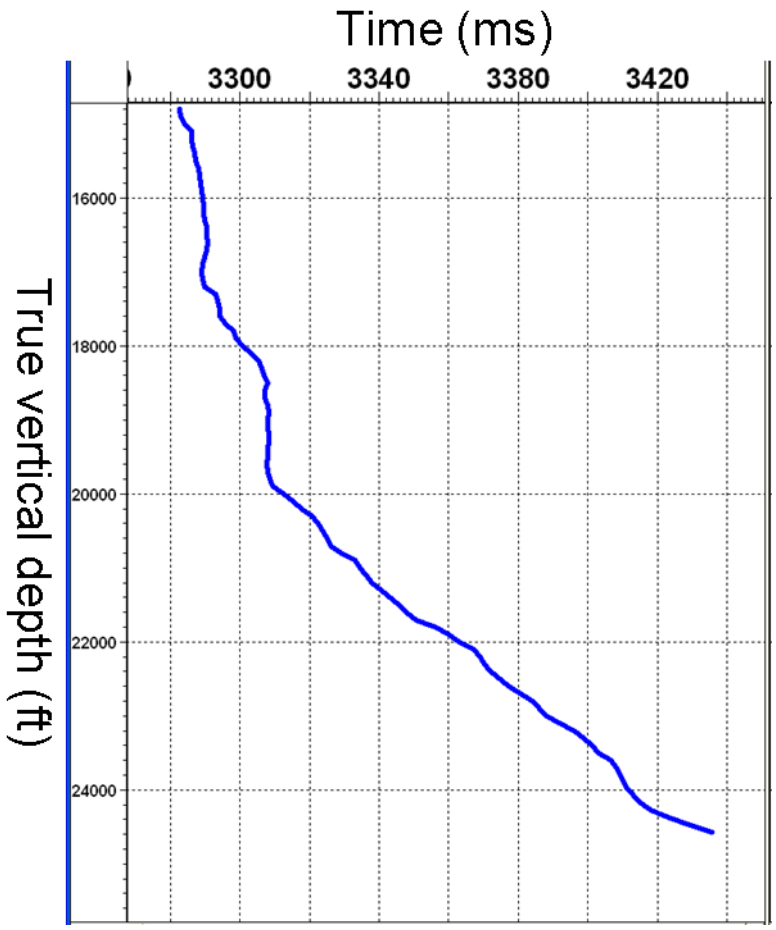

Figure 3-16: True vertical depth versus the first arrival time (one way time) curve.

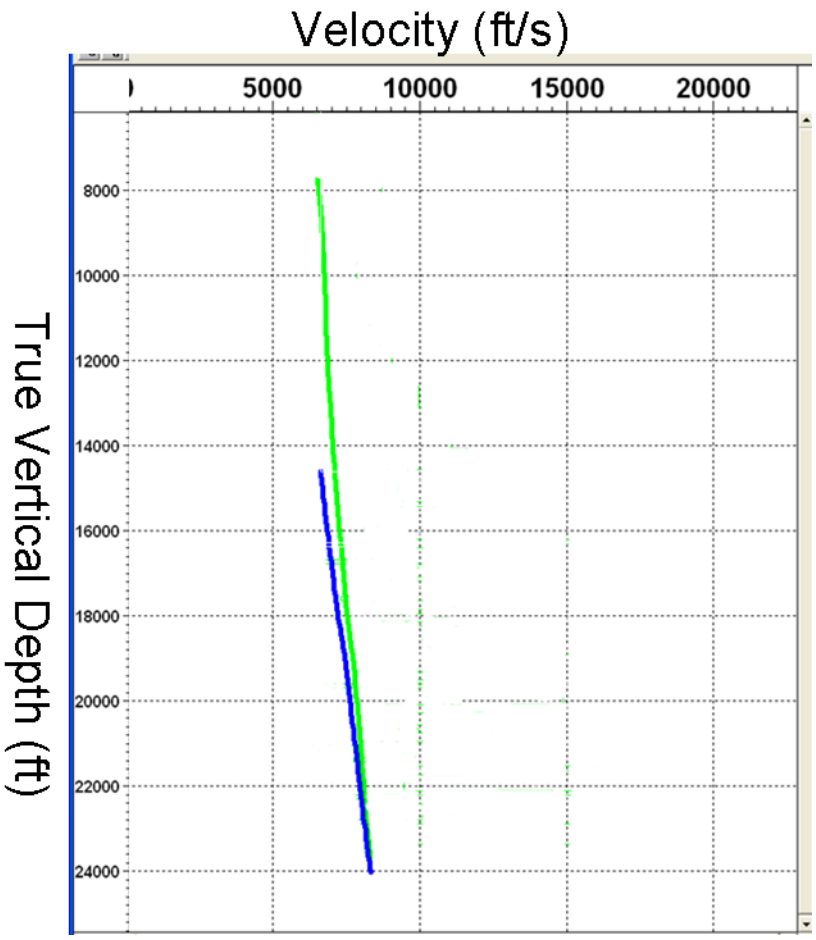

Figure 3-17: The OVSP average velocity (green line) overlay the VIVSP average velocity curve (blue line). VIVSP has lower average velocity compared to OVSP, since VIVSP is the average velocity to each vertical depth, and OVSP is the average velocity toward to the source.

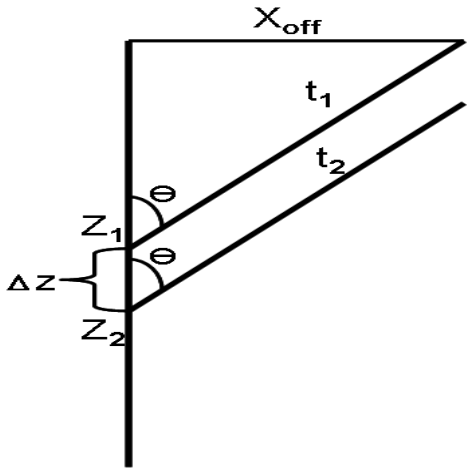

Figure 3-18: Illuminate of OVSP interval velocity calculation.

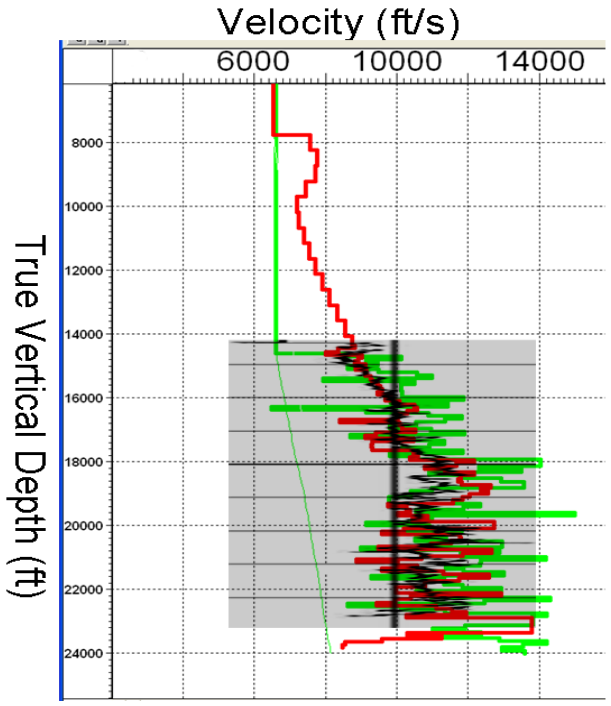

Figure 3-19: The OVSP vertical component interval velocity curve overlay with VIVSP vertical component interval velocity curve. It shows the velocity increasing at 17,000' depth, which agrees with the sonic logging interpretation.

3.5.2 OVSP synthetic generation

A synthetic OVSP was also generated, using a 26Hz Ricker wavelet based on the field OVSP (Fig. 3-20). The synthetic VSPs were compared with the vertical component field VSPs, since the synthetic VSPs just simulate the P wavefield. The difference between the synthetic and field VSPs are caused by the simplification in the synthetic VSPs, and different noise content. To display and process the synthetic VSPs, headers have been created using the depth of receiver and location of the shots. In this study, the synthetic data was used to understand the reflectivity from the existing field VSP geometry.

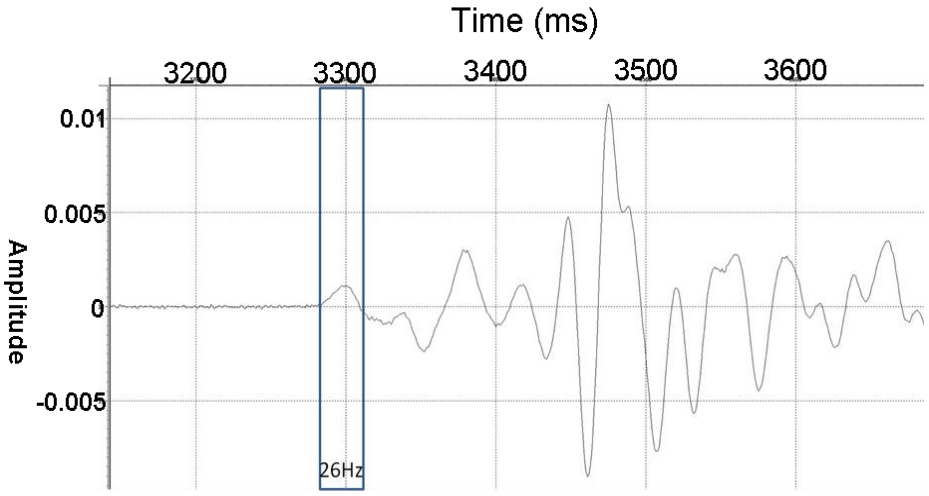

Figure 3-20: a) Wavelet extracted from the OVSP downgoing wave.

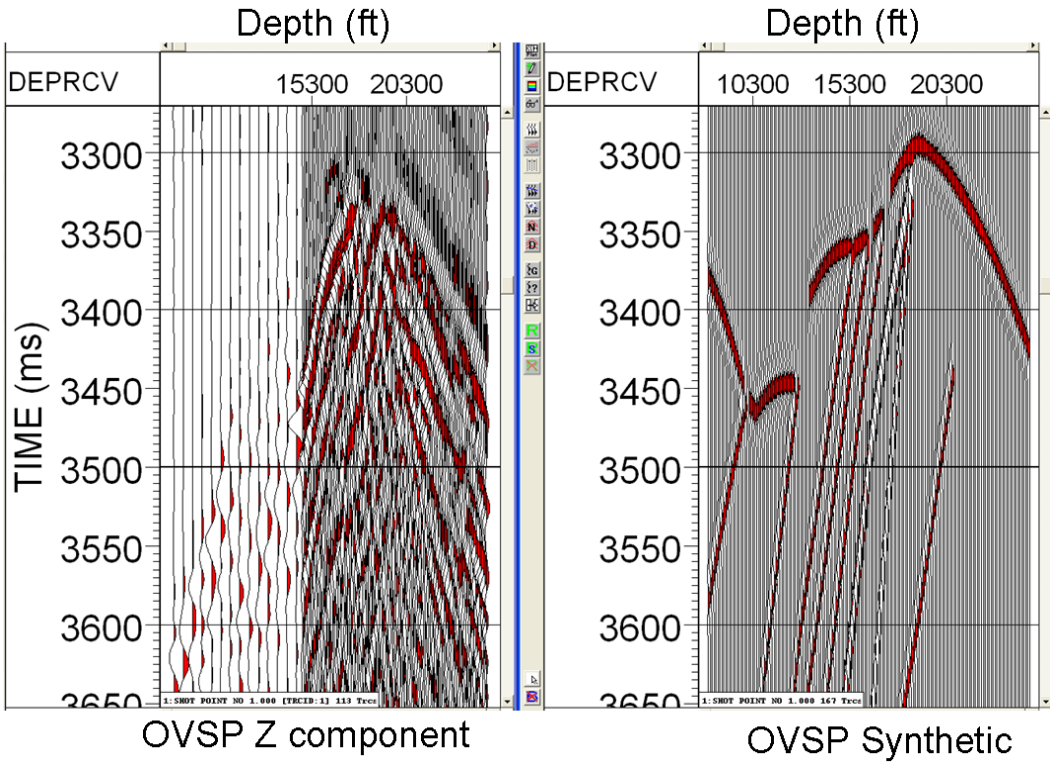

Figure 3-20: b) Synthetic OVSP (right) compared with the field OVSP vertical component data (left). Synthetic based on P wave only wavefield, OVSP Z component displayed with Ormsby filter (10-15-55-60Hz) and AGC. The large time gap at 3.4s caused by the high velocity contrast layer at 12,000ft (3700m) depth with P wave velocity of 9,000ft/s (2700m/s).

3.5.3 OVSP Hodogram rotations and P-P, P-S-S events analysis

The X and Y horizontal components randomly change directions in the borehole. The two horizontal components need to be polarized and corrected for this rotation effect to show consistent upgoing and downgoing wavefields (Fig. 3-21). Two rotations have been performed. First, rotate the X-Y components into well-source plane (Hmax is source-x orientation). Second, rotate the Hmax-Z component, so now Hmax' points to the source and Z' is perpendicular to Hmax'. The Hmax and Z coponents are used to get the mixed P and SV wavefields (Hinds et al., 1999). Z' has strong upgoing P-wave energy and downgoing converted PS-wave energy, and

Hmax' point toward the source, which has strong downgoing P-wave energy and upgoing converted PS-wave energy (Fig. 3-22).

To get the P-wave and S-wave velocities for the Vp/Vs value, the OVSP S-wave arrival have been analyzed as follows: The downgoing S-wave is from P-S transmissions through various high contrast layers. The Hmax' component contains less S wavefield than the Z' component, so the comparison between them provides an understanding of P-S events (Fig. 3-23).

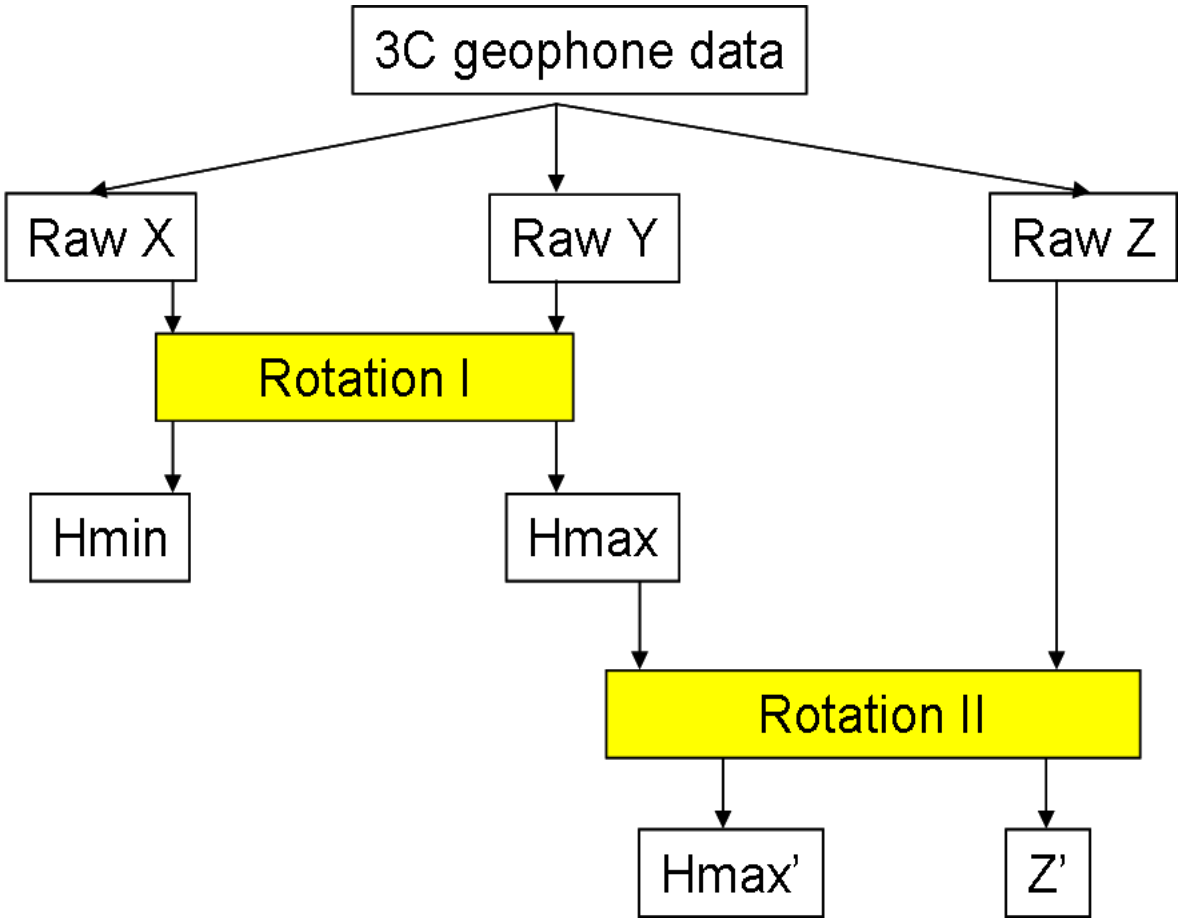

Figure 3-21: Rotation workflow (Adapted from Miong, 2008).

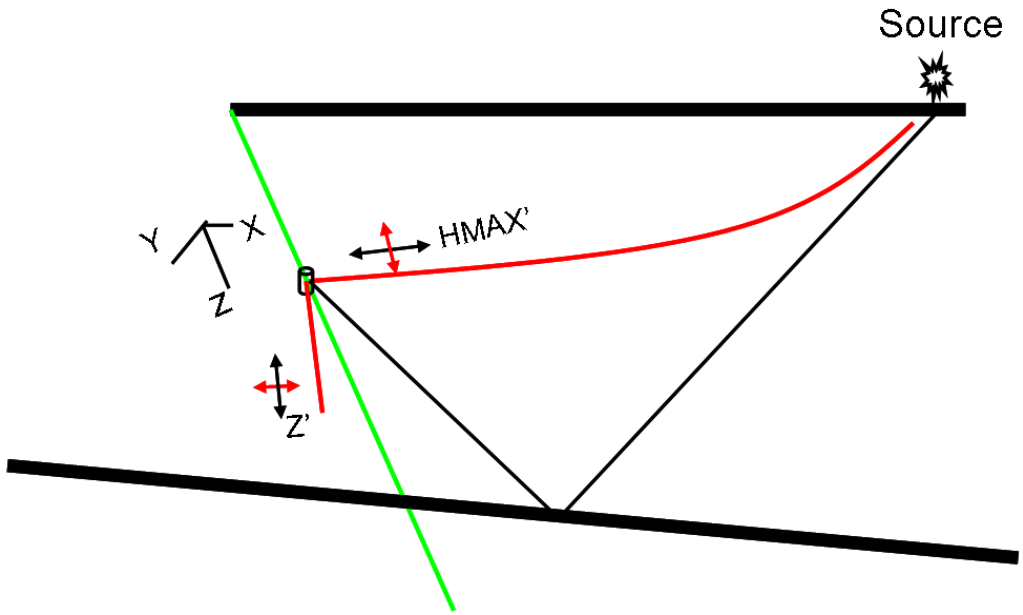

Figure 3-22: a) Illumination of rotation of downgoing and upgoing P, S wave fields from the OVSP geometry. The deviated well shows in green, ray before rotation shows in black line, ray after rotation shows in red line. It shows Z' has strong upgoing P wave energy and downgoing converted PS wave energy, and Hmax' point toward the source, which has strong downgoing P wave energy and upgoing converted PS wave energy.

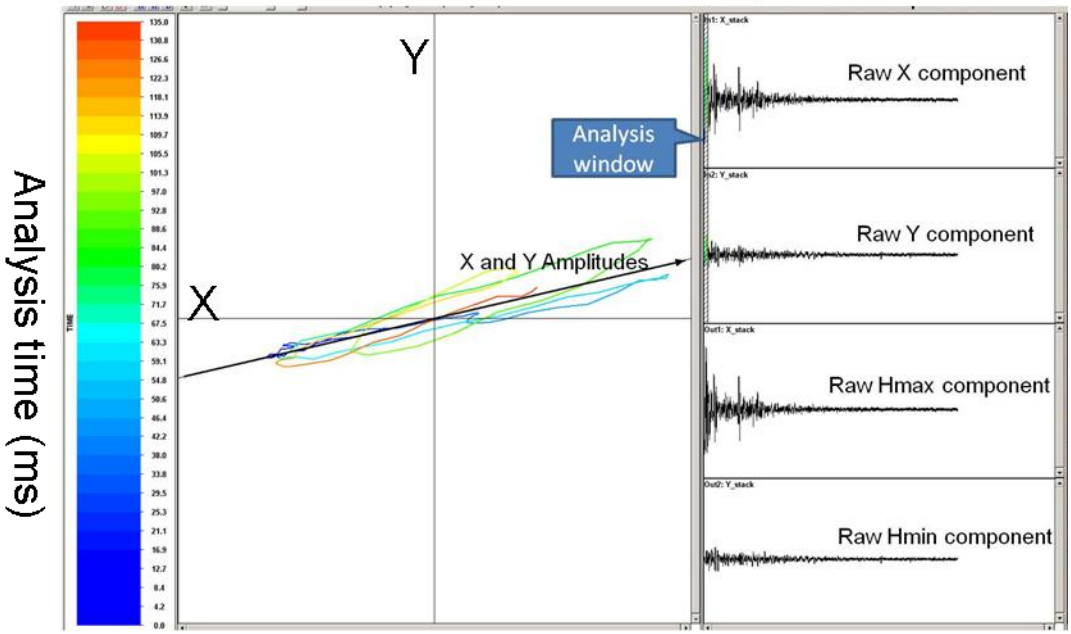

Figure 3-22: b) The hodogram rotation of X and Y components.

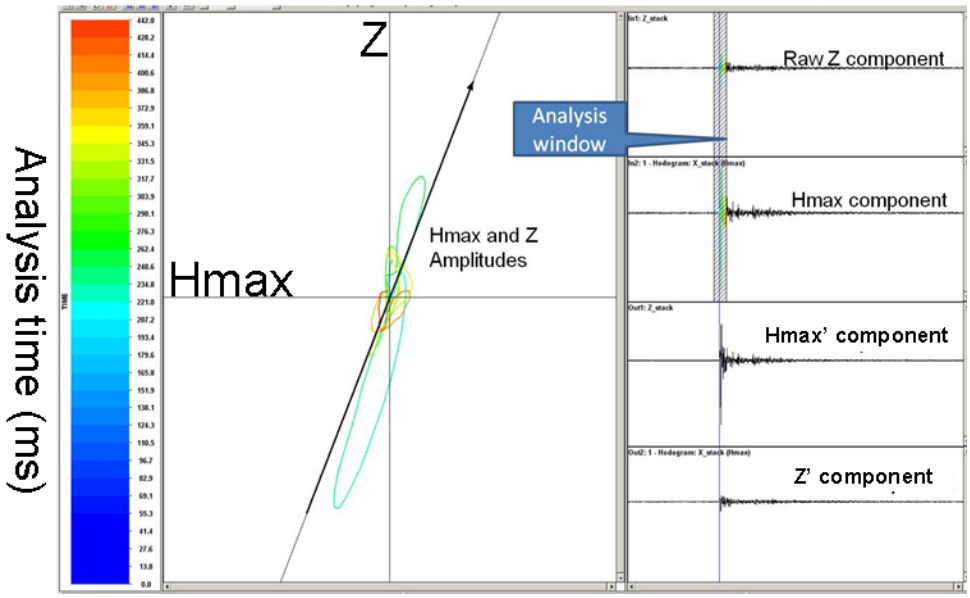

Figure 3-22: c) The hodogram rotation of Hmax and Z components.

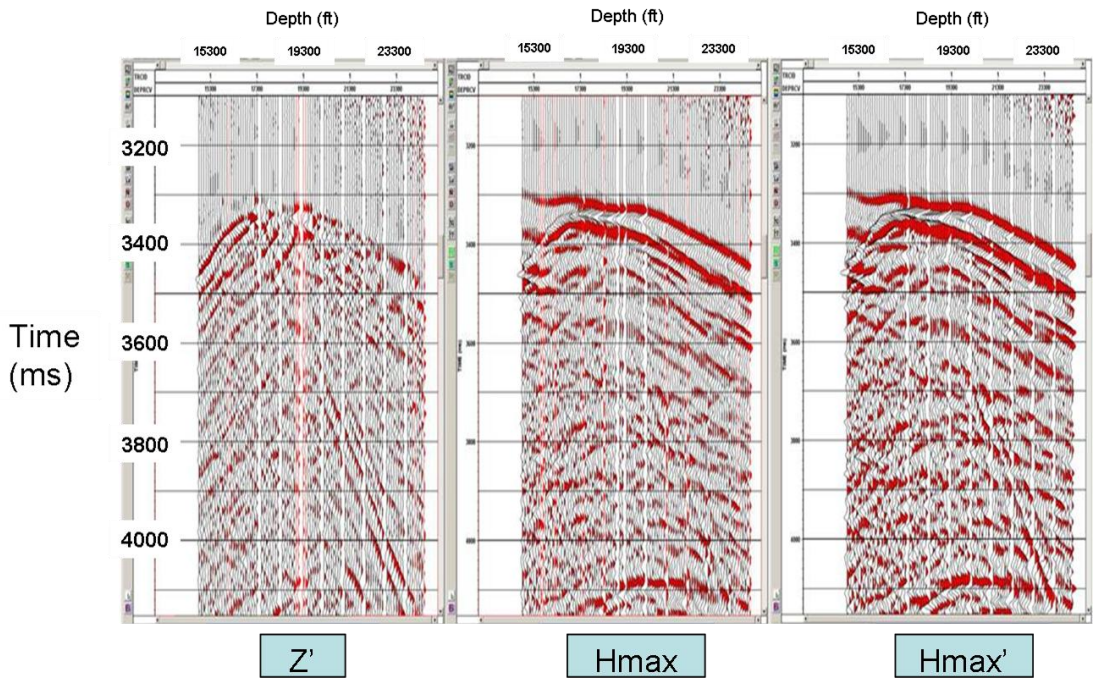

Figure 3-22: d) The rotation result of Z', Hmax, and Hmax', displayed with Ormsby filter and AGC.

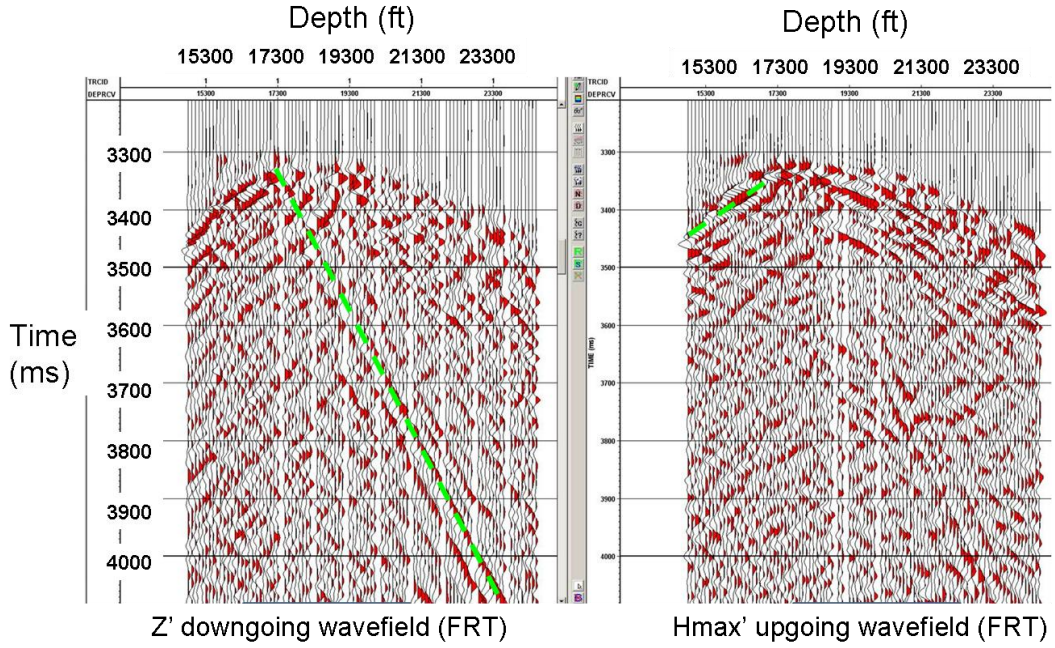

Figure 3-23: Downgoing wavefield of the Z' and upgoing wavefield of the Hmax' components, displayed with AGC. Downgoing and upgoing convert wave (P-S) are shown by the green dashed lines.

3.5.4 Energy partition analysis compare with Zoppritz theory prediction

The converted wave generated at 17,000ft (5200m) depth of velocity increase layer, based on this, downgoing PP-wave, downgoing PS-wave, upgoing PP-wave and upgoing PS-wave energy partitions have been analyzed (Fig. 3-24). The synthetic data based on different wavefields have been generated to determine different wave type arrival times (Fig. 3-25). From the predicted arrival time, the true amplitude has been picking from the 17,000ft (5200m) and 18,000ft (5500m) depth receivers (Fig. 3-26). The Zoeppritz theory amplitude prediction of PP, PS transmitted wavefields, and PP-, PS-reflected wavefields have been calculated by using CREWES Zoeppritz Explorer online module (Fig. 3-27). The PP- and PS-energy partitions field data result and Zoeppritz theory prediction show in table 3-2, they both show upgoing PS-wave has smallest energy, and downgoing PP-wave has highest energy. Downgoing PP-wave and downgoing PS-wave have reversed polarity. Similarly, upgoing PP-wave and ugoing PS-wave have reversed polarity.

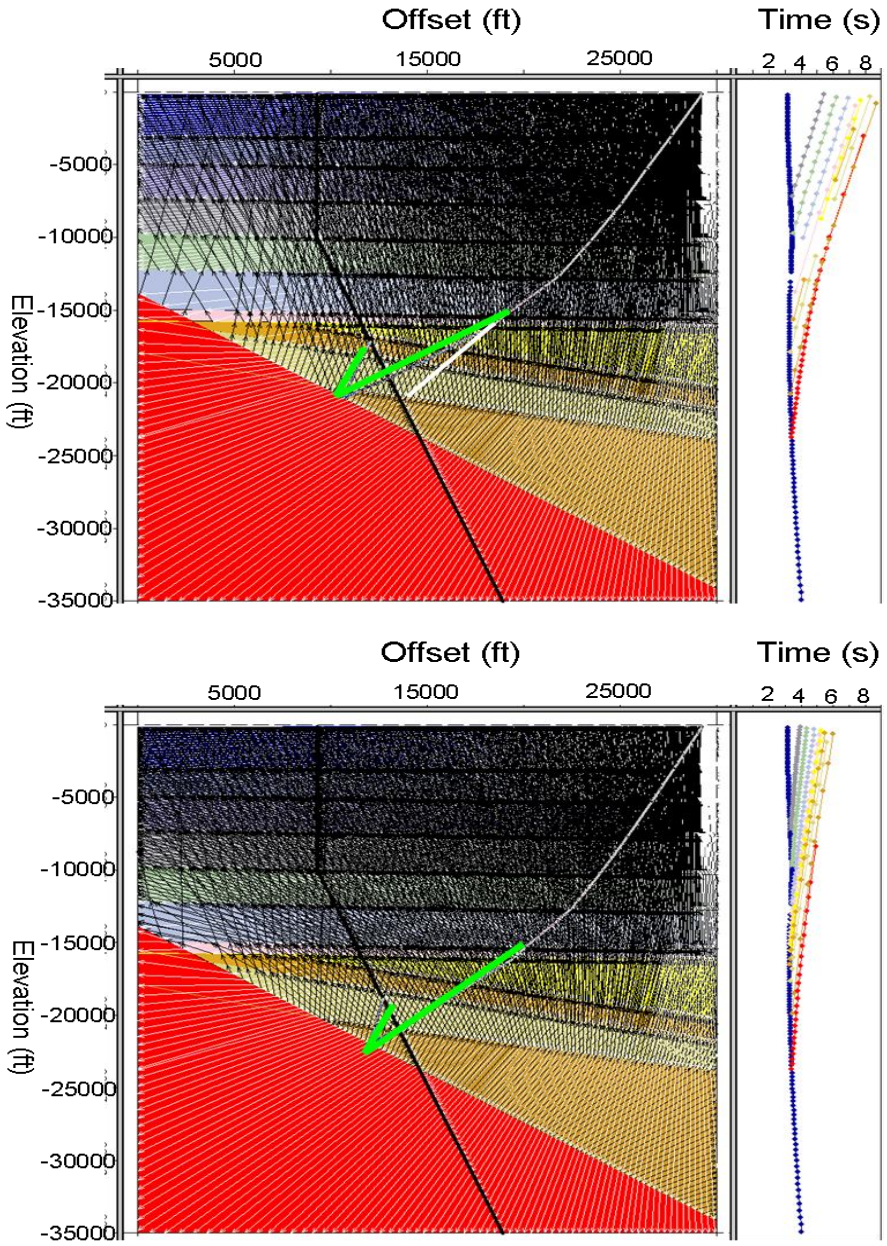

Figure 3-24: Analysis of the energy partition around 17,000ft (5200m) (layer of increased velocity). Upper: Ray tracing of converted wave field, the downgoing PS-wave is highlighted by the white line, the upgoing PS-wave is highlighted by the green line. Lower: Ray tracing of P wave field, the upgoing PP-wave is highlighted by the green line. The rays have been selected for PP upgoing wave and PS upgoing wave, because of their same reflection angle.

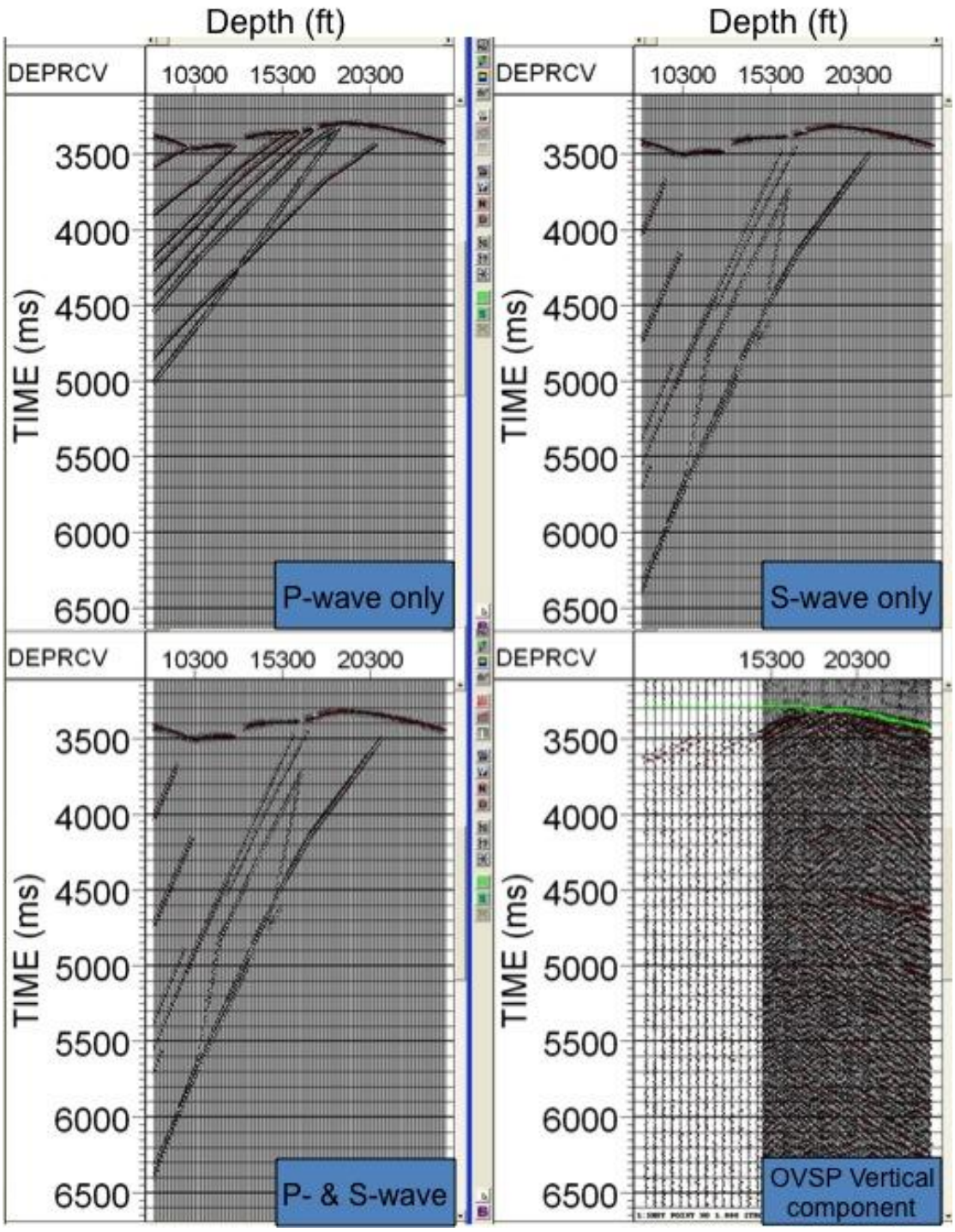

Figure 3-25: The synthetic data based on different wavefields, used to determine different wave type arrival times, these time are used for picking the amplitude of different wave partitions from the OVSP vertical component. Synthetic OVSP data displayed with AGC (500ms window length), OVSP vertical component displayed with Ormsby filter (10-15-55-60Hz) and AGC (500ms window length).

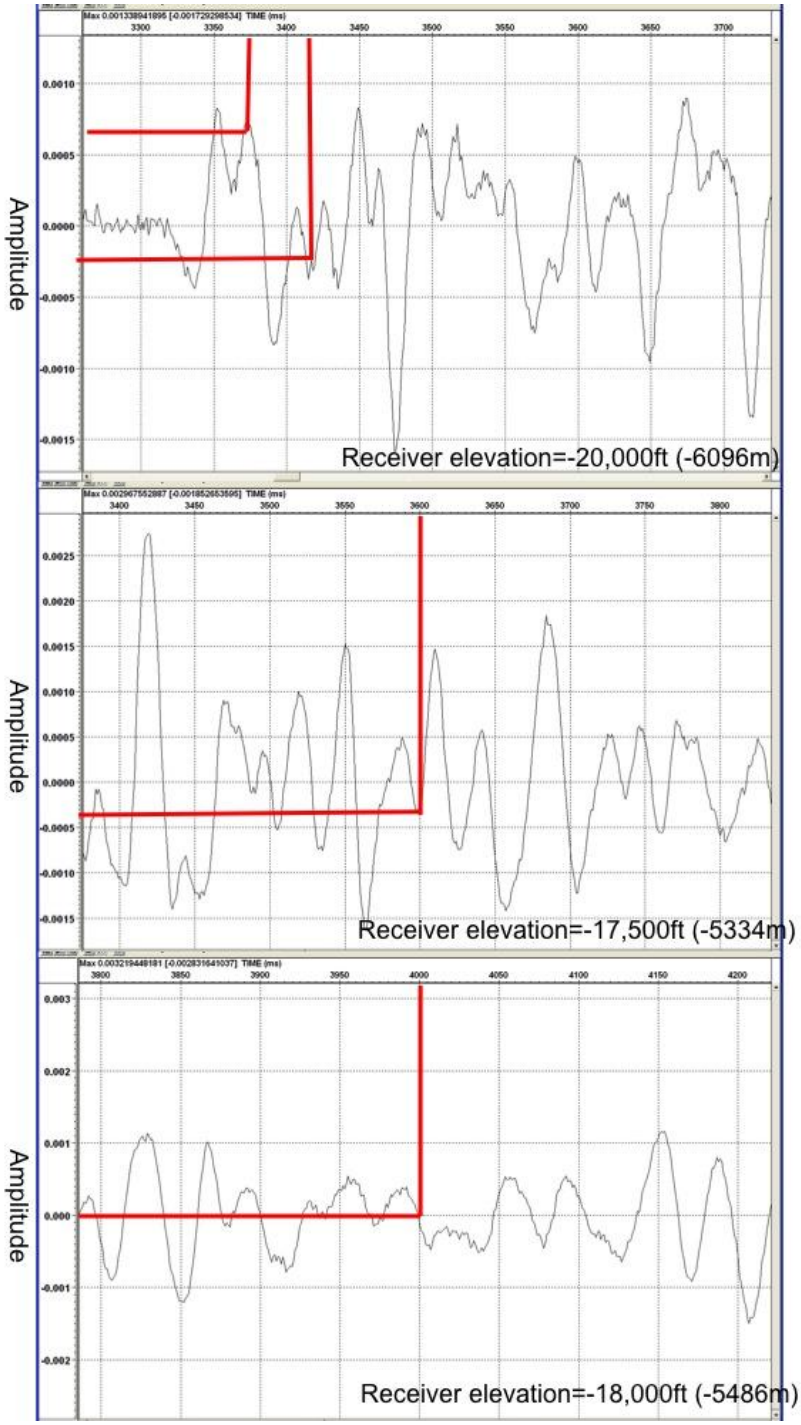

Figure 3-26: The amplitude picking from three different receivers using receiver depth from the ray tracing model and times from the synthetic data. PP & PS downgoing amplitude picked from 20,000ft (6100m) depth receiver. PP upgoing picked from 17,500ft (5300m) depth receiver, and PS upgoing picked from 18,000ft (5500m) depth receiver.

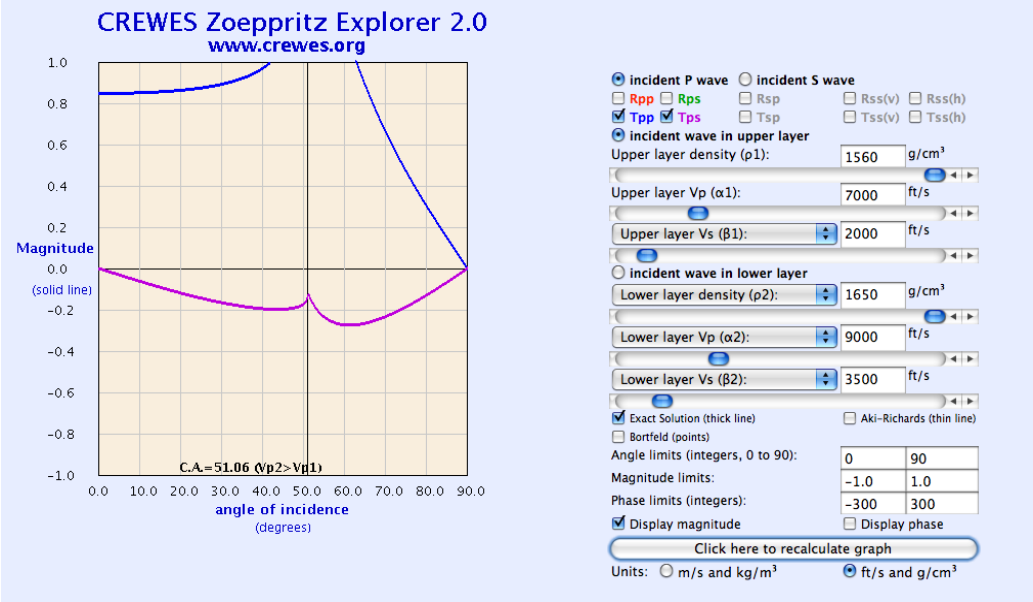

Figure 3-27: a) Zoeppritz theory prediction of PP (blue) and PS (purple) transmitted wave amplitudes at various incident angles, The transmitted PP wave amplitude increases from 0-40deg, then no transmitted PP wavefield until 63deg, from 63-90deg, its amplitude decreases from 1 to 0. The transmit PS wave negative amplitude magnitude increase from 0-50deg, and then decrease from 50-90deg;

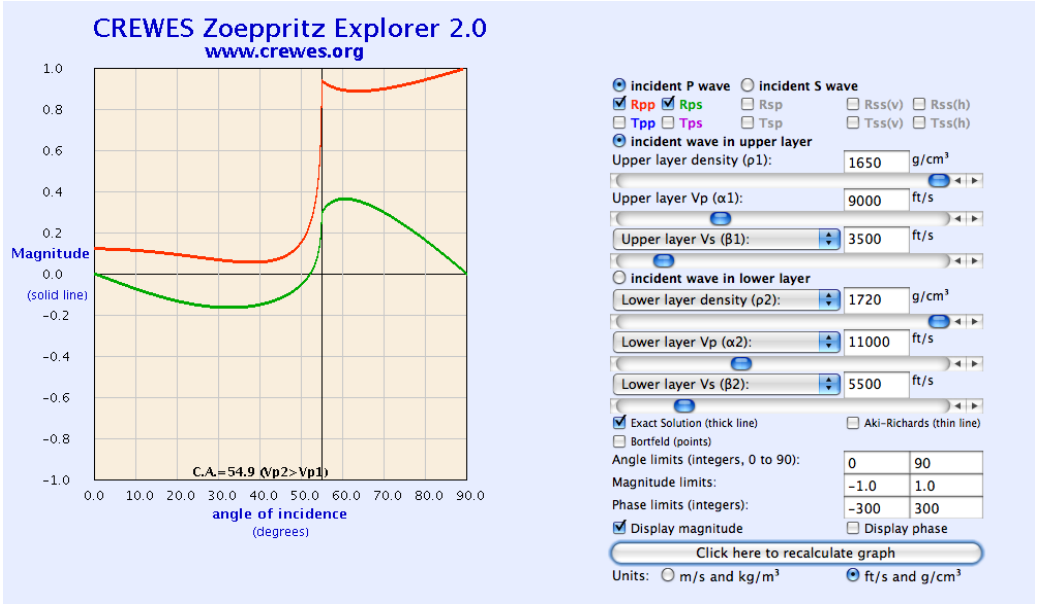

Figure 3-27: b) Zoeppritz theory prediction of PP (red) and PS (green) reflected wave amplitudes at various incident angles. The reflected PP wave amplitude slightly decreases from 0-50deg, and then jumps to 1 at 55deg. The reflected PS wave amplitude stay negative until 55deg, and then the positive amplitude decreases from 55-90deg.

Wave type	Receiver depth	Predict arrival time (s)	Picked amplitude	Theory amplitude
Downgoing P wave (Tpp)	20,000ft (6096m)	3.38s	0.0007	0.95
Downging PS wave (Tps)	20,000ft (6096m)	3.42s	-0.00025	-0.5
Upgoing PP wave (Rpp)	17,500ft (5334m)	3.5s	-0.0004	-0.25
Upgoing PS wave (Rps)	18,000ft (5486m)	4s	0	0

Table 3-2: the PP and PS energy partitions of reflected and transmitted waves around the velocity increase depth (17,000ft (5200m)) from field data and the Zoeppritz equation.

3.5.4 OVSP P-P wave processing— Hmax' component first break picking

After rotation, the Hmax' component contains most of the downgoing P wave energy, it has been chosen to process into P-P CDP mapping. Figure 3-28 shows the first break picks, the turning waves are caused by refractions.

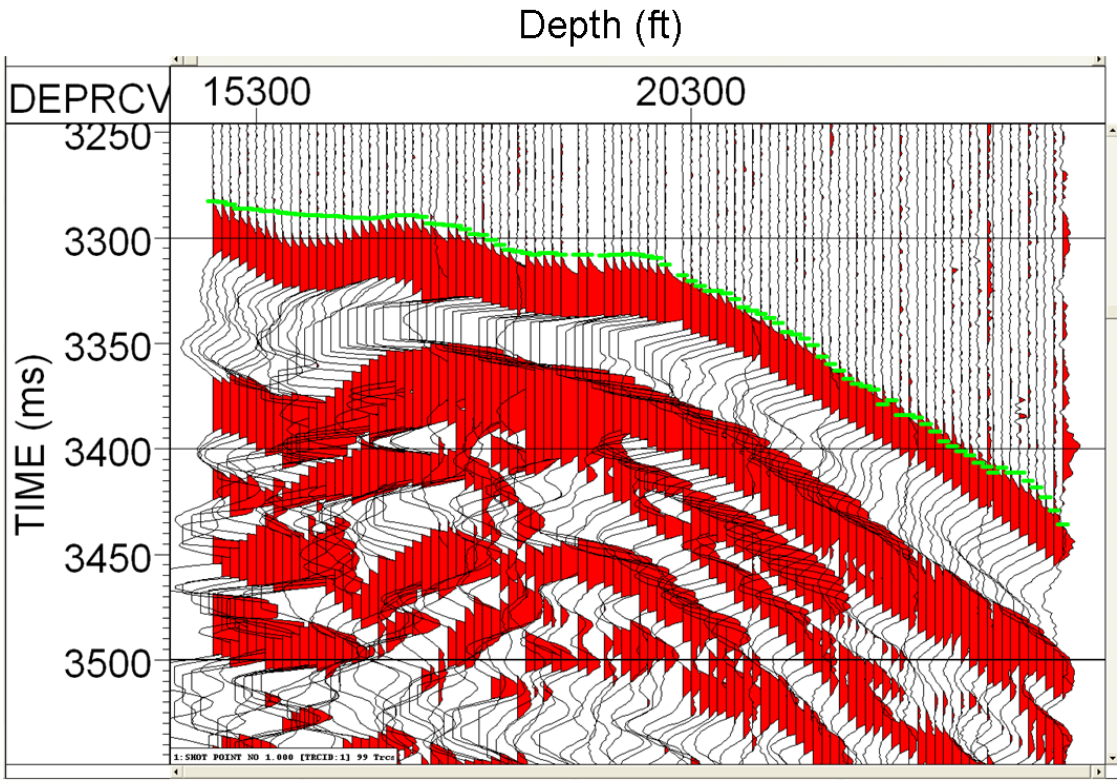

Figure 3-28: Hmax' component has first break picks in green. The first arrivals for the shallower receivers are caused by refractions (displayed without Ormsby filter and AGC).

3.5.5 OVSP Hmax' component wavefield separation by median filter

After flattening the total wavefield, a mean scaling is applied to enhance the first break amplitude before separation. The mean scaling is used to calculate a scale for each trace sample, which is then multiplied by the trace in a particular window (95-105ms to cover the flattened first break at 100ms in this study). A 17-point median filter was applied to separate the upgoing wavefield from the scaled, flattened wavefield. Then the upgoing wavefield was shifted back to the field record time (FRT) (Fig. 3-29).

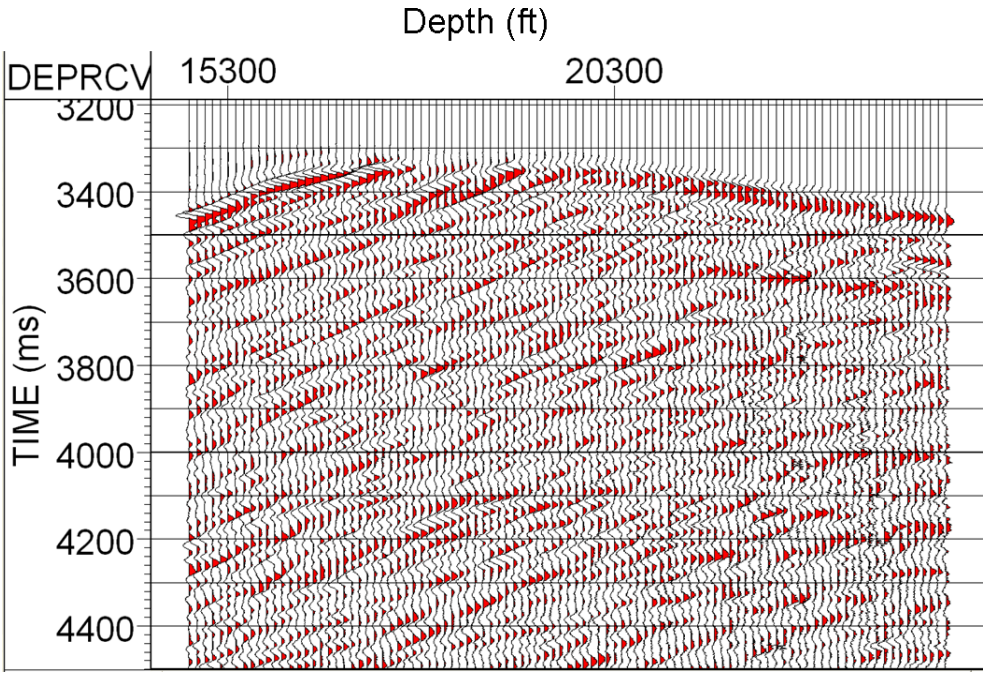

Figure 3-29: Hmax' component upgoing wavefield (FRT) after wavefield separation, displayed with Ormsby filter and AGC.

3.5.6 OVSP Hmax' component Deconvolution

A deconvolution operator window, 0-100ms in this case, is designed from the downgoing wavefield and applied to the upgoing wavefield. The deconvolution process appears successful because no significant multiples are apparent in the upgoing wavefield, which results in better-defined reflection events (Fig. 3-30).

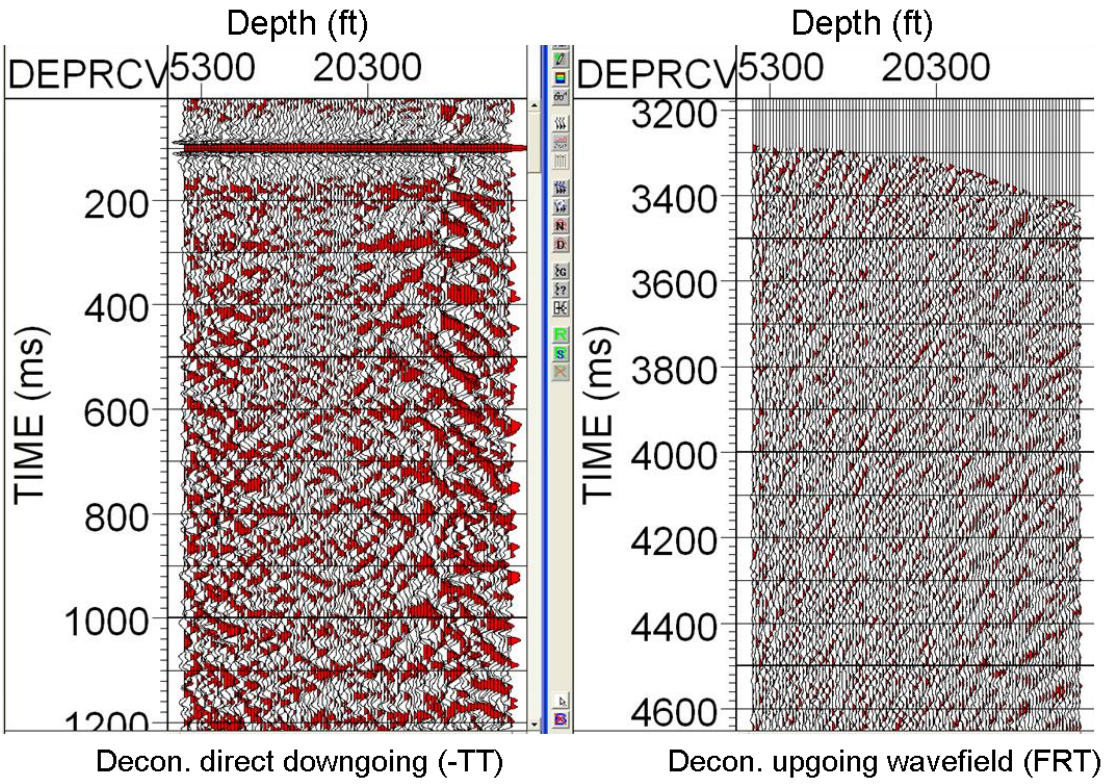

Figure 3-30: Hmax' component upgoing wavefield deconvolution (FRT), displayed with Ormsby filter and AGC.

3.5.7 OVSP Hmax' component CDP mapping

The VSP-CDP image can be built by mapping the seismic amplitudes from the receiver traces in the time domain to their spatial location. The data are trace-resampled to properly position the reflection points away from the well. The coverage is from the well out to about ½ of the shot offset. VSP-CDP is a conversion from depth of receiver and travel time to reflection point and offset (Fig. 3-31). The standard procedure for VSP-CDP mapping involves retracing through a P-wave velocity model to map the spatial locations of reflections. The algorithm takes sample

i of the trace (time=dt * i), gets the depth of that sample, then ray traces from the source to reflection point position by equal angles. The offset XB of the reflection point from the well for a P-wave arrival over an isotropic single-layer model is given in Stewart (1985) as,

$$X_B = \frac{x}{2}\left[\frac{vt_v - 2z}{vt_v - z}\right]$$

where x is the source-receiver offset, v is the velocity, tv is the normal incidence time of reflection, and z is the depth of the receiver.

A 150ft (45m) bin size has been chosen in this VSP-CDP calculation. One assumption is the time-depth function extends laterally from the well horizontally, thus if there is any structure the algorithm is not correct, so VSP-CDP is a zero dip migration.

The deconvolved Hmax' upgoing wavefield (FRT) is the input, since it has been rotated toward the source, it has the most downgoing P wave energy. The VSP-CDP mapping uses the receiver depths and the first break picks, which have to be edited in the data header. During the operation, the sorting selected is trace ID, since the algorithm operates trace by trace (Vista help) (Fig. 3-32).

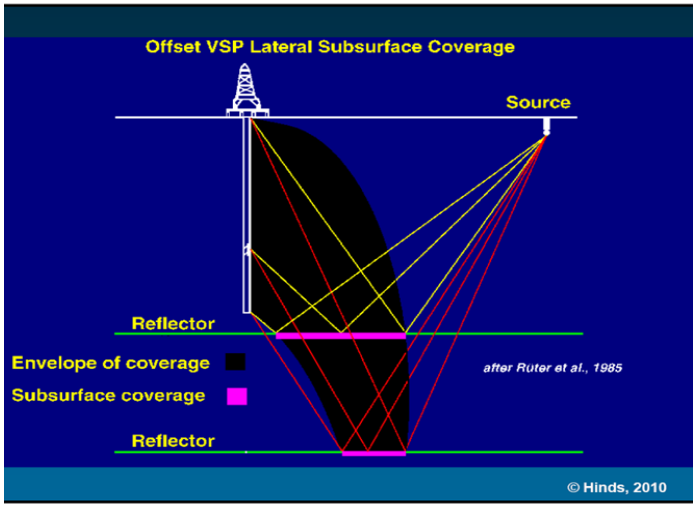

Figure 3-31: Illustration of far offset VSP-CDP mapping (Hinds, 2010)

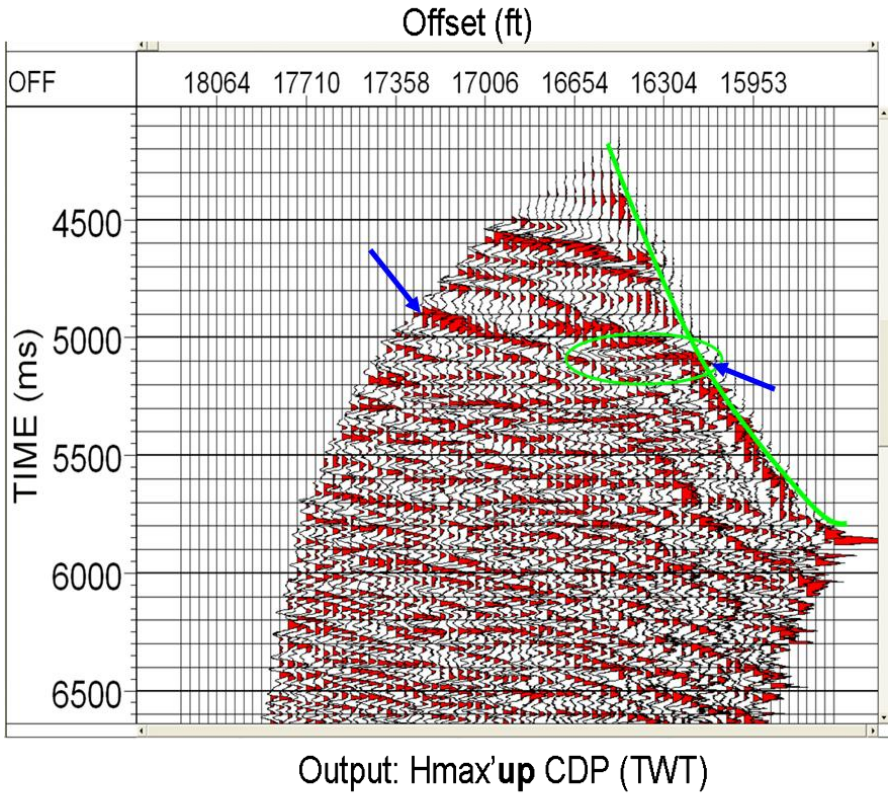

Figure 3-32: Hmax' upgoing wavefield OVSP-CDP mapping (TWT), Those flatten events means corrected velocity model. The result shows a continuous reflection at 17,000ft (5200m) (4.8s), which is the low velocity layer. There is a high amplitude layer at 19,000ft (5800m) (5.2s) and amplitude decease with offset increases. The two events illustrates by blue arrows.

3.6 VIVSP & OVSP AVO evaluations

The ray illumination technique was employed to investigate the fold, offset, and incident angle information within one bin. From the ray tracing model and analysis, bin A, from the existing VSP survey geometry, has the highest fold and widest incident angle range (Fig. 3-33). There are three shot-receiver pairs covered in bin A, which have 520ft (160m), 760ft (200m), and 2050ft (600m) offsets (Table 3-3). Based on the Zoeppritz equations for AVO calculation, those three offsets are not enough to get reliable AVO information (Fig. 3-34).

Bin size	100 × 100ft (30 × 30m)
Fold	6
Minimum offset	0ft (0m)
Maximum offset	20,000ft (6096m)
Variation offset	520ft (158m), 760ft (230m), 2050ft (625m)

Table 3-3: Existing VSP survey parameters.

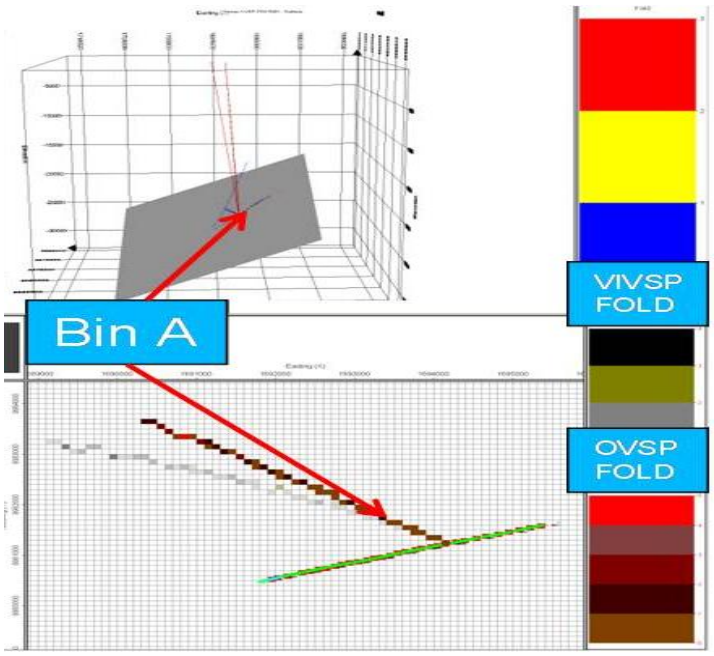

Figure 3-33: The field VSP geometries fold & offset analysis. The model was based on the field grid, which from N-S (Y) covers 9970000-9990000ft (3038800-3044900m), and from E-W (X) covers 1685000-1705000ft (513500-519600m).

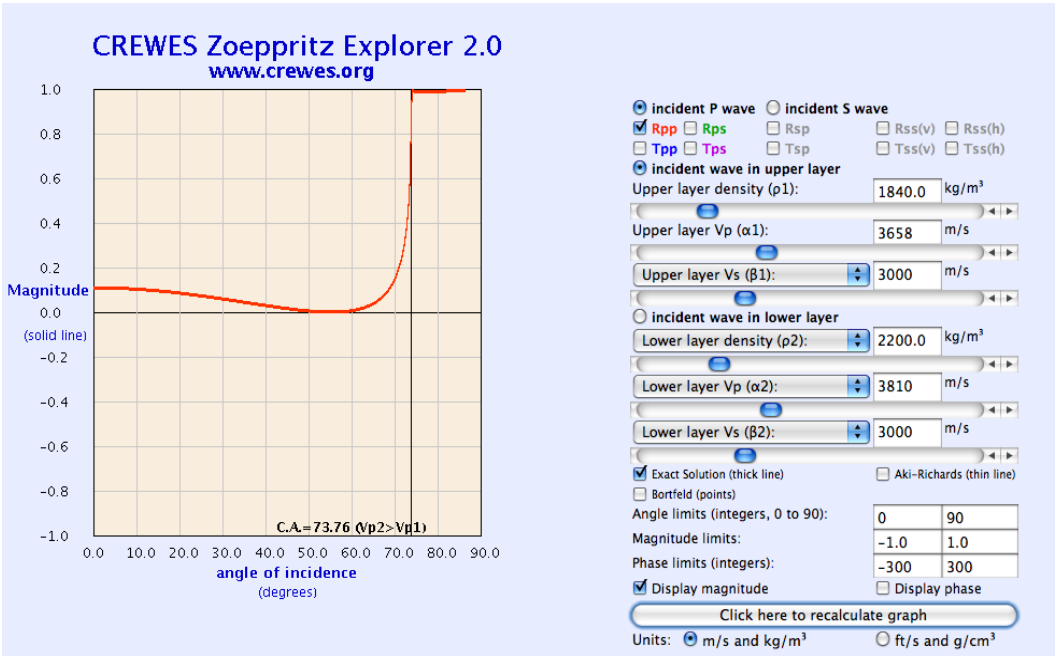

Figure 3-34: Theoretical Zoeppritz AVO value calculation in the Garden Banks target zone (from Crewes.org Zoeppritz explorer).

3.7 Walk-away VSP design for AVO analysis

For better AVO information, the walk-away VSP acquisition geometry listed in Table 3-4 was tested. In this walk-away VSP the source is moved along the surface and the receivers are fixed along the bushwood well from 14,800ft (4500m) to 24,700ft (7500m). From the ray tracing model and analysis, bin B, from this walk-away VSP survey geometry, has the highest fold and widest incident angle range (Fig. 3-35). There are six shot-receiver pairs covered in bin B, which have 800ft (250m), 1200ft (350m), 1500ft (460m), 1870ft (570m), 2240ft (680m), and 2610ft (800m) offsets (Table 3-5). This means that the AVO information can be achieved from this synthetic walk-away VSP dataset. The theoretical AVO value has been calculated in Figure 3-28. The AVO information can be further processed into lithologic information, such as the Lambda parameter, which can indicate lithology and pore-fluid values (Dumitrescu and Lines, 2007). The P-wave and S-wave velocities are naturally linked closely to rock properties, and are amenable to estimation from AVO analysis.

Shot number	Offset (N136E)
1	9,400ft (2865m)
2	11,800ft (3597m)
3	14,000ft (4267m)
4	16,100ft (4907m)
5	18,000ft (5486m)
6	20,000ft (6096m)

Table 3-4: Walk-away VSP geometry.

Bin size	25 × 25ft (7 × 7m)
Fold	30
Minimum offset	0ft (0m)
Maximum offset	20,000ft (6096m)
Variation offset	800ft (244m), 1200ft (365m), 1500ft (457m), 1870ft (570m), 2240ft (683m), 2610ft (795m)

Table 3-5: Walk-away VSP survey parameters.

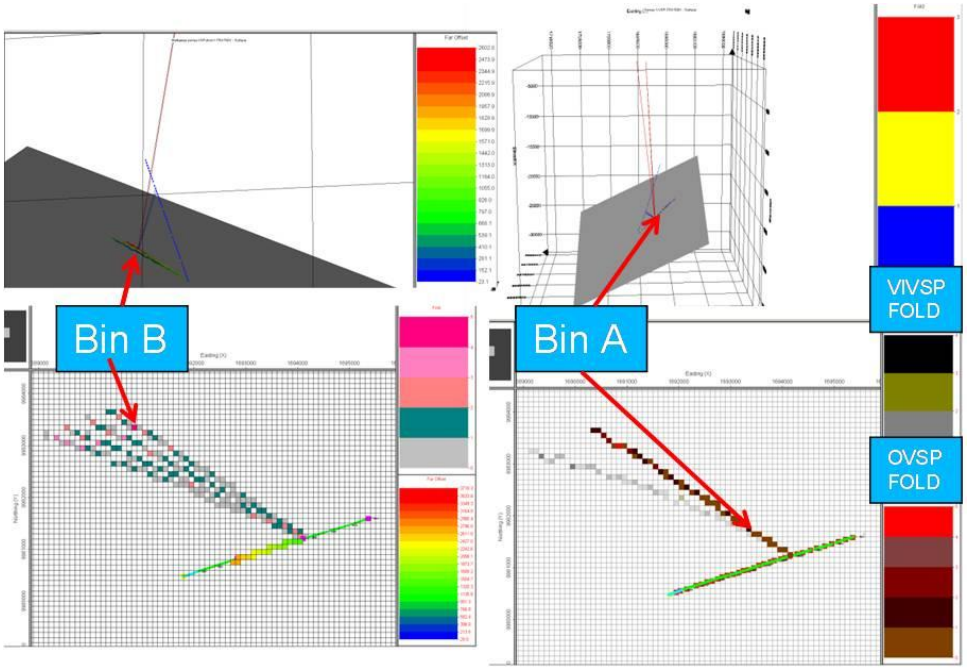

Figure 3-35: Comparison of the field and walk-away VSP geometries using fold & offset analysis. The model was based on the field grid, which from N-S (Y) covers 9970000-9990000ft (3038800-3044900m), and from E-W (X) covers 1685000-1705000ft (513500-519600m).

3.8 Discussion and conclusions

In VIVSP processing, the vertical Z component has the strongest P-P reflectivity. To isolate the upgoing wavefield, a 21-point median filter was applied. Deconvolution was performed on both the downgoing and upgoing wavefields. After deconvolution, sharper and better defined reflection events were produced.

In OVSP processing, rotations have been applied to access the strong P wavefields. A 17-point median filter was applied to separate the wavefields. A 100ms deconvolution operation window was applied to better define reflection events. A VSP-CDP mapping was applied to show the spatial distribution of the reflections by offset.

The velocity logging data at 17,000ft (5200m) depth shows a velocity increase from 10,000ft/s (3000m/s) to 12,000ft/s (3600m/s), this layer of increased velocity causes converted wavefields. Similarly, the OVSP interval velocity profiles show an increase at around 17,000ft (5200m). Based on this, downgoing P-wave, downgoing PS-wave, upgoing PP-wave and upgoing PS-wave energy partitions have been analyzed to compare their amplitude with the theoretical calculation from the Zoeppritz equation.

There are strong converted S-wave (P-S-S) reflections that have been detected after rotation. This means the P-S-S section can be processed. Besides the converted wave processing, the P-S-S incident angle can be tested for AVO potential evaluation, since the converted S wave reflection angle is smaller than the P-wave reflection angle (Stewart, 2002). In this study, the VSP-AVO potential has been tested, low incident angle range and low fold mean there is not enough information to perform AVO analysis based on the P-wavefields. A walk-away VSP design has been suggested and analyzed that would get better AVO information.

From the VIVSP-CDP mapping result, there are two dipping reflectors encountered with the well at 17,000ft (5200m) (4.8s), which is the low velocity layer, and it also resolves the events at 20,000ft (6100m) (5.35s) and 20,500ft (6200m) (5.45s) are two different reflection events, which agrees with the Schlumberger depth migration result.

From the OVSP-CDP mapping result, shows a continuous reflection at 17,000ft (5200m) (4.8s), where the velocity increases at this depth. There is a high amplitude layer at 19,000ft (5800m) (5.2s) and its amplitude decreases with offset increases (Fig. 3-36).

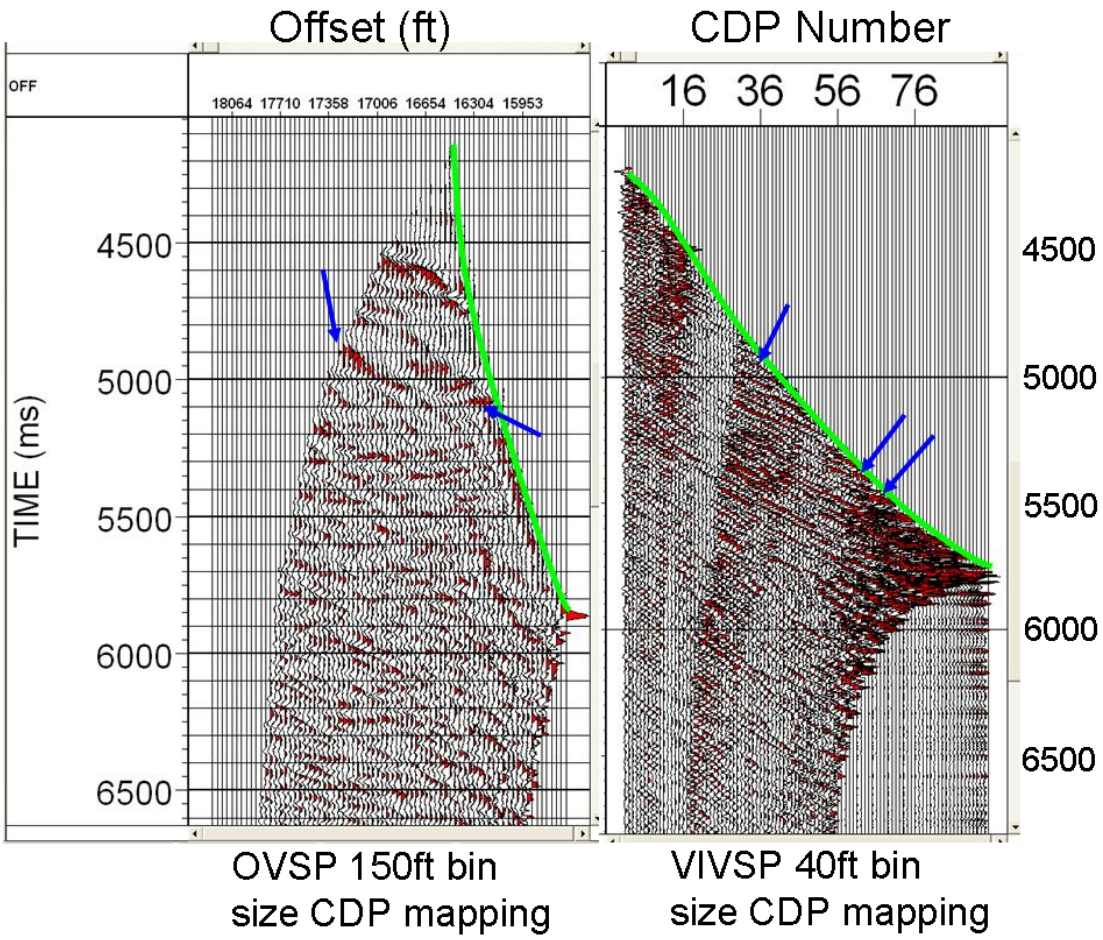

Figure 3-36: The comparison of OVSP-CDP mapping result and VIVSP-CDP mapping result. The deviated well track highlighted in green, the reflection events illustrate by blue arrows.

Chapter 4 Thesis summary

4.1 Summary of glacial terraces, Red Lodge, Montana

The VSP survey was acquired at the UH 2010 Montana field camp and had the goal of determining the thicknesses of glacial benches formed from glacial outwash from the Beartooth Mountains. We conducted a series of geophysical surveys to characterize a glacial bench deposit and underlying strata near Red Lodge, Montana. The well logs and VSP data were

acquired in a PVC-cased, 115m deep borehole. The multi-offset VSP was undertaken using surface sources (an accelerated weight drop and sledge hammer) with a hydrophone string and downhole, wall-clamping, 3-component geophone. The well logs included measurements of conductivity, radioactivity (gamma ray), temperature, and sonic velocity. Sonic and VSP velocities ranged from 1500m/s in the very near surface to 3000m/s at 85m depth. A distinct black clay layer (with high conductivity, high gamma ray, and low velocity) was penetrated at 85m. High-resolution 2D and 3D seismic surveys, using a sledge hammer source were designed and acquired near the well GB-1. On the L-plot composite displaying well log data, and the VSPs corridor stack, three reliable reflections were analyzed, and 50m depth one also shows on driller's report as a water zone. The VSPs velocities and sonic log show a velocity increase at 25m depth, which is interpreted as the total glacial deposits in this study.

Surface seismic refraction static analysis shows a layer at 25m depth. At 25m depth, VSPs and sonic log show a velocity change. This suggests a glacial till thickness of 25m. The 2D seismic brute stack shows a layer at 20ms depth, which may be the glacial till base. The L-plot shows three events, at 40m, 50m and 65m. 50m depth event, shows on geophone Z component stack, and hydrophone tubewave field stack. Also conductivity increases, velocity decreases at 50m depth. The driller's report shows a water perforation zones at 50m depth as well.

4.2 Summary of Garden banks, Gulf of Mexico

The VSP survey was acquired in the Gulf of Mexico, with the objective of acquiring petrophysical information to calibrate surface seismic anomalies by getting the time to depth conversion. A VSP was also acquired in the Garden Banks block at the Gulf of Mexico to provide

a basic time-to-depth relationship, and in situ velocities. An AVO investigation was completed for the deep-water (water depth around 2800ft (850m)) on the Louisiana slope, Gulf of Mexico. During the modeling part of this study, the incident angle of a 3D numerical model was tested. The analysis result shows that the field VSP geometry does not have enough information to perform adequate AVO analysis. For better AVO incident angle information, a walkaway VSP was designed and its synthetic data was also generated. VIVSP, OVSP and sonic log show a velocity increase at 17,000ft (5200m) depth, which causes converted wavefields. The downgoing P-wave, downgoing PS-wave, upgoing PP-wave and upgoing PS-wave energy partitions have been analyzed and compared with the theoretical calculations from the Zoeppritz equation. The field VSP data, after rotation and noise analysis, shows strong P-P and P-S reflection events and thus the potential to do further P-S VSP processing. The VIVSP P-P reflection has been processed into a 40ft (12m) bin size CDP section, which provides high-resolution reflection images. The OVSP P-P reflection has been processed into a 150ft bin size CDP section, which resolves the horizon at 18,000ft (5500m) (5.0s), and shows the reflection amplitude decrease with the offset increase. At 20,000ft (6100m) (5.35s) is a horizon with uncertain thickness, logging data shows it may extend to 20,500ft (6250m) (5.45s), which is also has low velocity, the VIVSP-CDP mapping resolves the boundary between those two horizons as two different low velocity layers.

VIVSP & OVSP interval velocity reasonably agrees with the sonic log, they show an increase at 17,000ft (5200m) depth. The VIVSP P-P reflection has been processed into a 40ft (12m) bin size CDP section, which resolves the boundary between the 20,000ft (6100m) (5.35s) horizon and another horizon at 20,500ft (6250m) (5.45s). Based on logging interpretation, at 20,000ft (6100m) depth is gas layer and 20,500ft (6248m) depth is tight gas layer.

The OVSP P-P reflection has been processed into a 150ft (45m) bin size CDP section, which resolves the horizon at 19,000ft (5800m) (5.2s), and shows the reflection amplitude decrease with the offset increase. From the modeling and bin analysis, the field data does not provide adequate AVO information. For better AVO analysis, a walk-away VSP is designed and recommended.

References

Coulombe, C.A., R.R. Stewart, and M.J. Jones, 1992, AVO analysis of VSP and well log data: CREWES Research Report, **4**, 15.1-15.29.

Coulombe, C.A., R.R. Stewart, and M.J. Jones, 1996, AVO processing and interpretation of VSP data: Can. J. Expl. Geophys., 32, 41-62.

Foose, R.M., D.U. Wise, and G.S. Garbarini, 1961, Structural geology of the Beartooth Mountains: Montana and Wyoming GSA Bulletin, 72, 1143-1172.

Galloway W., 1989, Genetic stratigraphic sequences in basin analysis II application to Northwest Gulf of Mexico Cenozoic basin: The American Association of Petroleum Geologists Bulletin, 73, 143-154.

Hardage, B.A., 1983, Vertical seismic profiling Part A: Principles Geophysical Press.

Heasler, H.P., C. Jaworowski, R.W. Jones, R.H. De Bruin, and A.J. Ver Ploeg, 1996, A self-guided geologic tour of the chief Joseph highway and surrounding area, Northwestern Wyoming in Wyoming State Geological Survey, No. 35, edited by G.B. Glass, 47th Annual Highway Geology Symposium, Cody Wyoming.

Hilterman F.J., 2001, Seismic amplitude interpretation: Soc. Explor. Geophys.

Hinds, R.C., N.L., Anderson, and R.D., Kuzmiski, 1996, VSP interpretive processing theory and practice: Soc. Explor. Geophys.

Hinds, R.C. and R.D. Kuzmiski, 2010, GeoCanada continuing education: Can. Soc. Expl. Geophys.

Huang, J.Q. and J. Wong, 2011, Integrated well-log, VSP, and surface seismic analysis of near-surface glacial sediments: Red Lodge, Montana: 81st Ann. Internat. Mtg., Soc. Expl. Geophys., Expanded Abstracts.

Jitendra, S.G., R.R. Stewart, and J.M. Parkin, 2004, Analyzing three-component 3D vertical seismic profiling data: Geophysics, 69, 386-392.

John, O.B., and R. Harris, 2006, Multicomponent VSP imaging of tight-gas sands: Geophysics, 71, 83-90.

Kramer, D., 1991, Multicomponent multioffset VSP processing: 61th Ann. Internat. Mtg., Soc. Expl. Geophys., Expanded Abstracts, 38-42.

Liner C.L., 2004, Elements of 3D seismology: Univ. of Tulsa.

Leaney, W.S., C.M. Sayers, and D.E. Miller, 1999, Analysis of multiazimuthal VSP data for anisotropy and AVO: Geophysics, 64, 1172-1180.

Li, Y.P., X.M. Zhao, R. Zhou, and D. Dushman, 2005, 3C VSP tomography inversion for subsurface P- and S- wave velocity distribution: 75th Ann. Internat. Mtg., Soc. Expl. Geophys., Expanded Abstracts, 2625-2629.

Lopez, D.A., 2005, Geologic map of the red lodge area, carbon county, Montana: Montana Bureau of Mines and Geology, 1-16.

Martin, G.S., K.J. Marfurt, and S. Larsen, 2002, Marmousi-2an updated model for the investigation of AVO in structurally complex areas: 72nd Ann. Internat. Mtg., Soc. Expl. Geophys., Expanded Abstracts, 1979-1982.

Maresh, J., R.S. White, R.W., Hobbs, and J.R. Smallwood, 2006, Seismic attenuation of Atlantic margin basalts observations and modeling: Geophysics, 7, 211-221.

Mahmoudian, F., 2006, Linear AVO inversion of Multi-component surface seismic and VSP data, M.Sc. thesis, Univ. of Calgary.

Miong, S.K., 2008, Borehole geophysical methods for near-surface characterization, M.Sc. thesis, Univ. of Calgary.

Mukherjee, T., and R.R. Stewart, 2010, Near-Surface borehole geophysical imaging in a highly structured area, Bear tooth Mountains, Montana: 79th Ann. Internat. Mtg., Soc. Expl. Geophys., Expanded Abstracts, 2044-2048.

Nottis, G.N., 2010, Predictive equations for soil shear-wave velocities: University at Buffalo, website, http://mceer.buffalo.edu/education/reu/01presentations/swvlwrhudson.htm.

Pilcher, R.S., B. Kilsdonk, and J. Trude, 2011, Primary basins and their boundaries in the deep-water northern Gulf of Mexico Origin, trap types, and petroleum system implications: American Association of Petroleum Geologists Bulletin, 95, 219-240.

Place, J., C. Naville, and I. Moretti, 2007, Fault throw determination using 4 component VSPAigion fault (Greece) case study: Tectonophysics, 440, 141-158.

Ritter, D.F., 1964, Terrace development along the front of the Beartooth mountains, southern Montana, Ph.D. thesis, Princeton University.

Robinson, E.A., S. Treitel, 2008, Digital imaging and deconvolution: The ABCs of seismic exploration and processing: Soc. Expl. Geophys.

Stewart, R.R., P.D. Huddleston, and T.K. Kan, 1982, Traveltime analysis and vertical seismic profiles: 52nd Ann. Internat. Mtg., Soc. Expl. Geophys., Expanded Abstracts, 158-159.

Stewart, R.R., P.D. Huddleston, and T.K. Kan, 1984, Seismic versus sonic velocities: A vertical seismic profiling study: Geophysics, 49, 1153-1168.

Stewart, R.R., 1984, VSP interval velocities from traveltime inversion: Geophysical Prospecting, 32, 608-628.

Stewart, R.R., 1985, Median filtering review and a new F/K analogue design: Can. J. Expl. Geophys, 21, 54-63.

Stewart, R.R., J.E. Gaiser, R.J., Brown, and D.C., Lawton, 2002, Tutorial: Coverted-wave seismic exploration methods: Geophysics, 67, 1348-1363.

Stewart, R.R., J.E. Gaiser, R.J., Brown, and D.C., Lawton, 2003, Tutorial: Coverted-wave seismic exploration applications: Geophysics, 68, 40-57.

Stewart, R.R., C.D. Xu, and N.L. Soubotcheva, 2007, Interpreting multicomponent (3C) seismic data example of sand channel identification: Journal of Seismic Exploration, 16, 1-25.

Stewart, R.R., S. Khan, S. Hall, C. Liner, and J. Wong, 2010, Geophysical field education: Better learning by doing: The Leading Edge, 29, 546-550.

Uyanik, O., 2010, Compresisnal and shear-wave velocity measurements in unconsolidated top-soil and comparison of the results: International Journal of the Physical Sciences, 5, 1034-1039.

Wise, D.U., 2000, Laramide structures in basement and cover of the Beartooth uplift near Red Lodge, Montana: American Association of Petroleum Geologists Bulletin, 84, 360-375.

Wong, J., S.K. Miong, R.R. Stewart, E.V. Gallant, and K.W. Hall, 2009, Shallow VSP survey using a small vibrator source: CSPG/CSEG/CWELS Convention, 628-631.

Wong, J., S.K. Miong, L. Bentley, and R.R. Stewart, 2008, VSP and well logs from a shallow test well: CSPG/CSEG/CWELS Convention, 363-367.

Appendix

1. **WELL OWNER:**
Name Dillon Mem. Harmont + Const. Inc
Mailing address P.O. Box 1529
Red Lodge, Mt 59068

2. **WELL LOCATION:** List ¼ from smallest to largest
¼ NE ¼ SE ¼ SE ¼, Section 17
Township 8 (N/S) Range 22 (E/W) County Carbon
Lot 13, Tract/Blk ___ Subdivision Name ___
Well Address ___
GPS ☒ Yes ☐ No
Latitude N45°01'47.9" Longitude W109° 16'45.5"
Error as reported by GPS locator (± feet) 49
Horizontal datum ☒ NAD27 ☐ WGS84

3. **PROPOSED USE:** ☒ Domestic ☐ Stock ☐ Irrigation
☐ Public water supply ☐ Monitoring Well ☐ Other: ___

4. **TYPE OF WORK:**
☒ New well ☐ Deepen existing well ☐ Abandon existing well
Method: ☐ Cable ☒ Rotary ☐ Other: ___

5. **WELL CONSTRUCTION DETAILS:**
Borehole:
Dia. 9 7/8 in. from 0 ft. to 380 ft.
Dia. ___ in. from ___ ft. to ___ ft.
Dia. ___ in. from ___ ft. to ___ ft.
Casing:
Steel: Wall thickness .250 ☐ Threaded ☒ Welded
Dia. 6 5/8 in. from +2 ft. to 45 ft.
Dia. ___ in. from ___ ft. to ___ ft.
Plastic: Pressure Rating 160 lbs. ☐ Threaded ☒ Welded
Dia. 4 in. from 40 ft. to 320 ft.
Perforations/Slotted Pipe:
Type of perforator used Factory
Size of perforations/slots .025 in. by 3 in.
160 no. of perforations/slots from 160 ft. to 180 ft.
160 no. of perforations/slots from 240 ft. to 320 ft.
Screens: ☐ Yes ☒ No 300 320
Material ___ 340 360
Dia. ___ Slot size ___ from ___ ft. to ___ ft.
Dia. ___ Slot size ___ from ___ ft. to ___ ft.
Gravel Packed: ☐ Yes ☒ No
Size of gravel ___
Gravel placed from ___ ft. to ___ ft.
Packer: ☐ Yes ☒ No
Type ___ Depth(s) ___
Grout: Material used Bentonite
Depth from ___ ft. to ___ ft. OR ☒ Continuous feed

6. **WELL TEST DATA:**
A well test is required for all wells. (*See details on well log report cover.*)
☐ Static water level ___ ft. below top of casing or
☐ Closed-in artesian pressure ___ psi.
How was test flow measured:
bucket/stopwatch, weir, flume, flowmeter, etc ___
Yellowstone groundwater closure area only - Water Temperature ___ °F
☐ AQUIFER TEST DATA FORM ATTACHED

Test - 1 hour minimum
Drawdown is the amount water level is lowered below static level.
All depth measurements shall be from the top of the well casing.
Time of recovery is hours/minutes since pumping stopped.

Air test* 4 gpm with drill stem set at 375 ft. for 2 hours
Time of recovery 3 hrs/min. Recovery water level 61 ft.

OR Bailer test*
___ gpm with ___ ft. of drawdown after ___ hours
Time of recovery ___ hrs/min. Recovery water level ___ ft.

OR Pump test*
Depth pump set for test ___ ft.
___ gpm pump rate with ___ ft. of drawdown after ___ hrs pumping
Time of recovery ___ hrs/min. Recovery water level ___ ft.

OR Flowing Artesian* LOWER well
___ gpm for ___ hours
Flow controlled by ___

**During the well test the discharge rate shall be as uniform as possible. This rate may or may not be the sustainable yield of the well. Sustainable yield does not include the reservoir of the well casing.*

7. **WELL LOG:**

Depth, Feet From	Depth, Feet To	Material: color/rock and type/descriptor (example: blue/shale/hard, or brown/gravel/water, or brown/sand/heaving)
0	1	Top Soil
1	44	Gravel
44	47	Limestone
47	75	Red Rock w/ Red Clay, Igneous?
75	80	Soft bentonite - Clay
80	85	Red Clay
85	115	Cobbles, broken Granite w/ Lots of Red 2½ gpm @ 120
115	130	Fractured Red granite
130	132	Soft red Clay
132	135	Light Iron
135	140	Red Clay
140	275	Fractured red rock
275	285	Black clay bentonite
285	380	Black, dry, with return but NO Cuttings

☐ ADDITIONAL SHEETS ATTACHED
8. **DATE WELL COMPLETED:** 11-7-99
9. **REMARKS:** ___

10. **DRILLER/CONTRACTOR'S CERTIFICATION:**
All work performed and reported in this well log is in compliance with the Montana well construction standards. This report is true to the best of my knowledge.
Name, firm, or corporation (print) B+H Drilling
Address Fishtail, MT 59028
Signature R B Murph
Date 11-9-99 License no. 309

Appendix 2-1: The GB-1 well drilling report.

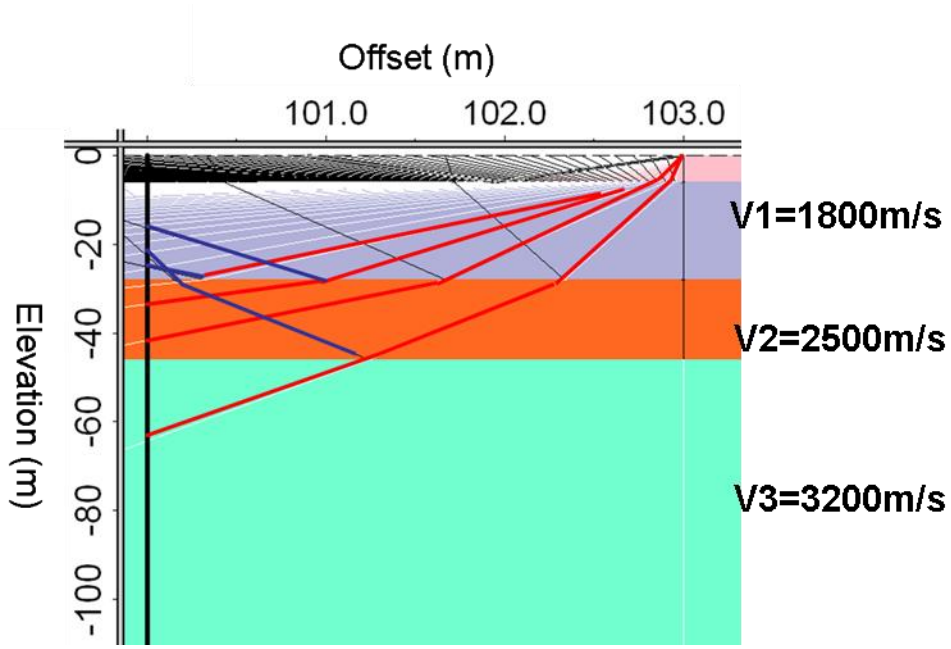

$$\frac{\sin\theta}{\sin 90^0} = \frac{V_1(1800\boldsymbol{m/s})}{V_2(2500\boldsymbol{m/s})}$$

$$\theta = 46^0$$

$$\boldsymbol{offset} = \tan 46^0 \times 55\boldsymbol{m} = 57\boldsymbol{m}$$

Appendix 2-2: 2D seismic refraction critical offset calculation using Snell's law, the offset was used in refraction first break picking for refraction static analysis.

Depth (m)	Vp (m/s)	Vs (m/s)	Density (g/cc)
6m	800m/s	372m/s	1.79
25m	1800m/s	487m/s	2.0
45m	2500m/s	552m/s	2.14
200m	3200m/s	665m/s	2.28

Appendix 2-3: 2D forward model parameters (Pers. Comm. D. Steve, 2011).

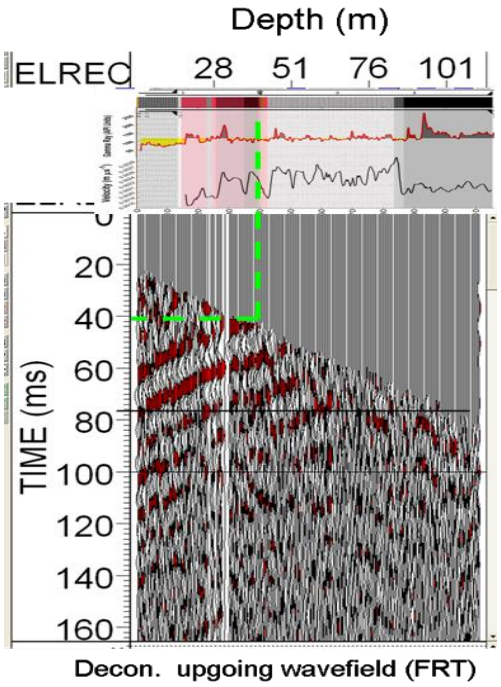

$$\tan\phi = \frac{offset(m)}{36(m)}$$

where, Ø is the incident angle, 36 is the depth of the receiver.

Offset (m)	Incident angle ø (deg)	Amplitude
3.2	5.08	-0.08
5.2	7.97	-0.24
7.2	11.31	-0.15
9.2	14.57	-0.07
11.2	17.22	-0.05
13.2	20.3	-0.12
15.2	22.78	-0.12
17.2	25.56	-0.3
19.2	27.92	-0.13
21.2	30.5	-0.076
23.2	32.62	-0.078
25.2	35	-0.112
27.2	37.1	-0.18

Appendix 2-4: 36m depth CRG amplitude table, blue indicates the reliable amplitudes have been chosen in the AVO analysis the 40m depth event.

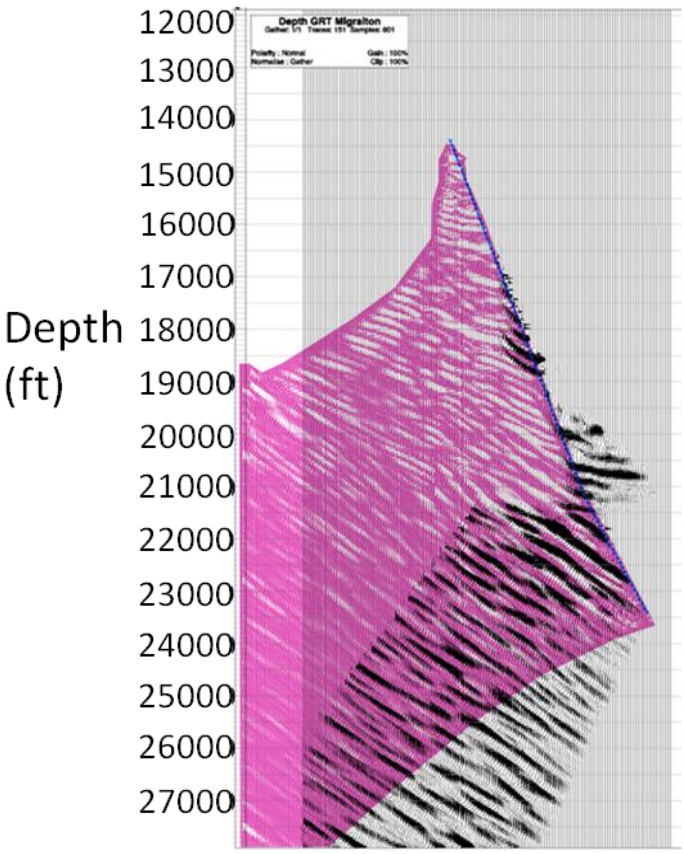

Appendix 3-1: Schlumberger processed VIVSP (pink color) and OVSP depth migration (black). It resolves the reflection at 18,700ft (5700m) (5.15s), and it shows the event at 20,000ft (6100m) (5.35s) and 20,500ft (6250m) (5.45s) are two different events.

Depth at NE corner	Dip angle (deg.)	Vp	Vs	Density (g/cc)
3,000ft (914m)	0	6,300ft/s (1920m/s)	1,585ft/s (483m/s)	2.0
5,000ft (1524m)	0	6,500ft/s (1981m/s)	1,757ft/s (536m/s)	2.0
7,000ft (2134m)	0	6,800ft/s (2073m/s)	2,016ft/s (614m/s)	2.0
9,500ft (2895m)	0	7,300ft/s (2225m/s)	2,447ft/s (746m/s)	2.0
12,000ft (3658m)	0	9,000ft/s (2743m/s)	3,912ft/s (1192m/s)	2.1
15,000ft (4572m)	0	9,500ft/s (2896m/s)	4,343ft/s (1324m/s)	2.25
16,500ft (5029m)	32	10,500ft/s (3200m/s)	5,205ft/s (1586m/s)	2.3
17,000ft (5182m)	32	13,000ft/s (3962m/s)	7,360ft/s (2243m/s)	2.35
18,000ft (5486m)	32	11,500ft/s (3505m/s)	6,067ft/s (1849m/s)	2.1
22,000ft (6705m)	32	11,800ft/s (3597m/s)	6,326ft/s (1928m/s)	2.2
24,000ft (7315m)	45	12,000ft/s (3658m/s)	6,498ft/s (1981m/s)	2.25

Appendix 3-2: Forward model parameters, at 17,000ft (5200m), there is a high velocity and high-density layer.